



University of Kentucky  
UKnowledge

---

Theses and Dissertations--Pharmacy

College of Pharmacy

---


2022

## BUILDING TOOLS FOR IMPROVED MODULATION OF THE HUMAN GABAA RECEPTOR, A CENTRAL NERVOUS SYSTEM TARGET FOR THE TREATMENT OF ANXIETY

Garrett Edward Zinck

University of Kentucky, garrett.zinck@gmail.com

Author ORCID Identifier:

 <https://orcid.org/0000-0001-9738-6576>

Digital Object Identifier: <https://doi.org/10.13023/etd.2022.038>

[Right click to open a feedback form in a new tab to let us know how this document benefits you.](#)

### Recommended Citation

Zinck, Garrett Edward, "BUILDING TOOLS FOR IMPROVED MODULATION OF THE HUMAN GABAA RECEPTOR, A CENTRAL NERVOUS SYSTEM TARGET FOR THE TREATMENT OF ANXIETY" (2022). *Theses and Dissertations--Pharmacy*. 134.

[https://uknowledge.uky.edu/pharmacy\\_etds/134](https://uknowledge.uky.edu/pharmacy_etds/134)

This Doctoral Dissertation is brought to you for free and open access by the College of Pharmacy at UKnowledge. It has been accepted for inclusion in Theses and Dissertations--Pharmacy by an authorized administrator of UKnowledge. For more information, please contact [UKnowledge@lsv.uky.edu](mailto:UKnowledge@lsv.uky.edu).

## **STUDENT AGREEMENT:**

I represent that my thesis or dissertation and abstract are my original work. Proper attribution has been given to all outside sources. I understand that I am solely responsible for obtaining any needed copyright permissions. I have obtained needed written permission statement(s) from the owner(s) of each third-party copyrighted matter to be included in my work, allowing electronic distribution (if such use is not permitted by the fair use doctrine) which will be submitted to UKnowledge as Additional File.

I hereby grant to The University of Kentucky and its agents the irrevocable, non-exclusive, and royalty-free license to archive and make accessible my work in whole or in part in all forms of media, now or hereafter known. I agree that the document mentioned above may be made available immediately for worldwide access unless an embargo applies.

I retain all other ownership rights to the copyright of my work. I also retain the right to use in future works (such as articles or books) all or part of my work. I understand that I am free to register the copyright to my work.

## **REVIEW, APPROVAL AND ACCEPTANCE**

The document mentioned above has been reviewed and accepted by the student's advisor, on behalf of the advisory committee, and by the Director of Graduate Studies (DGS), on behalf of the program; we verify that this is the final, approved version of the student's thesis including all changes required by the advisory committee. The undersigned agree to abide by the statements above.

Garrett Edward Zinck, Student

Dr. Joseph Chappell, Major Professor

Dr. David Feola, Director of Graduate Studies

BUILDING TOOLS FOR IMPROVED MODULATION OF THE HUMAN GABAA  
RECEPTOR, A CENTRAL NERVOUS SYSTEM TARGET FOR THE TREATMENT  
OF ANXIETY

---

DISSERTATION

---

A dissertation submitted in partial fulfillment of the  
requirements for the degree of Doctor of Philosophy in the  
College of Pharmacy  
at the University of Kentucky

By

Garrett Edward Zinck

Lexington, Kentucky

Co- Directors: Dr. Joseph Chappell, Professor of Pharmaceutical Sciences

and Dr. Robert Lodder, Professor of Pharmaceutical Sciences

Lexington, Kentucky

Copyright © Garrett Edward Zinck 2022

<https://orcid.org/0000-0001-9738-6576>

## ABSTRACT OF DISSERTATION

### BUILDING TOOLS FOR IMPROVED MODULATION OF THE HUMAN GABA<sub>A</sub> RECEPTOR, A CENTRAL NERVOUS SYSTEM TARGET FOR THE TREATMENT OF ANXIETY

In the U.S., anxiety is recognized as an increasing range of mentally and physically debilitating psychiatric health disorders with significant economic repercussions. Over the last 20 years, several novel anti-anxiety therapies have entered the drug development pipeline, but none have made it to market.

The work in this dissertation focused on structurally modifying valerenic acid (VA), a structurally unique carboxylated sesquiterpene acid found in *Valeriana officinalis*. VA is putatively reported to have allosteric modulatory activity of the human GABA<sub>A</sub> receptor, a ligand-gated ion channel responsible for attenuating neurotransmissions. Structural modeling of VA's GABA<sub>A</sub> receptor interaction suggests that constraining the isobutenyl group relative to the 5,6 membered ring system of VA could improve its binding specificity and affinity to the GABA<sub>A</sub> receptor. In planta, valerena-1,10-diene (VLD) is synthesized from farnesyl pyrophosphate (FPP) valerenadiene synthase (VDS), a sesquiterpene synthase. VLD is then carboxylated at one of its isobutenyl terminal methyl groups to yield VA. Our first objective was to engineer the VDS enzyme for altered product specificity and a more chemically constrained VLD scaffold.

Using computational homology modelling and phylogenetic sequence analysis of characterized sesquiterpene synthases, amino acid residues in or near the active site and potentially impinging on catalytic specificity of VDS were identified. Residues were mutated via site-directed mutagenesis and mutants evaluated *in vivo* and *in vitro*. While wild type VDS' products were 66 % VLD, 5 % alloaromadendrene, and 29 % bicyclogermacrene (BCG), mutant Y535F yielded solely BCG. VDS with alanine or serine substituted for asparagine at position 455 lost all its ability to produce any of the wild type products and instead yielded a suite of seven new

products dominated by germacrene-D-ol ( $\geq 40\%$ ).

To install a carboxylic acid functional group onto the sesquiterpene hydrocarbon scaffolds, we focused on the development of a host platform harboring an endomembrane system suitable for the expression of eukaryotic cytochrome P450 enzymes (P450s). As an example, plasmid co-expression of VDS, *Lactuca sativa* germacrene-A oxidase, and *Artemisia annua* cytochrome P450 oxidoreductase yielded an average 2mg/L of VA.

For biological evaluation of sesquiterpene analogs, HEK293 cells transiently transfected with the human GABA<sub>A</sub> receptor subunit genes  $\alpha_1$ ,  $\beta_3$ , and  $\gamma_{2L}$ , as well as a HEK293 cell line stably expressing the same GABA subunit genes, were optimized for sensing changes in membrane potential using a fluorescent bioassay. Effective concentration of test compounds and absolute magnitude of membrane depolarization in the transiently transfected cells gave the greatest responsiveness as determined for  $\gamma$ -aminobutyric acid ( $EC_{50} = 808 \pm 206$  nM,  $E_{max} = 13,309 \pm 953$  AFU's), clonazepam ( $EC_{50} = 15 \pm 8$  nM,  $E_{max} = 4,211 \pm 334$  AFU's), and VA ( $EC_{50} = 2,397 \pm 341$  nM,  $E_{max} = 5,935 \pm 104$  AFU's). Abscisic acid, gibberellic acid, and cyclopartheniol demonstrated little to no detectable activity for modulating the human GABA<sub>A</sub> receptor.

KEYWORDS: anxiety, terpene synthase engineering, yeast engineering, fluorescent bioassay, GABA<sub>A</sub> receptor allosteric modulators

---

Garrett Edward Zinck

---

February 27, 2022

---

Date

BUILDING TOOLS FOR IMPROVED MODULATION OF THE HUMAN  
GABAA RECEPTOR, A CENTRAL NERVOUS SYSTEM TARGET FOR THE  
TREATMENT OF ANXIETY

By

Garrett Edward Zinck

Dr. Joseph Chappell

---

Co-Director of Dissertation

Dr. Robert Lodder

---

Co-Director of Dissertation

Dr. David Feola

---

Director of Graduate Studies

February 27, 2022

---

Date

## DEDICATION

To my loving and patient wife, Melissa.

## ACKNOWLEDGMENTS

I wanted to first acknowledge my advisor, Dr. Joe Chappell, PhD. for his mentorship and unwavering encouragement throughout my tenure in the Chappell lab. While under his guidance, I was fully indoctrinated into the three pillars of scientific research: rigor, robustness, and reproducibility. I have the greatest respect for scientific wisdom and more importantly, his friendship.

Secondly, I would like to thank former members of the Chappell lab, Scott Kinison, Dr. Kirsten Linscott, Ph.D, M.D., and Dr. Chase Kempinski, Ph.D – all of whom inculcated fundamental scientific skill sets and provided invaluable advice to me along the way.

Finally, I would like to thank Dr. Steven Van Lanen, Ph.D., Dr. Jim Pauly Ph.D., Dr. Robert Lodder Ph.D., Dr. Ann Morris Ph.D., and Dr. Olivier Thibault Ph.D. for serving as my doctoral advisory committee. Each of you availed his or herself, at one time or another, and to provide sound scientific guidance during my tenure as a graduate student which all positively impacted the success of the work covered in this dissertation.



## TABLE OF CONTENTS

ACKNOWLEDGMENTS .....	iii
LIST OF TABLES .....	vii
LIST OF FIGURES .....	viii
LIST OF EQUATIONS .....	ix
CHAPTER 1. INTRODUCTION .....	1
1.1 Prevalence and economic burden of anxiety psychiatric disorders in the US .....	1
1.2 Psychotherapies for the treatment of AD .....	4
1.3 Pharmacotherapies for the treatment of AD .....	4
1.4 BZDs mechanism of action.....	7
1.5 Mechanism of GABA <sub>A</sub> receptor activation .....	9
1.6 The future of anxiolytic drug discovery.....	10
1.7 Use of valerian for its anxiolytic properties.....	11
CHAPTER 2. STRUCTURALLY GUIDED REPROGRAMMING OF VALERENADIENE SYNTHASE .....	13
2.1 Introduction.....	13
2.2 Materials and Methods.....	17
2.2.1 Molecular Modeling.....	17
2.2.2 Site-directed mutagenesis of VDS .....	17
2.2.3 <i>In vivo</i> product analysis .....	20
2.2.4 <i>In vitro</i> mutant expression for enzyme assays .....	24
2.2.5 Steady-State Kinetic determinations.....	24
2.2.6 <i>In Vitro</i> Product Analysis.....	25
2.2.7 Immunodetection of VDS Enzymes .....	25
2.3 Results and Discussion .....	28
2.3.1 Building an Accurate 3D Structural Representation of VDS .....	28
2.3.2 Selection Criteria for Candidate Residues .....	32
2.3.3 Evaluation Procedure for Candidate Residues.....	35
2.3.4 Tyr535 is likely the proton donor in VDS .....	42
2.3.5 Probing the role of Cys415 and Cys452 .....	48
2.3.6 Contributions of residues proximal to a metal binding domain.....	50
2.3.7 Asn455 suppress a dormant cyclization cascade in VDS .....	52
2.4 Conclusions.....	53

CHAPTER 3. TOWARDS BUILDING A VALERENIC ACID ANALOG BIOSYNTHESIS PLATFORM IN YEAST.....	54
3.1 Introduction.....	54
3.2 Materials and Methods.....	59
3.2.1 Chemicals and reagents.....	59
3.2.2 VoVDS cloning and amplification.....	59
3.2.3 LsGAO amplification and cloning.....	60
3.2.4 <i>S. pyogenes</i> Cas9-NLS amplification and cloning.....	64
3.2.5 BTS1, Rox1, YPL062W, & YJL064W gRNA cassettes .....	64
3.2.6 Homology-armed VDS DNA oligo .....	65
3.3 Construction and maintenance of utilized yeast lines.....	69
3.3.1 ZXB yeast line .....	69
3.3.2 CRISPR/Cas9 engineered yeast lines from ZXB.....	71
3.4 Detection of VLD and VA from engineered yeast lines.....	74
3.4.1 Plasmid-based expression system .....	74
3.4.2 CRISPR/Cas9 VDS knock in yeast line system .....	75
3.5 Results and Discussions.....	78
3.5.1 Successive oxidation of valerenadiene to valerenic acid.....	78
3.5.2 Improvement in valerenadiene yeast titers using CRISPR/Cas9 .....	81
3.6 Conclusions.....	84
CHAPTER 4. ESTABLISHING & VALIDATING A HUMAN CELL LINE-BASED FLUORESCENCE ASSAY FOR MODULATION OF THE HUMAN GABAA $\alpha_1\beta_3\gamma_{2L}$ RECEPTOR .....	85
4.1 Introduction.....	85
4.2 Materials and Methods.....	90
4.2.1 Chemicals and reagents.....	90
4.2.2 Culturing wildtype HEK293 cells.....	90
4.2.3 Culturing transfected HEK293 cells .....	91
4.2.4 Culturing HEK293 cells stably expressing human GABA <sub>A</sub> receptors .....	92
4.2.5 FMP RED dye assay 96 well plate preparation .....	93
4.2.6 CLARIOstar optical settings and run mode.....	94
4.2.7 Immunoblot confirmation of the $\alpha_1$ , $\beta_3$ , & $\gamma_{2L}$ human GABA <sub>A</sub> subunit total expression in transfected naïve HEK293 whole cell lysates.....	95
4.2.8 Data analysis parameters.....	98
4.3 Results and Discussion .....	101
4.3.1 Validating heterologously expressed human GABA <sub>A</sub> ( $\alpha_1$ , $\beta_3$ , $\gamma_{2L}$ ) receptors display GABA concentration-dependance within the confines of the FMP Red Dye activity assay .....	101

4.3.2	Recombinantly expressed GABA <sub>A</sub> ( $\alpha_1$ , $\beta_3$ , $\gamma_{2L}$ ) receptors are directly potentiated by GABA, CZP, & VA in a concentration dependent manner in the absence of GABA and in the presence of the FMP Red Dye .....	106
4.3.3	The sesquiterpenoids ABA & CPol along with diterpenoid GA3 showed no detectable level of potentiation for transiently expressed human GABA <sub>A</sub> ( $\alpha_1$ , $\beta_3$ , $\gamma_{2L}$ ) receptors.....	111
4.3.4	Varying the $\alpha_1$ , $\beta_3$ , & $\gamma_{2L}$ subunits' availability directly impacts GABA's, CZP's, &VA's potency and efficacy for transiently expressed GABA <sub>A</sub> receptor in naive HEK293 cells .....	113
4.4	Conclusions.....	117
CHAPTER 5. CONCLUSIONS AND PERSPECTIVES.....		118
5.1	Conclusions and perspectives .....	118
REFERENCES .....		120
VITA.....		139

## LIST OF TABLES

Table 1.1 The Seven Subtypes of Anxiety Disorders Recognized by the DSM-V .....	3
Table 1.2 List of Current FDA-Approved Drugs for Treating AD.....	6
Table 2.1 VDS mutagenic primers, with mutated codon colored in red and underlined..	19
Table 2.2 Comparison of the <i>In Vivo</i> Reaction Products from WT and Mutant VDS Enzymes .....	37
Table 2.3 Steady-State Kinetic Parameters and <i>In Vitro</i> Product Distributions (%) by WT and Mutant VDS Enzymes.....	38
Table 3.1 List of VoVDS and LsGAO forward and reverse cloning primers .....	62
Table 3.2 List of CRISPR/Cas9 cloning primers.....	67
Table 3.3 BTS1, Rox1, YPL062W, & YJL064W gRNA cassette nucleotide sequences.	68
Table 3.4 Genotypes of yeast lines used in this study .....	72
Table 3.5 Valerenadiene (VLD) and valerenic acid (VA) titers from plasmids transformed into ZXB .....	79
Table 3.6 VLD titers from plasmid expression of VDS vs. chromosomal insertion within ZXB.....	83
Table 4.1 GABA potency for the CYL3053 PrecisION hGABA-A $\alpha 1/\beta 3/\gamma 2$ -HEK Recombinant Cell Line independently observed by the Chappell and Pessah research groups using the FMP Red Dye assay. ....	105
Table 4.2 GABA, CZP, & VA potency (nM) and efficacy (AFUs) of transiently vs. stably expressed human GABA <sub>A</sub> receptors in HEK293 cells .....	110
Table 4.3 Potency and efficacy of GABA, CZP, & VA for transiently expressed human GABA <sub>A</sub> receptors with varying $\alpha 1$ , $\beta 3$ , & $\gamma 2L$ subunit availability.....	115

## LIST OF FIGURES

Figure 1.1 The human GABAA receptor.....	8
Figure 2.1 Valerena-1,10-diene revised catalytic cascade.....	16
Figure 2.2 EI-Mass spectra of detected sesquiterpenes .....	22
Figure 2.3 (Figure 2.2 (con't)) .....	23
Figure 2.4 Quantitation of wildtype and mutant VDS enzymes.....	27
Figure 2.5 <i>In silico</i> 3D structural VDS tertiary model.....	30
Figure 2.6 Superimposition of TEAS-FHP ribbon structure and the VDS-FPP model....	31
Figure 2.7 Alignment of amino acid residues mutated within VDS.....	34
Figure 2.8 Michaelis-Menten plots of wild type and mutant VDS enzymes.....	39
Figure 2.9 Steady-state kinetics of wild type VDS.....	40
Figure 2.10 GC chromatogram of the detected hydrocarbon products.....	41
Figure 2.11 GC-MS comparisons of bicyclogermacrene standard.....	45
Figure 2.12 Sesquiterpene metabolite comparisons.....	46
Figure 2.13 Overlay of the observed and predicted <sup>13</sup> C labeling pattern for VLD.....	47
Figure 3.1 VA and VA analog factory in our ZXB yeast host system .....	57
Figure 3.2 Hypothetical reaction oxidation scheme .....	58
Figure 3.3 Molecular constructs co-transformed into the ZXB yeast line.....	63
Figure 3.4 Molecular constructs used to knock in VDS in specific yeast genomic loci...	66
Figure 3.5 Overview of the CRISPR/Cas9-DNA Repair System.....	73
Figure 3.6 The genomically integrated VDS DNA expression oligo .....	77
Figure 3.7 Retention time and EI mass spectral validation of valerenic acid.....	80
Figure 4.1 Compounds used to validate the FMP Red Dye assay .....	88
Figure 4.2 Conceptualization of the FMP Red Dye assay .....	89
Figure 4.3 Immunodetection of the $\alpha_1$ , $\beta_3$ , $\gamma_{2L}$ human GABA <sub>A</sub> receptor subunits .....	97
Figure 4.4. Dose response curves for GABA, CZP, VA, ABA, CPol, & GA3 .....	99
Figure 4.5 Wildtype naïve HEK293 cells response to 1000nM of GABA.....	104
Figure 4.6 Varied GABAA receptor subunit responses to GABA,VA, & CZP.....	116

## LIST OF EQUATIONS

Equation 4.1 The four parameter, non-linear regression formula.....	100
---	-----

## CHAPTER 1.INTRODUCTION

### 1.1 Prevalence and economic burden of anxiety psychiatric disorders in the US

Excessively worrying about (or perceiving there is) an imminent threat with no evidence to suggest it is harmful, results in an emotional state of enhanced vigilance and hyperarousal (Russell, 1980) concomitantly accompanied by physiological changes, such as increases in sweating, dizziness, and heart rate, clinically summarizes the debilitating psychiatric mental health disorder classified as anxiety (Calhoun & Tye, 2015; Davis et al., 2010; Robinson et al., 2019; Shackman & Fox, 2016). Succinctly, anxiety is clinically characterized as a subjective emotional mental state originating from unfounded worrying about past or current events which can lead to physical disruption of the neurochemical equilibrium within the limbic system, resulting in irrational social behavior(s) (Calhoun & Tye, 2015; Robinson et al., 2019). In the US, anxiety disorders (AD), codified into seven subtypes under the DSM-V (American Psychiatric, 2013) (**Table 1.1**), burden approximately 32% of the US adult population (18yrs. & older) over the course of his and her lifetime (Kessler et al., 2012). Each AD subtype's etiology and disorder pathogenesis framed the chosen specifiers for the proper psychiatric diagnosis (Kupfer, 2015). Out of the seven AD subtypes, Kessler et al. (Kessler et al., 2012) found social anxiety (social phobia) and specific phobias were the most prevalent AD subtypes among US adults, with a lifetime prevalence of 13% and 13.8%, respectively. Separation anxiety disorder (SAD) generalized anxiety disorder (GAD), panic attack disorder (PD), and agoraphobia were the least prevalent among the US adult population, with lifetime prevalence's estimated at 6.6%, 6.2%, 5.2%, and 2.6%, respectively. It should be noted, Kessler et al.'s report

(Kessler et al., 2012) preceded the release of fifth edition of the DSM, which was the first edition to include selective mutism (SM) as an AD subtype.

Beyond the classification as the most prevalent mental health disorder in the US to date (Cryan & Sweeney, 2011; Garakani et al., 2020), treating AD incurs substantial cost to both the healthcare system and the patient, placing significant strain on a nation's potential economic growth (Greenberg et al., 1999; Shirneshan, 2013; Wittchen et al., 2011). For example, from 2009 to 2010 the total estimated direct costs (i.e., the consumed medical and non-medical resources) for treating AD in the US was estimated at \$1657.57 per person, or \$33.7 billion in 2013 US dollars (Shirneshan, 2013). This is equivalent to 24% of all 2013 US healthcare expenditures and 0.2% of the US' 2013 GDP<sup>1</sup> (Konnopka & König, 2020). AD is a debilitating, costly psychiatric condition that will only continue to burden the US' healthcare system preventing future economic growth. One way to remedy the AD societal burden may be to increase the volume of FDA-approved drugs specifically designed to target novel anxiolytic pathways with the overall goal of equivalent or greater efficacy, lower abuse potential, and a reduced number of adverse effects.

---

<sup>1</sup> Gross Domestic Product



**Table 1.1** The Seven Subtypes of Anxiety Disorders Recognized by the DSM-V

Anxiety Disorder Subtypes	Brief Description
Generalized Anxiety Disorder (GAD)	Excessive anxiety and worry (apprehensive expectation), occurring more days than not for at least 6 months, about a number of events or activities (such as work or school performance)
Panic Attack Disorder (PD)	An abrupt surge of intense fear or intense discomfort that reaches a peak within minutes.
Separation Anxiety Disorder (SAD)	Developmentally inappropriate and excessive fear or anxiety concerning separation from those to whom the individual is attached.
Social Anxiety Disorder	Marked fear or anxiety about one or more social situations in which the individual is exposed to possible scrutiny by others.
Specific Phobia (SP)	Marked fear or anxiety about a specific object or situation.
Agoraphobia	A marked fear or anxiety about two (or more) of the following five situations: using public transportation, being in open spaces, being in enclosed spaces, standing in line or being in a crowd, or being outside the home alone.
Selective Mutism (SM)	Continual failure to speak in specific settings (e.g., school, social situations) despite speaking normally in others (e.g., at home).

## 1.2 Psychotherapies for the treatment of AD

Psychotherapies, which encompasses cognitive behavioral therapy (CBT) (Bandelow et al., 2015) and transcranial magnetic stimulation (TMS) (Zhang et al., 2019), offer AD patients a clinically supported alternative to or a supplemental treatment option with pharmaceutical-based AD approved treatments. Though vitally important to the AD treatment regimen, the rest of this section will be spent focused on the pharmacological anxiolytic advances made to help those struggling daily with anxiety. For a more in-depth understanding of CBT and TMS methodology, the reader is encouraged to view (Kaczurkin & Foa, 2015) and (Lefaucheur et al., 2014), respectively.

## 1.3 Pharmacotherapies for the treatment of AD

As of August 2021, there were 17 drugs (**Table 1.2**) currently still Food & Drug Administration (FDA)-approved for treatment of AD recognized under the DSM-V (**Table 1.1**), including obsessive compulsive disorder (OCD) and post-traumatic stress disorder (PTSD) (American Psychiatric, 2013). OCD and PTSD were removed from the list of AD subtypes and placed into their own separate categories with the release of the fifth edition of the DSM in 2013. Currently, the anti-depressant drug class remains the first line of treatment for chronic AD, more specifically- the selective serotonin re-uptake inhibitors (SSRIs) (**Table 1.2**, drug #'s 8-12,) (Garakani et al., 2020; Sartori & Singewald, 2019). SSRI's increase the synaptic serotonin concentration via blocking the 5-HT<sub>1</sub> re-uptake transporter, resulting in the migration of feelings and emotions associated with AD (Griebel & Holmes, 2013). Though documented as safe and highly efficacious (compared with the

placebo in RCTs<sup>2</sup> (Jakubovski et al., 2019)), SSRI's are known to have undesirable adverse effects such as, weight gain, sexual dysfunction, and insomnia (Ferguson, 2001). For acute AD treatment (typically less than a month), the benzodiazepine (BZD) drug class (drug #'s 1-6, **Table 1.2**) remains highly favored among clinicians, given this drug class has a clinical history of rapidly (within minutes) mitigating symptoms of AD via reduction in excitatory action potentials in the postsynaptic neuron through GABAergic inhibitory neurotransmission within the CNS dating back to 1963 with the FDA approval of diazepam (Valium<sup>®</sup>) for GAD (Olfson et al., 2015; Sartori & Singewald, 2019). Greater details on BZDs' mechanism of action are detailed below. Although efficacious, the benzodiazepines have an alarming risk of physical dependence and addictive properties among young adults (Cryan & Sweeney, 2011; Licata & Rowlett, 2008; Tauseef, 2012) and were reported to cause anterograde amnesia within geriatric populations (Mejo, 1992).

---

<sup>2</sup> Randomized Clinical Trial

**Table 1.2** List of Current FDA-Approved Drugs for Treating AD

Number	Generic (Brand) Name	Drug Class	FDA Approval Year	AD Approval Subtype
1.	Alprazolam (Xanax)	BZD	1981	GAD, PD
2.	Clonazepam (Klonopin)	BZD	1975	GAD
3.	Chlorazepate (Tranxene)	BZD	1972	GAD
4.	Diazepam (Valium)	BZD	1963	GAD
5.	Lorazepam (Ativan)	BZD	1977	GAD
6.	Oxazepam (Serax)	BZD	1965	GAD
7.	Clomipramine (Anafranil)	TCA	1989	OCD
8.	Escitalopram (Lexapro)	SSRI	2003	GAD
9.	Fluoxetine (Prozac)	SSRI	1995	OCD, PD
10.	Fluvoxamine (Luvox)	SSRI	1997	OCD, SAD
11.	Paroxetine (Paxil)	SSRI	1996	OCD <sup>b</sup> , PD, SAD,PTSD <sup>b</sup> ,GAD
12.	Sertraline (Zoloft)	SSRI	1996	OCD <sup>b</sup> , PD, PTSD <sup>b</sup> , SAD
13.	Venlafaxine (Effexor XR)	SNRI	1999	GAD, SAD, PD
14.	Duloxetine (Cymbalta)	SNRI	2007	GAD
15.	Buspirone (Buspar)	Other <sup>c</sup>	1986	GAD
16.	Meprobamate (Miltown)	Other <sup>d</sup>	1955	GAD
17.	Trifluoperazine (Stelazine)	APY	2001	GAD

#### 1.4 BZDs mechanism of action

For anxiety disorders, it is clinically documented that excessive or in-appropriate worry can be rapidly mitigated by enhancing the GABAergic inhibitory neurotransmission with use of BZD class of drugs (#'s 1-6, **Table 1.2**) (Low et al., 2000; Rudolph & Knoflach, 2011). In the mid 1950's, the first benzodiazepine, chlordiazepoxide, was synthesized by Sternbach at the Hoffman La Roche Pharmaceutical Company (Cryan & Sweeney, 2011). This drug class, formed from the fusion of a benzene and a diazepine ring, binds to a set of specific amino acid residues located at the interface of an  $\alpha$  and  $\gamma$  subunit, which induces a conformation shift within the receptor, resulting in an increase in the affinity for  $\gamma$ -aminobutyric acid (GABA), its natural agonist. Concomitantly, increasing the frequency at which the chloride ion-selective channel is in the open vs. closed state (**Figure 1.1**).

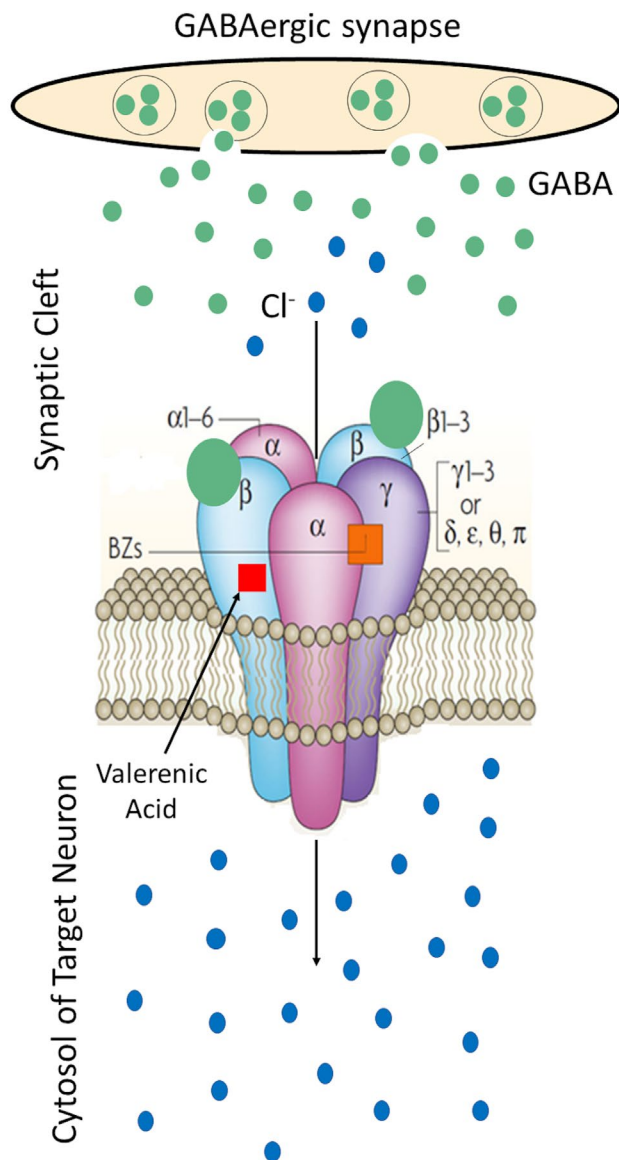


**Figure 1.1** The human GABA<sub>A</sub> receptor is a vitally important ligand-gated ion channel responsible for inhibitory neurotransmission in the central nervous system. The chloride ion (blue circles) selective channel opens after a GABA molecule (green circle) binds to one of its two binding sites (at interface of the  $\alpha$  &  $\beta$  subunits) (Kim et al., 2020; Masiulis et al., 2019). BZDs allosterically modulate the GABA<sub>A</sub> receptor, via binding to the BZ site (orange square) resulting in an increase in the receptor's affinity for GABA. Khom and company (Benke et al., 2009; Khom et al., 2007; Khom et al., 2016; Khom et al., 2010) demonstrated valerianic acid acts as a positive allosteric modulator after binding to the  $\beta$ 2,3 subunits (red square) below 30  $\mu$ M and as direct activator above, observed within in vitro electrophysiology models. Figure was adapted from Jacob et. al. (Jacob et al., 2008).

## 1.5 Mechanism of GABA<sub>A</sub> receptor activation

In the mammalian brain, there must be a balance between excitatory and inhibitory neurotransmission for the brain to function properly (i.e., cortical rhythmic activity) (Bannai et al., 2015). Most of the inhibitory transmission is carried out via the GABAergic synapses, which releases gamma amino-butyric acid (GABA) into the synaptic cleft where it binds to presynaptic neurons inhibiting the release of excitatory neurotransmitters, such as glutamate. In concert, up to two molecules GABA will bind to postsynaptic GABA<sub>A</sub> receptors, inducing a conformational shift, moving the receptor from a “closed” to an “open” state (**Figure 1.1**). In the “open” state, negative chloride ions move freely from the presynaptic cleft down the ion-selective channel into cytosol of the target neuron down their electrochemical gradient. The rapid influx of chloride ions hyperpolarizes the cell, moving the resting membrane potential (typically -80mV for a neuron) in the negative direction reducing the likelihood of an excitatory action potential in the neighboring postsynaptic neuron (Mohler et al., 2005; Tauseef, 2012; Tretter et al., 2008). Structurally, GABA receptors are pentameric ligand-gated ion channels comprised of two  $\alpha$  and two  $\beta$  subunits with a variable subunit of either  $\gamma$ ,  $\epsilon$ ,  $\pi$ ,  $\theta$ , or  $\delta$  in a pseudosymmetric orientation (Jacob et al., 2008; Kim et al., 2020; Masiulis et al., 2019). The  $\alpha_2$  subunit containing GABA<sub>A</sub> receptors (preferentially expressed in the hippocampus, striatum, and the olfactory bulb) are responsible for anxiolysis and preferentially targeted by the barbiturate, benzodiazepine, ethanol, and neurosteroid drug classes (Engin et al., 2012). Hence, play a vital role in the fields of anesthesia and acute anxiolytic treatment (Althaus et al., 2020; Jurd et al., 2003; Pritchett et al., 1988).

## 1.6 The future of anxiolytic drug discovery

Since 2007, the FDA has granted approval designation for only two anxiety disorder pharmacotherapies: duloxetine (Cymbalta<sup>®</sup>) for the treatment of GAD and fluvoxamine maleate (Luvox<sup>®</sup>) for the treatment of OCD. To date, there have been no approvals of New Drug Applications (NDAs) with the FDA specifically designated for the treatment of AD, despite the long list of ongoing FDA-approved clinical trials (Garakani et al., 2020; Sartori & Singewald, 2019). One plausible reason for the recent reduced output of AD approved drugs is the common perception that they are efficacious (**Table 1.2**), though the literature supports a different perspective (Garakani et al., 2020). Dr. Bystritsky (Bystritsky, 2006) reported only 60-85% AD patients respond (experience at least a 50% improvement) to the current psycho and pharmacological US approved AD treatments, hence exploration of alternative AD treatments with greater efficacy, limited adverse effects, and reduced abuse liabilities are warranted. The latest pre-clinical and clinical efforts in AD treatments have looked to target novel receptors in the CNS putatively linked to the anxiety neural circuitry (Sartori & Singewald, 2019), such as the N-methyl-D-aspartate (NMDA) (Sterpenich et al., 2019), cannabinoid type 1 (CB) (Christine & Phan, 2014), and vasopressin type 1A (V<sub>1A</sub>) (Lee et al., 2013) receptors. Interestingly, nicotine, a psychostimulant, was evaluated as an anxiolytic remedy; however, it exhibited paradoxical anxiolytic and anxiogenic pharmacodynamic properties in pre-clinical animal models (Picciotto et al., 2002). Currently, ketamine (NMDA receptor antagonist) and cannabis (complex mixture of chemistries with known agonistic activity for the CB receptor) are under phase 2/3 clinical trials for their anxiolytic activities.



## 1.7 Use of valerian for its anxiolytic properties

For millennia, civilizations have exploited the diverse, biologically active chemistry within plants to provide for their medicinal needs (Barrett et al., 1999; Cragg & Newman, 2013; Dias et al., 2012). Our earliest records indicate, the Mesopotamians (ca. 2600 B.C.) extracted oils from *Cupressus sempervirens* and *Commiphora* species to treat ailments such as the common cough, cold, and infections (Cragg & Newman, 2013; Dias et al., 2012). In Greece 2<sup>nd</sup> century A.D., Galen, a physician and pharmacist, prescribed valerian, a crude extract from the roots of *Valeriana officinalis* to patients suffering from insomnia. Intriguingly, valerian was later re-purposed as an anxiolytic agent to treat shell shock syndrome during WWII in England (Bent et al., 2006; Houghton, 1988, 1999; Ricigliano et al., 2016). Due to its unique anxiolytic properties, valerian's biological chemistry has been under investigation since the 1950's. To date, scientists have discovered that valerenic acid (VA), a carboxylated sesquiterpenoid produced within the roots of *V. officinalis*, binds to specific amino acid residues on the GABA<sub>A</sub> receptor  $\beta_{2,3}$  subunits (**Figure 1.1**) (Benke et al., 2009; Khom et al., 2007; Khom et al., 2016; Khom et al., 2010). VA binding induces a conformational change within the GABA<sub>A</sub> receptor leading to a post-synaptic inhibition of the target neuron, which by itself has been noted to incite anxiolytic effects *in vitro* and *in vivo* (Benke et al., 2009; Houghton, 1988; Khom et al., 2007; Khom et al., 2016; Kopp et al., 2010; Luger et al., 2015; Murphy et al., 2010). *In vitro*, VA has bifurcating mechanisms of actions at the GABA<sub>A</sub> receptor. It acts as an allosteric modulator below 30  $\mu$ M and as a direct activator above the 30  $\mu$ M threshold. These are comparable to the benzodiazepine and barbiturate drug classes, respectively. Previous *in silico* work by Luger et al. (Luger et al., 2015), posited VA's flexible isobutenyl side chain forms a network of hydrophobic and van der Waals interactions with several amino acid residues within a

specific region of the  $\beta_{2,3}$  subunits. Khom and company (Khom et al., 2016) tested several VA analogs for improved potency and selectivity, however; none of the analogs physically constrained VA's "floppy" isobutenyl side chain. Physically constraining VA's isobutenyl side chain by such measures as cyclization would potentially lower its entropic barrier to reaching its active confirmation within the GABA<sub>A</sub> receptors. Such hypotheses are supported by the literature (Allen et al., 2016; Pan et al., 2013).

Hence, the following body of work explores various strategies for the biosynthesis of novel constrained VA analogs within a yeast host system. The immediately following chapter dives into the rational, directed evolution of VDS towards more constrained hydrocarbon precursors (**CHAPTER 2**). Afterwards, **CHAPTER 3** lays out the initial blueprint for enhancing the titers of carboxylated sesquiterpenoids within an endomembrane yeast host platform. Then, **CHAPTER 4** concludes the work with the outline of an optimized *in vitro* biological screening assay for detecting novel chemistries which directly modulate recombinantly expressed human GABA<sub>A</sub> receptors. A summary chapter concludes this entire body of work reflects on the experimental paths undertaken by the author and those which were left explored (**CHAPTER 5**). It is the opinion of this author that these unexplored experimental paths should be considered for continuation of synthesizing and testing novel chemistries with enhanced modulation activity of the GABA<sub>A</sub> receptor with the end downstream goal of greater potency, reduced abuse potentials and minimized adverse effects.

## CHAPTER 2. STRUCTURALLY GUIDED REPROGRAMMING OF VALERENADIENE SYNTHASE

### 2.1 Introduction

Terpenes and terpenoids arise from the condensation of ubiquitous 5 carbon isoprenoid building blocks isopentyl pyrophosphate and dimethylallyl pyrophosphate into linear precursors that undergo complex regio- and stereochemical cyclization reactions catalyzed by terpene synthases, TPSs. The elegance of these cyclized terpenes is most easily captured by noting the multiple ring systems, multiple stereocenters and variety of substituent groups captured in small molecules of 500 Daltons or less (Christianson, 2017; Poulter & Rilling, 1978; Ruzicka, 1953; Tantillo, 2011). Estimates for the number of naturally occurring terpenes identified to date exceeds 100,000, but this only accounts for 1 to 10% of the theoretical possibilities (Christianson, 2017; Poulter & Rilling, 1978; Ruzicka, 1953; Tantillo, 2011). To achieve such chemodiversity, TPSs begin with the generation of a highly reactive carbocation intermediate species through the ionization of their allylic diphosphate substrate (**Figure 2.1**). Then, through a series of well-defined intramolecular bond formations; stereospecific hydride, methyl, and methylene migrations; and various ring openings/closings, TPSs form penultimate terpene/terpenoid scaffolds. The catalytic cascade is finally halted and the hydrocarbon product released from the active site when the reactive carbocation intermediate is either quenched by the capture of a water molecule within the active site or supplied by the bulk solvent (generating hydroxylated terpene species (Grundy et al., 2016)), a stereospecific proton is abstracted to form a double bond (Felicetti & Cane, 2004), or by a nucleophilic addition (alkylation) from a side chain of an amino acid within the active site (Kersten et al., 2015). Interestingly, TPSs utilize one or various combinations of these reaction mechanisms to produce some of the worlds most

renowned therapeutics, agrochemicals, fragrances, and nutraceuticals (Singh & Sharma, 2015).

From a biotechnological point of view, to access the diversity of terpenoid scaffolds (Paddon et al., 2013) it is imperative to gain a fundamental comprehension of the primary catalytic cascades the TPS uses to cyclize the ionized isoprenoid substrate into highly-desired terpene product(s) (Christianson, 2017). This can be achieved through structure-function mapping of key amino acid residues responsible for the catalytic plasticity found within the TPS (Abdallah et al., 2018; Dixit et al., 2017; Greenhagen et al., 2006; Salmon et al., 2015; Schrepfer et al., 2016; Yoshikuni, Ferrin, et al., 2006). Previously, the Ro and Chappell groups independently characterized valerena-1,10-diene synthase (VDS) from *Valeriana officinalis* (Pyle et al., 2012; Yeo et al., 2013). VDS is a class I sesquiterpene synthase which converts the acyclic, all trans farnesyl diphosphate (FPP) into a 5- and 6-fused member ring system with an unusual isobutenyl substituent group known as valerena-1,10-diene (VLD). Therapeutically, valerenic acid (VA), VLD's carboxylated derivative arising from the action of a cytochrome P450(s) localized to the roots of *V. officinalis* (Bos et al., 1996; Ricigliano et al., 2016), was shown to allosterically modulate the mammalian GABA<sub>A</sub> receptor *in vitro* and mitigate the physical signs of stress in murine animal models (Benke et al., 2009; Khom et al., 2007; Khom et al., 2010). *In silico* models predict VA's flexible isobutenyl acidic tail forms hydrophobic interactions with specific amino acid residues within the  $\beta_2$  &  $\beta_3$  subunits of the GABA<sub>A</sub> receptor (Luger et al., 2015). While the Khom group had moderate successes in generating valerenic acid analogs with improved selectivity and potency for the  $\beta$ -subunit *in vitro*, none of these analogs physically constrained the flexible isobutenyl side chain (Khom et al., 2016). The literature

supports the theory that if one constrains a ligand (ex. a drug), one lowers the entropic barrier of reaching its “active” binding conformation, naturally enhancing its ability to bind to its target receptor (Allen et al., 2016; Pan et al., 2013). One such way of introducing conformational constraint is through the stabilization of the ligand’s side chains via cyclization which, by default, reduces the ligand’s number of rotatable bonds (Allen et al., 2016). Hence, the aim of the current work was to identify key amino acids within VDS which mapped to reaction products that offered structural constraint at VLD’s isobutenyl side chain (**Figure 2.1**). Using the information and experimental strategies from previous efforts to alter TPS specificity (Bell et al., 2014; Greenhagen et al., 2006), we discovered amino acid substitutions that altered the product specificity towards native, structurally constrained terpene reaction products or completely derailed the catalytic trajectory towards abortive, structurally constrained reaction products not previously identified for VDS.

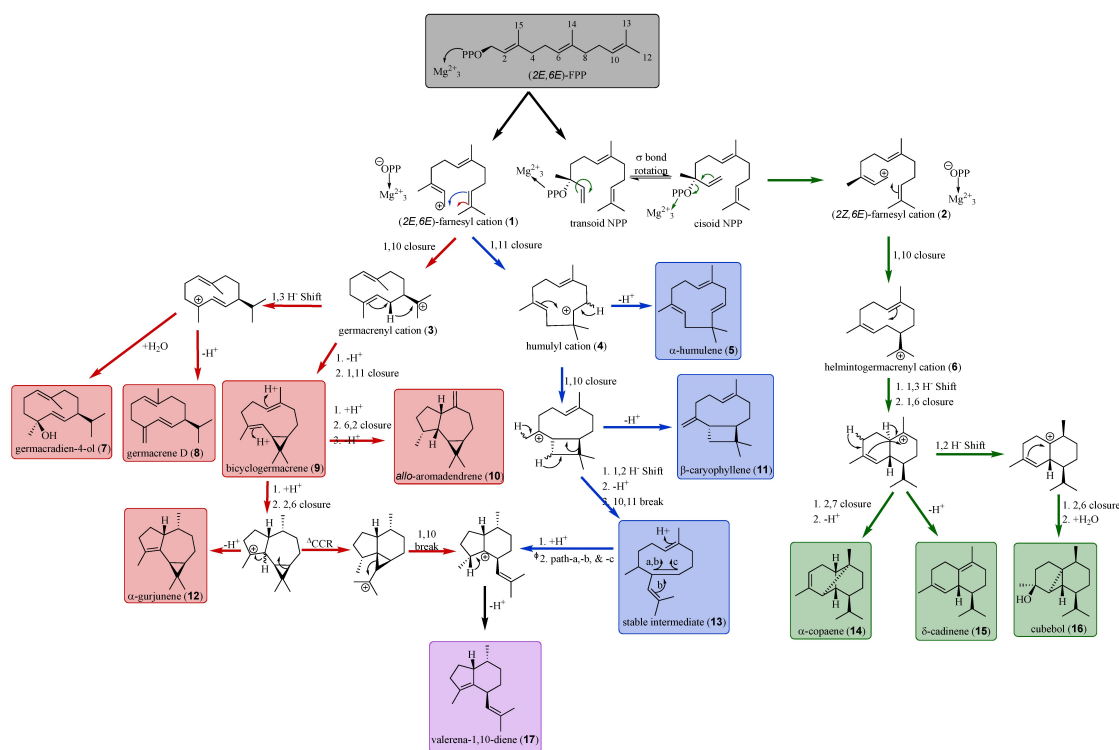


**Figure 2.1** Valerena-1,10-diene (**17**) is the predominate reaction product of the wild type VDS and can arise from two possible routes, initiated by either a 1,10 (germacrenyl route, red arrows and highlighting) or a 1,11 (humulyl route, blue arrows and highlighting) ring closure of **1** (Paknikar et al., 2013; Pyle et al., 2012; Yeo et al., 2013). The other major products **9** and **10**, generated by the wild type VDS, could arise from a germacrenyl cation route as suggested previously (Stefan Garms et al., 2010; Vattekkatte et al., 2017). An earlier study also used specifically labeled FPP to suggest the biosynthetic origin of  $\alpha$ -gurjunene (**12**) via a germacrenyl route (Schmidt et al., 1999). Mutant VDS enzymes lose their ability to biosynthesize the dominant products (**9**, **10**, and **17**), and instead generated a diverse set of sesquiterpenes: germacrene D (**8**) - (germacrenyl cation route) (Picaud et al., 2006);  $\alpha$ -humulene (**5**) and  $\beta$ -caryophyllene (**11**) - (humulyl cation route) (Cai et al., 2002);  $\alpha$ -copaene (**14**),  $\delta$ -cadinene (**15**), and cubebol (**16**) - possibly arising from a helmintogermacrene cation (green arrows and highlighting) (**6**) (Stefan Garms et al., 2010).  $\Delta$ CCR, the cyclopropylcarbinylcation-cyclopropylcarbinylcation rearrangement (Poulter & Rilling, 1978) was suggested by Paknikar et. al. (Paknikar et al., 2013). Details of the  $\phi$ Paths-a, -b, & -c are provide in Yeo et. al. (Yeo et al., 2013).

## 2.2 Materials and Methods

### 2.2.1 Molecular Modeling

Homology modeling of enzymes were carried out with MODELLER v9.21 (University of California, San Francisco, CA) (Sali & Blundell, 1993) using the *Nicotiana tabacum* (tobacco) 5-epi-aristolochene synthase (EAS) coordinates (Protein Data Bank entry 5EAT) (Starks et al., 1997) as the template. Model was evaluated for accuracy with the freely available SaliLab Model Evaluation v2.1 program (Eramian et al., 2008; Melo et al., 2002; Shen & Sali, 2006). The model with the smallest predicted root-mean-squared deviation and DOPE score was subsequently used for docking studies. Proposed reaction intermediates were constructed in CHEMDRAW (PerkinElmer) and were energy-minimized using MOPAC2016 (Stewart Computational Chemistry, Colorado Springs) (Stewart, 2016). Proposed reaction intermediates were docked into the VDS model using Autodock Vina v1.1.2 (The Scripps Research Institute, La Jolla, CA) (Trott & Olson, 2010). Images were made using PYMOL v1.8 (Delano Scientific, South San Francisco, CA) (Schrodinger, 2015).

### 2.2.2 Site-directed mutagenesis of VDS

Site-directed mutagenesis was carried out using a modified version of the QuikChange Lightning Site-Directed Mutagenesis Kit (Agilent) according to the manufacturer's instructions. In brief, PrimeSTAR® HS DNA Polymerase (Takara) was used in a "round-the-horn" *in vitro* PCR mutagenesis reaction (98° C for 2 min, 55° C for

15 s, 72° C for 7 min for 18 cycles; 72° C for 7 min final extension for 1 cycle). DpnI digestion of template plasmid and transformation into *E. coli* DH5 $\alpha$  competent cells were carried out per the manufacturer's protocols. All mutations were verified by single-pass DNA sequencing (UK HealthCare Genomics Laboratory). The template construct for all site-directed mutagenesis reactions was pET-28a(+)-VDS (NCBI Accession #AGB05610) as described previously (Yeo et al., 2013). Mutagenic primers are listed in **Table 2.1**.



**Table 2.1** VDS mutagenic primers, with mutated codon colored in red and underlined

Mutation	Direction	5' -Sequence- 3'
I307L	FWD REV	TCTCGTGCAAGAAAGATGTTTGTCAAAGTA <u>CTT</u> AATTTGACATCT ATGTGTCGTCTATGAGAGATGTCAAATT <u>AAG</u> TACTTTGACAAACA
T310A	FWD REV	AGAAAGATGTTTGTCAAAGTAATTAATTT <u>GGC</u> ATCTCTCATAGAC GTCATATGTGTCGTCTATGAGAGAT <u>GCC</u> AAATTAATTACTTTGAC
T310I	FWD REV	AGAAAGATGTTTGTCAAAGTAATTAATTT <u>GAT</u> ATCTCTCATAGAC GTCATATGTGTCGTCTATGAGAGAT <u>TAT</u> CAAATTAATTACTTTGAC
T310M	FWD REV	AGAAAGATGTTTGTCAAAGTAATTAATTT <u>GATG</u> TCTCTCATAGAC GTCATATGTGTCGTCTATGAGAGAT <u>CAT</u> CAAATTAATTACTTTGAC
T310S	FWD REV	AGAAAGATGTTTGTCAAAGTAATTAATTT <u>GTC</u> ATCTCTCATAGAC GTCATATGTGTCGTCTATGAGAGAT <u>GAC</u> AAATTAATTACTTTGAC
S311A	FWD REV	AAGATGTTTGTCAAAGTAATTAATTTGAC <u>AGCT</u> CATAGACGAC CATACGAGTCATATGTGTCGTCTATGAG <u>AGCT</u> GTCAAATTAATTA
S311I	FWD REV	AAGATGTTTGTCAAAGTAATTAATTTGACA <u>ATT</u> CATAGACGAC CATACGAGTCATATGTGTCGTCTATGAG <u>AATT</u> GTCAAATTAATTA
S311F	FWD REV	AAGATGTTTGTCAAAGTAATTAATTTGACAT <u>TCT</u> CATAGACGAC CATACGAGTCATATGTGTCGTCTATGAG <u>AGAT</u> GTCAAATTAATTA
S311T	FWD REV	AAGATGTTTGTCAAAGTAATTAATTTGACA <u>ACT</u> CATAGACGAC CATACGAGTCATATGTGTCGTCTATGAG <u>AGTT</u> GTCAAATTAATTA
C415A	FWD REV	ACGAGTATCTTAAAGTTGCATTGATATCA <u>GCT</u> GGTTATATGTTAC AATGAAATAGTTGAGAGTAACATATAACC <u>AGCT</u> TGATATCAATGCA
C415S	FWD REV	ACGAGTATCTTAAAGTTGCATTGATATCA <u>TCT</u> GGTTATATGTTAC AATGAAATAGTTGAGAGTAACATATAACC <u>AGAT</u> TGATATCAATGCA
C452A	FWD REV	ACGAATAACCCTTTGATTCTTATAGCCTCG <u>GCT</u> ACTATCAATAGA ACCTTATCATCCGCGAGTCTATTGATAGT <u>AGCC</u> GAGGCTATAAGA
N455A	FWD REV	CCTTTGATTCTTATAGCCTCGTGTACTATC <u>GCT</u> AGACTCGCGGAT CCAACCTTATCATCCGCGAGTCT <u>AGCG</u> GATAGTACACGAGGCTATA
N455C	FWD REV	CCTTTGATTCTTATAGCCTCGTGTACTATC <u>TGT</u> AGACTCGCGGAT CCAACCTTATCATCCGCGAGTCT <u>ACAG</u> GATAGTACACGAGGCTATA
N455S	FWD REV	CCTTTGATTCTTATAGCCTCGTGTACTATC <u>TCT</u> AGACTCGCGGAT CCAACCTTATCATCCGCGAGTCT <u>AGAG</u> GATAGTACACGAGGCTATA
N455T	FWD REV	CCTTTGATTCTTATAGCCTCGTGTACTATC <u>ACT</u> AGACTCGCGGAT CCAACCTTATCATCCGCGAGTCT <u>AGT</u> GATAGTACACGAGGCTATA
M531L	FWD REV	GCGGCCTCTTTATTTGGCATGCTTT <u>TG</u> AATGTATTCTACAAAGA ACCAATCTTCATCTTTGTAGAATACATT <u>CAAAA</u> AGCATGCCAAAT
M531V	FWD REV	GCGGCCTCTTTATTTGGCATGCTTT <u>GTG</u> AATGTATTCTACAAAGA ACCAATCTTCATCTTTGTAGAATACATT <u>CACAAA</u> AGCATGCCAAAT
Y535F	FWD REV	CCTCTTTATTTGGCATGCTTTATGAATGTATT <u>TTC</u> AAAGATGAA TTAGAGTGTGTGTACCAATCTTCATCTTTGAA <u>GAA</u> TACATTGATA

### 2.2.3 *In vivo* product analysis

Reaction products of mutant proteins were profiled via heterologous expression in BL21 (DE3) cells. Plasmids harboring the correct coding sequence for mutant enzymes were co-transformed into *E. coli* BL21(DE3) with pBbA5c-MevT(CO)-MBIS(CO,ispA) (obtained from Addgene, plasmid #35151) (Peralta-Yahya et al., 2011). Recombinant bacterial colonies were selected with kanamycin (25 µg/mL) and chloramphenicol (17.5 µg/mL) and 3 independent colonies from each plate were inoculated into 1 mL of 2xYT + 2 % glycerol liquid media with antibiotics and incubated at 37° C for 16-20 h with shaking. The next morning, cells from overnight seed culture were diluted into 10 mL of 2xYT + 2 % glycerol liquid media at an OD<sub>600</sub> = 0.05 supplemented with antibiotics and overlaid with 10 % n-dodecane. Shake flask fermentations were incubated at 37° C for 2 h before cooling the flasks at 4° C for 10 min. After addition of IPTG (Isopropyl β-D-1-thiogalactopyranoside) to 0.4 mM, the flasks were incubated at 28° C for an additional 20 h. The cultures were then centrifuged at 920g for 10 min and the dodecane overlay removed for GC-MS analysis. To ensure sufficient extraction (>80 %) of the total hydrophobic enzymatic products, optimization studies were conducted prior to this work in which a known concentration of hexadecane (a non-native enzymatic product) was spiked into the bacterial culture to measure the extraction efficiency with the dodecane overlay.

Aliquots of the dodecane overlay were analyzed on an Agilent 7890 GC (1:9 split injection; HP-5MS column, 30 m x 0.25 mm, 0.25 µm film, 250° C inlet temperature; oven temperature was 100° C initially, ramped to 140° C (10° C/min), then to 200° C (5° C/min), and finally increased to 300° C (120° C/min) and held for 5 min; 0.9 mL/min He flow rate)

connected to a 5975C Agilent Technologies mass spectrometer (run in positive ionization mode, 70 eV, scanning 40-500 amu). Sesquiterpene products were identified by comparison of mass spectra to authentic standards, matches to the NIST v2.0 library, and those reported by Yeo et. al. (Yeo et al., 2013) (**Figure 2.2**, **Figure 2.3**). The classified sesquiterpene products, whose peak areas were greater than or equal to 1 % of the total sesquiterpene peak areas, were quantified against known concentrations of  $\beta$ -caryophyllene, a bicyclic ring constrained sesquiterpene (Cai et al., 2002). The results from the detected and quantified sesquiterpene products are summarized in **Table 2.2** & **Table 2.3**.

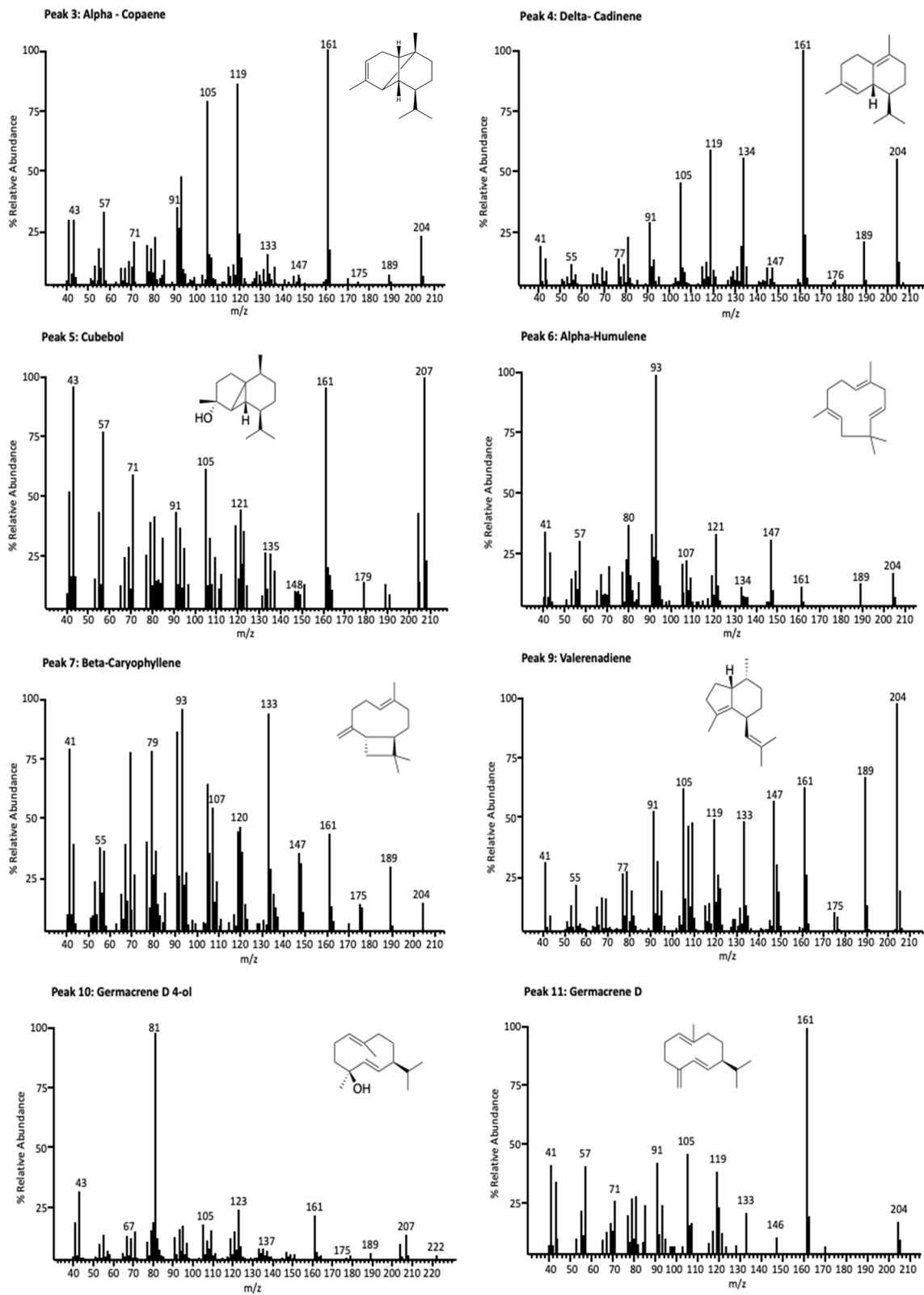


**Figure 2.2** EI-Mass spectra of sesquiterpenes detected from in vivo expression in *E. coli* BL21(DE3) cells of wildtype and mutant VDS enzymes.

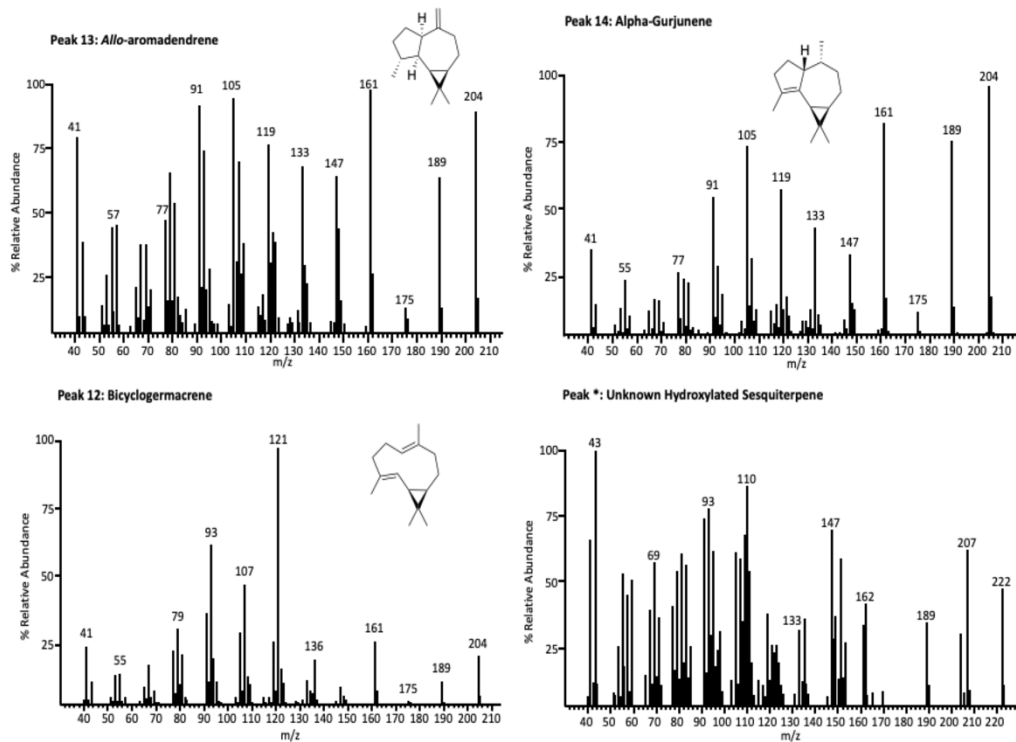


**Figure 2.3** (Figure 2.2 (con't)) EI-Mass spectra of sesquiterpenes detected from in vivo expression in *E. coli* BL21(DE3) cells of wildtype and mutant VDS enzymes.

#### 2.2.4 *In vitro* mutant expression for enzyme assays

Plasmids harboring wild type or mutant genes coding for VDS were expressed in BL21(DE3) cells as described above. Overnight, saturated cultures were inoculated into 2xYT + 2 % glycerol liquid media containing kanamycin (25 µg/mL) at an OD<sub>600</sub> equal to 0.05 and grown at 37° C until an OD<sub>600</sub> of 0.5 to 1.0. The cultures were then induced with 400 mM IPTG and incubated at 23° C for 20 h before collecting the cells at 6,000g for 10 min. The cell pellets were stored at -80° C until processed.

Cell pellets were lysed in 50 mM NaH<sub>2</sub>PO<sub>4</sub>, pH 7.4, 300 mM NaCl, 5 mM imidazole, and 5 % glycerol (v/v) by sonification (30 % power, 5 bursts, 20 s each, 1 min rest in between) using a QSonica® 500 equipped with a 1.6 mm probe. The cell debris was removed by centrifugation at 21,000g for 30 min at 4° C. Total protein concentrations were estimated by the Bradford assay (Bio-Rad) using bovine serum albumin as the standard.

#### 2.2.5 Steady-State Kinetic determinations

Michaelis-Menten kinetics were determined for each mutant enzyme and compared with wildtype using radiolabeled [1-<sup>3</sup>H] FPP (20 Ci mmol<sup>-1</sup>, American Radiolabeled Chemicals) under similar assay conditions as detailed in Yeo et. al. (Yeo et al., 2013). Briefly, 10 µL (1-3 µg/µL crude protein) of the cleared lysate was incubated with 1-60 µM [1-<sup>3</sup>H] FPP in a 50 µL total reaction volume for a 15 min reaction time at 37° C. Reactions were stopped with 50 µL of 2x Stop Buffer (0.4 M NaOH, 0.2 M EDTA) and the <sup>3</sup>H-labeled hydrocarbon products extracted with 200 µL n-hexanes. After a silica scrub of the hexane

extract to remove unreacted prenyl diphosphates and prenyl alcohols (Bell et al., 2014), aliquots were counted in a liquid scintillation counter. A crude lysate from bacteria transformed with the empty pET28(a)+ vector (Novagen) was used for background subtraction. Michaelis-Menten kinetic analysis was performed using GraphPad enzyme kinetic software v9 (San Diego, CA). Kinetic assays were performed in technical triplicate from a single transformed bacterial colony.

#### 2.2.6 *In Vitro* Product Analysis

For GC-MS profiling of wildtype and mutant enzymes, reactions were carried out as previously described by Yeo et. al. (Yeo et al., 2013), with a few modifications. Aliquots of the cleared bacterial lysate (1-3  $\mu\text{g}/\mu\text{L}$  total crude protein) were incubated with 230  $\mu\text{M}$  cold FPP in 250 mM Tris-HCL, pH 7.0, 50 mM  $\text{MgCl}_2$  (1 mL total reaction volume), overlaid with 1 mL n-hexanes at 37° C in 4 mL glass vials. After 16 h, 600  $\mu\text{L}$  aliquots of the organic overlay were carefully dried down under a gentle nitrogen stream while kept on ice. Concentrated samples were resuspended in n-hexanes and small volumes injected onto the GC-MS for profiling as described above.

#### 2.2.7 Immunodetection of VDS Enzymes

Expression levels of wildtype and mutant enzymes were determined by separating aliquots of soluble cleared *E. coli* lysates by SDS-PAGE under reducing conditions, as previously detailed in Bell et. al. (Bell et al., 2014). Proteins were transferred to a

nitrocellulose membrane, blocked with 5 % non-fat dry milk, and probed with a mouse monoclonal anti-polyHistidine antibody conjugated to alkaline phosphatase (Sigma Aldrich, Cat# A5588) according to the manufacturer's recommended protocol. Immobilized proteins were visualized by incubation with a working solution of 5-bromo-4-chloro-3-indoyl-phosphate (BCIP) and nitro blue tetrazolium (NBT) ("Rapid measurement of protein concentration by western analysis using colorimetric detection by bcip-nbt," 2006). Alkaline phosphatase detected VDS immune complexes were estimated using a purified wildtype enzyme standard curve and ImageJ software (**Figure 2.4**) (Schneider et al., 2012).



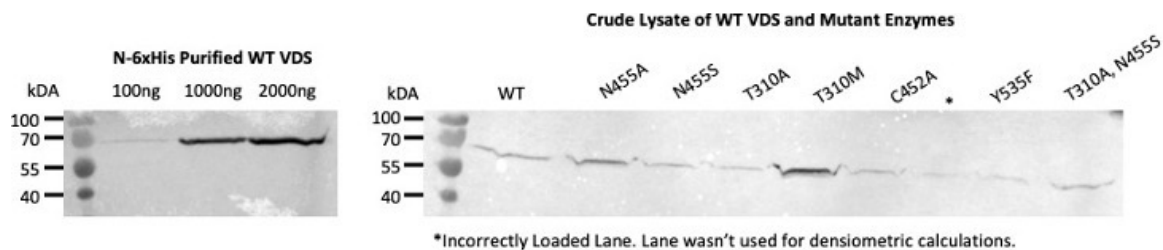


**Figure 2.4** Quantitation of wildtype and mutant VDS enzyme amounts in cell lysates. Cell lysates were prepared from *E. coli* cells induced for expression of the VDS or mutant genes and 20  $\mu$ g of total protein separated by SDS-PAGE prior to transferring to nitrocellulose (right panel). The blots were incubated with mouse polyclonal anti-polyHistidine antibody conjugated with alkaline phosphatase and immune complexes detected using colorimetric reactions with BCIP/NBT (5-bromo-4-chloro-3-indoyl-phosphate/nitro blue tetrazolium, respectively) as substrates. The immune complexes were captured using ImageJ software and quantification calculated against standard curves constructed using purified wild type VDS (left panel).

## 2.3 Results and Discussion

### 2.3.1 Building an Accurate 3D Structural Representation of VDS

To target amino acid residues within VDS which might govern product specificity, an energy-minimalized model of VDS was rendered upon the molecular coordinates of the TEAS-FHP-Mg<sup>2+</sup><sub>3</sub> complex (PDB: 5eat) (Starks et al., 1997) using MODELLER (Sali & Blundell, 1993) (**Figure 2.5, Panel A**). The VDS model exhibited the classical “terpene fold” consisting of  $\alpha$ -helices connected by loops and turns adopting the  $\alpha\beta$  domain architecture (**Figure 2.5, Panel A**) (Christianson, 2017; Lesburg et al., 1997; Starks et al., 1997). The active site cavity (shape analogous to a cylinder) measured approximately 14.1 Å tall (Trp286 to Asp318) by 10.9 Å wide (Ser311 to Asp539) (total volume of 1316 Å<sup>3</sup>) surrounded by predominantly non-polar amino acid residues, akin with previously crystallized sesquiterpene synthases (**Figure 2.5, Panel B**) (Lesburg et al., 1997; Starks et al., 1997; Tarshis et al., 1994). The model’s C $\alpha$ ’s deviated by 2.154 Å with 92 % of its atoms within 3.5 Å of their structural positions in TEAS (referred to as native overlap (Eramian et al., 2008)). Finally, we identified the evolutionarily conserved  $\alpha$ -helices in the COOH terminus through superimposition of the TEAS crystal structure (**Figure 2.5, Panel A**). Using the default scoring function of Autodock Vina (Trott & Olson, 2010), we anchored FPP (MOPAC energy-minimalized (Stewart, 2016)) into the VDS active site using the restricted search space of 1 Å spacing with a 15 Å grid box. We generated nine theoretical binding confirmations of FPP, all with similar binding energies (-7.7 to -7.9 kcal/mol). To visually determine the most reasonable spatial orientation of FPP, we aligned the TEAS-FHP-Mg<sup>2+</sup><sub>3</sub> complex with each of the VDS-FPP complex models for visual

inspection. Of the nine theoretical binding confirmations, one binding confirmation, #6, geometrically docked FPP in the characteristic “U” shape with the terminal pyrophosphate group anchored between the tri-nuclear magnesium cluster, angled towards the G1/G2 helix break (**Figure 2.6**). With our substrate docked in a feasible orientation and an accurate 3D molecular model of VDS, we set out to establish the amino acid residues forming the active site topography. Through a cavity detection radius constrained to 7 Å and cavity detection cutoff at three solvent radii, we identified twenty-four residues which formed the solvent inaccessible active site shell, structurally poised to influence the catalytic trajectory of VDS (**Figure 2.5, Panel B**).

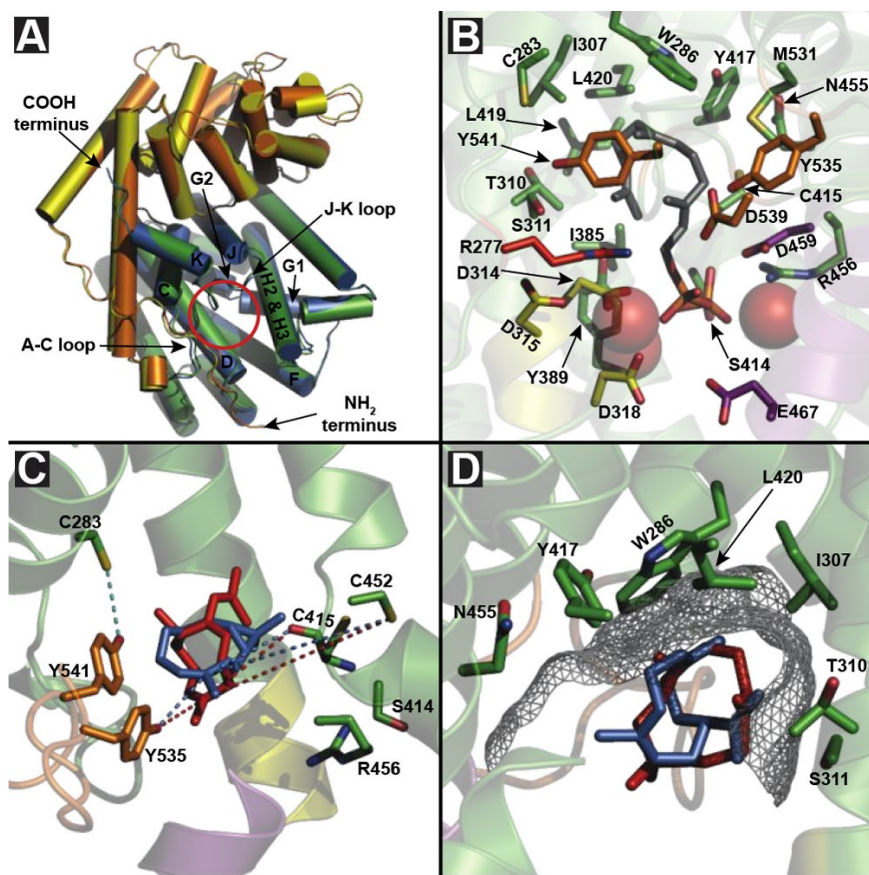


**Figure 2.5** (A). *In silico* 3D structural superimposition of energy minimized VDS tertiary model (NH<sub>2</sub> terminus - orange rods; COOH terminus - green rods; GenBank: AGB05610 (Yeo et al., 2013)) and the template crystal structure TEAS (NH<sub>2</sub> terminal residues - yellow rods; COOH terminal residues - blue rods; PDB:5EAT) (Starks et al., 1997). Red circle highlights VDS' proposed catalytic pocket. (B). VDS' active site cavity complexed with Mg<sup>2+</sup><sub>3</sub>-FPP (Mg<sup>2+</sup><sub>3</sub> atoms (red spheres); FPP carbon atoms (gray), phosphorous atoms (orange), and oxygen atoms (red)); "DDXXD" and "NSE/DTE" metal-binding domains are colored in yellow and purple, respectively; J-K and A-C loops are colored in orange and red, respectively). (C). Snapshot of proposed H<sup>+</sup> donor residues within VDS interacting with **9** (blue sticks) and **13** (red sticks) and other active site residues. Tyr535's -OH group (J-K loop) is 3.8 Å (blue dotted line) and 4.3 Å (red dotted line) from C7 on **9** and **13**, respectively. Cys452's SH group (H2/3 helix) is 10.5 Å (blue dotted line) and 11.9 Å (red dotted line) from C7 on **9** and **13**, respectively. Cys415's carbonyl group is approximately 5.0 Å (blue dotted line) and 5.8 Å (red dotted line) from C7 on **9** and **13**, respectively. (D). Back side view of VDS displaying the influence on active site topology (grey meshwork) by select residues flanking the two metal-binding domains resulting in either the 1,10 or 1,11 initial ring closures of **1** (1,10 forms **3** - blue; 1,11 forms **4** - red). Trp286 (C helix), Ile307 (D helix), Tyr417 (G2 helix), and Leu420 (G2 helix) form the bottom of the active site cavity. Asn455 is structurally aimed at C1 on **4**, while Thr310 and Ser311 (D helix) are poised at C12,13 on **3**.

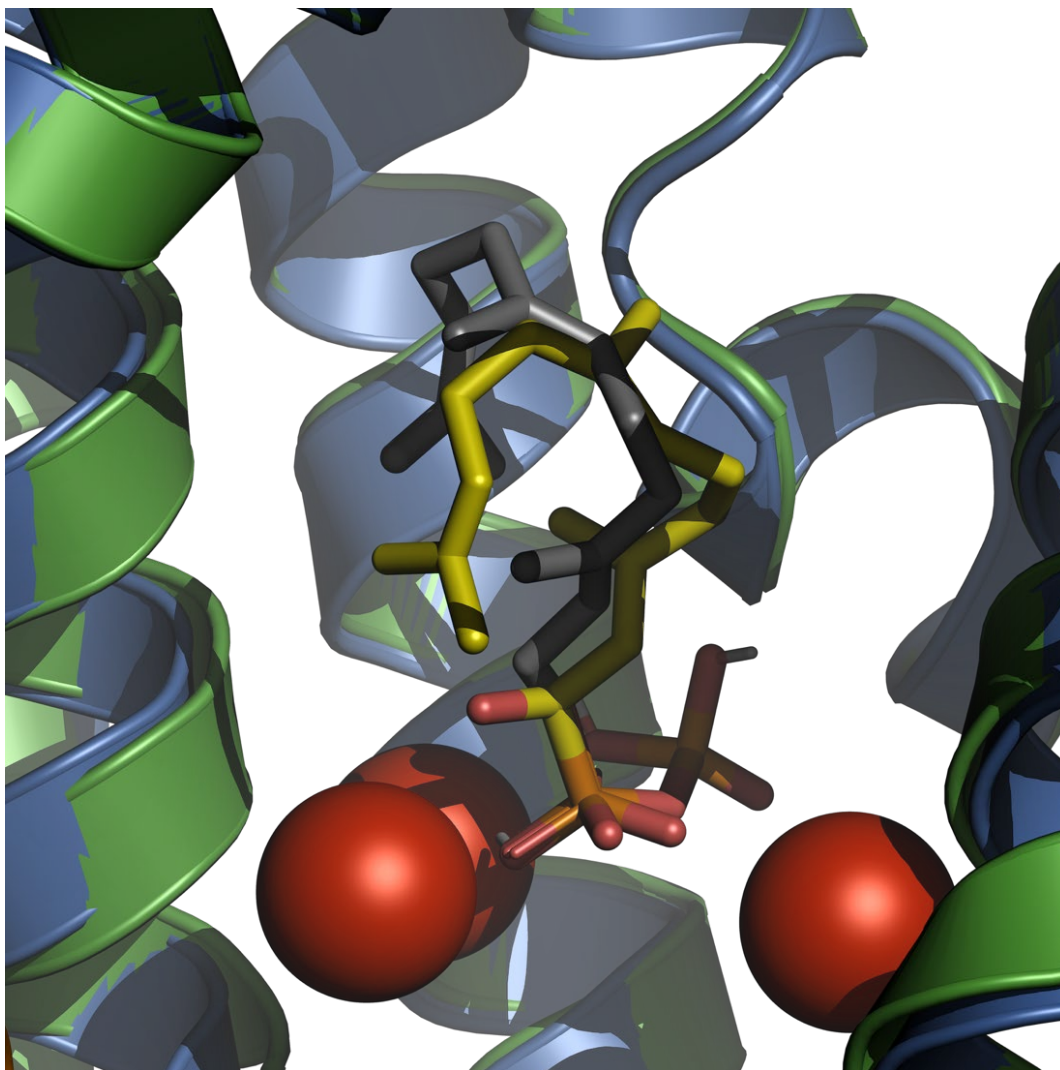


**Figure 2.6** Superimposition of the TEAS-FHP ribbon structure (blue) (PDB 5EAT) (Starks et al., 1997) onto the selected energy-minimized VDS-FPP model (green) generated with Modeller (Sali & Blundell, 1993) and Autodock Vina (Trott & Olson, 2010) programs. The overlay image of the TEAS-FHP and VDS-FPP structures was made using PYMOL v1.8 (Delano Scientific, South San Francisco, CA) (Schrodinger, 2015). Note the close overlap between FHP (yellow) and FPP (grey), the “U” shape of both, and the juxtaposition of C10 and C11 in proximity to the initial carbocation that will be generated at C1. The three magnesium ions (red spheres) are located near the entrance to TEAS’ active site poised to ionize the phosphate group on FHP, thus initiating the catalytic cascade.

### 2.3.2 Selection Criteria for Candidate Residues

Recognizing terpene product specificity is predominantly determined by those residues lining the active site, we chose to restrict our candidate selection to primarily 1<sup>st</sup> tier residues identified by our contact map strategy (**Figure 2.5, Panel B**). (Greenhagen et al., 2006; Yoshikuni, Ferrin, et al., 2006) Several residues classified as 1<sup>st</sup> tier residues with well-documented catalytic roles in sesquiterpene synthases were excluded from consideration because of their essential contributions to the general catalytic process (**Figure 2.5, Panel B**): Arg277 conserved among all terpene synthases and necessary for offsetting the negative charge from the ionized pyrophosphate group of FPP (Starks et al., 1997); Trp286 is responsible for active site contour and stabilization of carbocation intermediates through  $\pi$ -cation interactions (Christianson, 2017); Asp314 part of class I terpene synthase conserved metal binding domain (DDXXD motif) which is necessary for Mg<sup>2+</sup> coordination and catalysis (Kersten et al., 2015); Asp459 part of class I terpene synthase 2<sup>nd</sup> metal binding domain triad (NSE/DTE motif) necessary for the Mg<sup>2+</sup> coordination and catalysis (Aaron & Christianson, 2010) (**Figure 2.5, Panel B**).

Instead, we focused on residues inferred to be associated with two other biochemical and structural criteria: 1) residues with the capability of initiating the second half reaction of VDS's catalytic cascade via donation of a proton across a double bond; and 2) residues surrounding the metal binding domains that could restrict substrate binding confirmations. Previously, our group postulated cysteine and tyrosine residues, structurally aligned to interact with the substrate, are capable of acting as catalytic acids through the donation of a proton from their hydroxyl or thiol side chains to re-initiate the catalytic cascade at a stable reaction intermediate (Greenhagen, 2003). This was further supported by site-

directed mutagenesis studies, which demonstrated that a loss of the residue's proton donor functional group halted the catalytic cascade at a neutral reaction intermediate limiting continuation of the cyclization cascade to the final hydrocarbon product (Greenhagen, 2003; Rising et al., 2000). With this rationale, we sought to map the potential proton donor amino acid residues within VDS. From our contact map, we identified residues Cys415 (G1/G2 helix break), Cys452 (H helix) and Tyr535 (J/K loop) as potential proton donor candidates warranting further investigation (**Figure 2.5, Panel B**).

Several research groups have found that while mutating residues within the metal binding domains of terpene synthases often leads to loss of enzyme activity, targeting the residues just outside these domains diversify the product specificity (Abdallah et al., 2018; Fang et al., 2017; Rynkiewicz et al., 2002; Salmon et al., 2015; Yoshikuni, Martin, et al., 2006). When we compared the locations of the 1<sup>st</sup> tier residues with respect to VDS' two metal binding domains (D<sup>314</sup> DTYD<sup>318</sup> & D<sup>459</sup> GE<sup>467</sup>), we selected Ile307, Thr310, Ser311 and Asn455 as potential candidates which look to restrict FPP's binding confirmation through hydrogen bonding, van der Waals interactions, and substrate steric hinderance, thus poised to directly influence the catalytic outcome. From our 3D homology model, we noticed these residues appear to exert the greatest regio- and stereo-chemical control over FPP binding conformations, making them prime candidates for our site-directed mutagenesis study (**Figure 2.5, Panel B**).

```

275          286 307          318 385 389 413 420 452 456 459          467 531 535 539 541
AaADS  CLRDRIVECYFW--VAVITLIDDTYD---F---L---TGGANLL---GILGR--NDLMTHKAE---L---Y---DNF
AaBFS  YVRDRVVEGYFW--CMWLVLVDDTYD---E---T---TGTYGLM---CVIVR--DDIVSHKEE---C---Y---DGF
AaBCS  YARDRMVECYFW--ISLATVLDDTYD---F---Y---SSGYSML---CAIAR--DDIHSQKEE---M---Y---DGF
GaDCS  YARDRVVEGYFW--IAMASIVDDTYD---L---Y---TCGYAML---TII CR--DDVAEHKFK---M---Y---DGY
NtEAS  YARDRVVECYFW--ISMISIVDDTYD---V---Y---TTTTYYL---VIICR--DDTATYEVE---V---Y---DGY
ObGDS  FARDRVVECYFW--IAMTSIIDDTYD---L---Y---SGAYMML---SVICR--DDVVGHGIE---I---Y---DSY
PdBCGS YARDRIVETYFW--QSLFSIIDDTYD---L---Y---TCGYTSL---LTINR--DDIVGHED E---I---Y---DWY
ScGAS  YVRDRLVELYFW--IKMAAILDDTYD---L---Y---TGGYKML---SDISR--NDIVGHKEE---M---Y---DNL
VoVDS  YARDRFVECYFW--INLTSIIDDTYD---I---Y---SCGYMLL---CTINR--DDKVGHELE---M---Y---DWY
ZmACS  YGRDRIVECYFW--IMLASLLDDTYD---L---Y---SAGIQVL---AEVTR--DDMADFRRG---M---F---DRY

```

**Figure 2.7** Alignment of amino acid residues mutated within VDS and representative class I sesquiterpene synthases. The “DDXXD” and “NSE/DTE” metal binding domains are highlighted in gray. The numbering corresponds to the amino acid positions within VDS. Alignments were performed with the Multiple Sequence Comparison by Log-Expectation (MUSCLE) alignment package (v3.8.31) within the MacVector software program (version 18.1.5), and the C-terminal domains of AaADS: *Artemisia annua* amorpho-4,11-diene synthase (GenBank: AAF61439); AaBFS: *Artemisia annua* beta-farnesene synthase (GenBank: AAX39387); AaBCS: *Artemisia annua* beta-caryophyllene synthase (GenBank: AAL79181); GaDCS: *Gossypium arboretum* delta-cadinene synthase (GenBank: AAA93065); NtEAS: *Nicotiana tabacum* 5-epi-aristolochene synthase (GenBank: AAA19216); ObGDS: *Ocimum basilicum* germacrene-D synthase (GenBank: AAV63786); PdBCGS: *Phyla dulcis* bicyclogermacrene synthase (GenBank: AFR23369); ScGAS: *Solidago canadensis* germacrene-A synthase (GenBank: CAC36896); VoVDS: *Valeriana officinalis* valerena-1,10-diene synthase (GenBank: AGB05610); ZmACS: *Zea mays* alpha-copaene synthase (GenBank: AAX99148).



### 2.3.3 Evaluation Procedure for Candidate Residues

We utilized a well-documented *in vivo* terpene screening platform (Bell et al., 2014; Nybo et al., 2017) to detect and quantify the various sesquiterpene reaction products generated by the 1<sup>st</sup> tier residue mutants while expressed in a living host cell. Briefly, expression plasmids with the mutant VDS genes were transformed into *E. coli* cells and incubated for 24 h with a n-dodecane overlay designed to “capture” the hydrophobic, volatile reaction products. At 24 h, small aliquots (1  $\mu$ L) of the dodecane layer were injected onto a GC-MS for product detection, identification (**Figure 2.2** & **Figure 2.3**) and quantification (**Table 2.2**). We evaluated each mutant’s ability to alter VDS’ product specificity by comparing the percent change in the sesquiterpene product distribution compared with wildtype VDS’ percent reaction product distribution, providing a relative measure of the mutant’s activity compared with wildtype. Mutants which were active and demonstrated at least a 10 % shift from VLD (**17**) (66 % of the wildtype’s sesquiterpene products) were considered for further enzyme characterization. Results from all the mutants evaluated in this work are shown in **Table 2.2**. For the mutants which met our criteria in the *in vivo* screen, we confirmed their reaction products by a secondary *in vitro* product profile assay, using the cleared crude lysate from freshly transformed *E. coli* cells as our source of enzyme. Results from the *in vitro* reactions are summarized in **Table 2.3** and generally agree with our *in vivo* results **Table 2.2**. However, it should be noted discrepancies in the percent product distributions between our *in vivo* and *in vitro* reactions are likely attributed to the presence of various TPS conformers present in the *in vivo* assay yet absent in our *in vitro* reactions. This is directly correlated to the *E. coli* cell’s protein degradation pathways (Sauer & Baker, 2011). Finally, we characterized each mutants’

steady-state kinetic parameters using a radiolabeled [1-<sup>3</sup>H] FPP assay (1-60 μM) (Figure 2.8). We chose to use the crude cleared lysate as our enzyme source for the kinetic assays due to the potential loss of catalytic activity during the purification process (Bell et al., 2014). For validation of our experimental accuracy, we compared the crude lysate of wildtype VDS against the purified wildtype VDS's kinetic parameters and observed no significant difference in their  $K_M$  (μM) values (20.1 vs. 29.8 μM clarified lysate and column purified, respectively), but approximately a 50 % reduction in the purified enzyme's turnover rate,  $k_{cat}$  (s<sup>-1</sup>), (0.018 vs. 0.009 s<sup>-1</sup> clarified lysate and column purified, respectively, **Figure 2.9**). For  $k_{cat}$  determinations, we calculated each mutant's concentration in pmoles within the crude lysate with reference to a standard curve constructed with purified VDS detected by immunodetection against their N-terminal polyHistidine tag (**Figure 2.4**). Although the *in vitro* assays were incubated for 16 h, shorter incubation periods gave similar product profiles, only with less total product yield (**Figure 2.10**).

**Table 2.2** Comparison of the *In Vivo* Reaction Products from WT and Mutant VDS Enzymes

	Amino Acid Position in VDS								In Vivo % Product Distributions & Total Sesquiterpene Productivity													
	307	310	311	415	452	455	531	535	5 <sup>c</sup>	7 <sup>d</sup>	8 <sup>d</sup>	Unk <sup>f</sup>	9 <sup>c</sup>	10 <sup>d</sup>	11 <sup>c</sup>	12 <sup>d</sup>	14 <sup>d</sup>	15 <sup>d</sup>	16 <sup>d</sup>	17 <sup>c,e</sup>	Total <sup>g</sup>	
WT	I	T	S	C	C	N	M	Y		tr. <sup>b</sup>		tr. <sup>b</sup>	29	5							66	1.96
I307L	L	T	S	C	C	N	M	Y					69	17							14	
T310A	I	A	S	C	M	N	M	Y		tr. <sup>b</sup>		tr. <sup>b</sup>	40	4							56	1.76
T310I	I	I	S	C	M	N	M	Y					62	13		tr. <sup>b</sup>					25	
T310M	I	M	S	C	M	N	M	Y		3			61	3		27					6	1.16
T310S	I	S	S	C	C	N	M	Y				tr. <sup>b</sup>		tr. <sup>b</sup>							tr. <sup>b</sup>	
S311A <sup>a</sup>	I	T	A	C	C	N	M	Y														
S311I <sup>a</sup>	I	T	I	C	C	N	M	Y														
S311F <sup>a</sup>	I	T	F	C	C	N	M	Y														
S311T <sup>a</sup>	I	T	T	C	C	N	M	Y														
C415A	I	T	S	A	C	N	M	Y					51	12							37	
C415S	I	T	S	S	C	N	M	Y					51	tr. <sup>b</sup>							49	
C452A	I	T	S	C	A	N	M	Y		tr. <sup>b</sup>		tr. <sup>b</sup>	65	4							31	1.96
N455A	I	T	S	C	C	A	M	Y	tr. <sup>b</sup>	41	tr. <sup>b</sup>			tr. <sup>b</sup>	11		13	31	3	tr. <sup>b</sup>	0.63	
N455C	I	T	S	C	C	C	M	Y		65		6		22	tr. <sup>b</sup>		tr. <sup>b</sup>			7		
N455S	I	T	S	C	C	S	M	Y	4	51	5			tr. <sup>b</sup>	10		12	14	3	tr. <sup>b</sup>	0.63	
N455T	I	T	S	C	C	T	M	Y		80	10	tr. <sup>b</sup>		tr. <sup>b</sup>	tr. <sup>b</sup>		10			tr. <sup>b</sup>		
M2	I	A	S	C	C	S	M	Y	6	48	12			tr. <sup>b</sup>	18		5	12	tr. <sup>b</sup>	tr. <sup>b</sup>	0.85	
M531L	I	T	S	C	C	N	L	Y				86									14	
M531V	I	T	S	C	C	N	V	Y				73		tr. <sup>b</sup>							27	
Y535F	I	T	S	C	C	N	M	F					100								0.48	

Product distributions were calculated as percentages of individual peak areas in relation to the total peak areas and quantified relative to a caryophyllene standard. <sup>g</sup>The total sesquiterpene productivity (Total) was calculated by averaging the individual sesquiterpene productivities (mg/L/OD<sub>600</sub>) from three independent bacterial cultures measured after 24 h of aerobic fermentation at 28° C and is reported for only select mutants. The gold and light blue shadings signify codon mutations to neutral or proton donor amino acid residues, respectively. Colored product numbers correspond to their structural assignment and catalytic cascade cation route (germacrenyl (red), humulyl (blue), and helmintogermacrenyl (green)) in **Figure 2.1**. <sup>a</sup>No detected sesquiterpene products; below GC-MS limit of detection. <sup>b</sup>Trace amounts (tr.) represent less than 1% of the detectable reaction products. Product identifications are based upon comparisons to <sup>c</sup>authentic standards, <sup>d</sup>mass spectral comparisons found in the NIST library 2.0, or those reported by <sup>e</sup>Yeo et al. (Yeo et al., 2013). <sup>f</sup>Mass spectrum of unknown sesquiterpene alcohol (Unk) can be found in **Figure 2.3**.

**Table 2.3** Steady-State Kinetic Parameters and *In Vitro* Product Distributions (%) by WT and Mutant VDS Enzymes

	Steady-State Kinetic Parameters			<i>In Vitro</i> Product Distribution (%)												
	$K_M$ ( $\mu\text{M}$ )	$k_{\text{cat}}$ ( $\text{sec}^{-1}$ )	$k_{\text{cat}}/K_M$ ( $\mu\text{M}^{-1}\text{s}^{-1}$ )	5 <sup>b</sup>	7 <sup>c</sup>	8 <sup>c</sup>	Unk <sup>e</sup>	9 <sup>b</sup>	10 <sup>c</sup>	11 <sup>b</sup>	12 <sup>c</sup>	14 <sup>c</sup>	15 <sup>c</sup>	16 <sup>c</sup>	17 <sup>b,d</sup>	
WT	20.1 ± 7.8	0.018 ± 0.003	8.96 X 10 <sup>-4</sup>	5			22	28	tr. <sup>a</sup>							44
T310A	12.4 ± 4.2	0.007 ± 0.001	5.65 X 10 <sup>-4</sup>	9			12	39	tr. <sup>a</sup>							35
T310M	22.8 ± 11.3	0.002 ± 0.0003**	8.77 X 10 <sup>-5</sup>	23				55	tr. <sup>a</sup>		19					4
C452A	20.7 ± 9.5	0.038 ± 0.008**	18.4 X 10 <sup>-4</sup>	6			11	63	tr. <sup>a</sup>							20
Y535F	9.35 ± 2.75	0.005 ± 0.0004*	5.35 X 10 <sup>-4</sup>	8				92								
N455A	6.79 ± 2.04	0.020 ± 0.0002**	2.95 X 10 <sup>-4</sup>	90	tr. <sup>a</sup>					tr. <sup>a</sup>		tr. <sup>a</sup>	tr. <sup>a</sup>		10	
N455S	10.6 ± 4.3	0.007 ± 0.001	6.60 X 10 <sup>-4</sup>	91	tr. <sup>a</sup>					tr. <sup>a</sup>		tr. <sup>a</sup>	tr. <sup>a</sup>		9	
N455S, T310A	20.8 ± 6.08	0.007 ± 0.0007	3.37 X 10 <sup>-4</sup>	93	tr. <sup>a</sup>					tr. <sup>a</sup>		tr. <sup>a</sup>	tr. <sup>a</sup>		7	

Colored product numbers correspond to their structural assignment and catalytic cascade cation route (germacrenyl (red), humulyl (blue), and helmintogermacrenyl (green)) in **Figure 2.1**. <sup>a</sup>Trace amounts (tr.) represent less than 1% of the detectable reaction products. Product identifications are based upon comparisons to <sup>b</sup>authentic standards, or <sup>c</sup>mass spectral comparisons found in the NIST library v2.0, or those reported by <sup>d</sup>Yeo et al. (Yeo et al., 2013) <sup>e</sup>Mass spectrum of the unknown sesquiterpene alcohol (Unk) can be found in **Figure 2.3**. Error bars ±SEM. One-way ANOVA using Dunnett’s multiple comparisons was performed to determine the statistical differences between the observed WT’s  $K_M$ ,  $k_{\text{cat}}$ , &  $k_{\text{cat}}/K_M$  to those of the mutants. \*P < 0.05, \*\*P < 0.005.

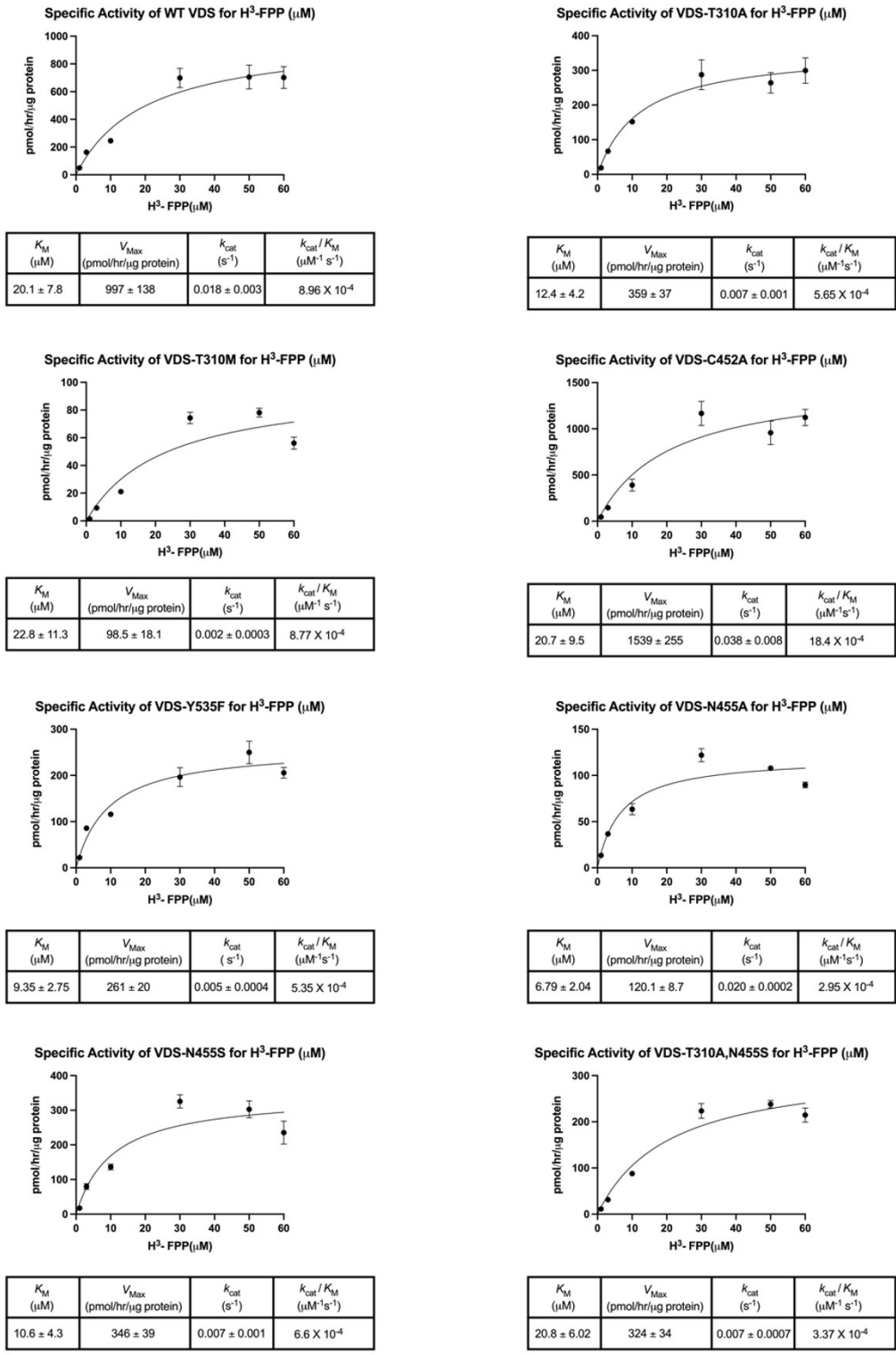
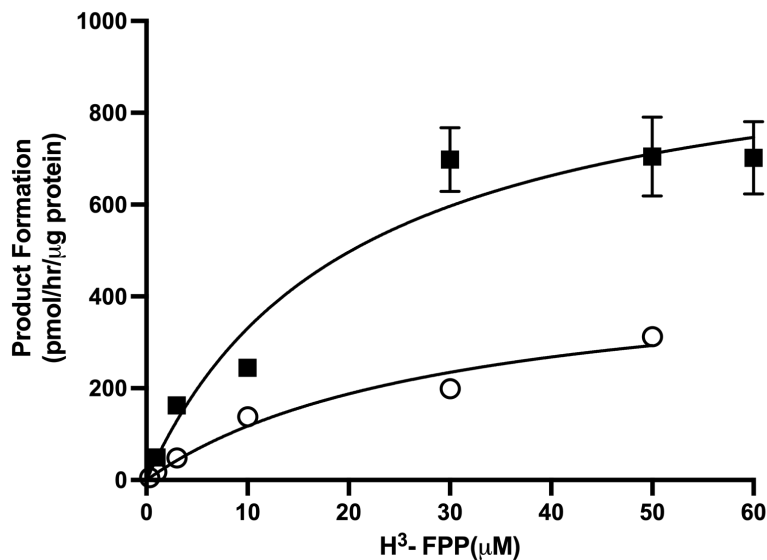


**Figure 2.8** Michaelis-Menten plots of wild type and mutant VDS enzymes. Crude lysates were used as enzyme source and the amount of VDS protein in each was calculated from their immune detection as noted in **Figure 2.4**.



Symbol	Enzyme Preparation	$K_M$ ( $\mu\text{M} \pm \text{SEM}$ )	$V_{\text{Max}}$ ( $\text{pmol/hr}/\mu\text{g}$ protein $\pm \text{SEM}$ )	$k_{\text{cat}}$ ( $\text{s}^{-1} \pm \text{SEM}$ )	$k_{\text{cat}}/K_M$ ( $\text{M}^{-1} \text{s}^{-1} \pm \text{SEM}$ )
■	Clarified Lysate	$20.1 \pm 7.8$	$997 \pm 138$	$0.018 \pm 0.003$	$896 \pm 385$
○	Column Purified	$29.8 \pm 9.4$	$468 \pm 70$	$0.009 \pm 0.001$	$302 \pm 106$

**Figure 2.9** Comparison of steady-state kinetics of wild type VDS from clarified bacteria lysate (squares) and his-tagged column purified wildtype VDS (circles). VDS protein amounts were quantified for the clarified lysate as in **Figure 2.4** and for the purified VDS using the Bradford assay. The purified protein gave a single protein as evident from Coomassie Blue stained PAGE (data not shown), while the VDS protein in the clarified lysate was evident amongst many other soluble proteins.

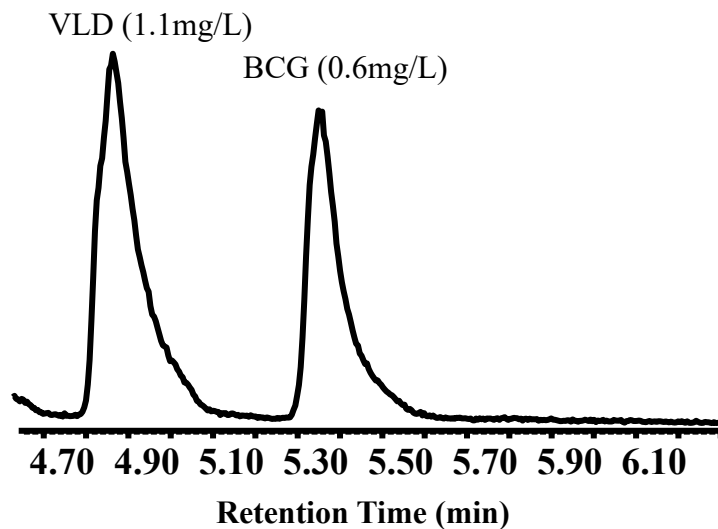


**Figure 2.10** GC chromatogram of the detected hydrocarbon products from a single *in vitro* reaction with 100-500 ng of purified VDS and 10  $\mu$ M FPP incubated for 2 h at room temperature overlaid with n-hexanes, as detailed in Yeo et. al. (Yeo et al., 2013). Valerena-1,10-diene (VLD) and bicyclogermacrene (BCG) productivities were estimated with a caryophyllene external standard. Note, ~60 % VLD's and ~30 % BCG's percent product distribution is consistent with the results listed in **Table 2.2** & **Table 2.3** for wildtype VDS' product distribution profile, observed at 16 and 24 h, respectively.

### 2.3.4 Tyr535 is likely the proton donor in VDS

Following the same biochemical rationale as Rising et. al. (Rising et al., 2000), we mutated Tyr535 (J/K loop, 4.3 or 3.8 Å from C7 of either **9** or **13**, respectively) to a phenylalanine residue (**Figure 2.5, Panel C**). This afforded us the ability to maintain the spatial geometry previously provided by the tyrosine residue in the active site, all the while removing any potential contribution of a proton donation into the active site matrix. From our modeling and previous terpene mechanism studies, we hypothesized this mutation would halt the cyclization cascade at one of the proposed stable intermediates within VLD's catalytic cascade (**9** or **13, Figure 2.1**) (Rising et al., 2000). From our *in vivo* assay, we detected bicyclogermacrene (**9**), identified by its mass fragmentation pattern compared to an authentic standard provided by F. Bohlmann (Jakupovic et al., 1987) (**Figure 2.11**), as 100 % of the reaction products (**Table 2.2**). This is a significant shift from wildtype VDS' product distribution percentages which naturally produces 66 % of **17**, 5 % of **10** and 29 % of **9** (**Table 2.2, Figure 2.10**). *In vitro*, Y535F's substrate affinity constant,  $K_M$ , improved to half of that for wildtype VDS (9.35 vs. 20.1  $\mu\text{M}$ ), while its turnover rate,  $k_{\text{cat}}$ , decreased about 3-fold (0.005 vs. 0.018  $\text{s}^{-1}$ ) and its overall catalytic efficiency ( $k_{\text{cat}}/K_M$ ) decreased to ~60 % of that relative to the wild type VDS (**Table 2.3**).

Could **9** be the neutral stable intermediate in VLD's catalytic cascade? According to Paknikar et. al. (Paknikar et al., 2013), it is conceivable to propose Tyr535 reprotonates C7 of **9**. Thus, allowing the concomitant formation of the aromadenrenyl-like cation and permitting the catalytic cascade to continue onto **17**. However, such a conclusion is tempered by the conservation of Tyr535 amongst other sesquiterpene synthases, including a bicyclogermacrene synthase (*PdBCGS*) in **Figure 2.7** (Attia et al., 2012; Bennett et al.,



2002; Bouwmeester et al., 2002; Cai et al., 2002; Chen et al., 1996; Iijima et al., 2004; Starks et al., 1997; van Der Hoeven et al., 2000). If Tyr535 is the Brønsted acid in VDS' active site which re-initiates the catalytic cascade, then it might be a unique feature of VDS and not serve such a role in other bicyclogermacrene synthases. Additionally, our previous efforts to elucidate putative VDS's reaction intermediates using  $^{13}\text{C}$  labeling revealed the biogenic origin of VLD's unique isobutenyl tail likely arose from formation of a C1 to C11 bond, which could proceed through a caryophyllenyl carbocation intermediate or the germacrene cation intermediate as suggested by Paknikar et al. (Paknikar et al., 2013) (**Figure 2.1, Figure 2.13**) (Yeo et al., 2013). The involvement of a caryophyllenyl intermediate in the biogenesis of sesquiterpenes containing this enigmatic isobutenyl side chain was first proposed by Connolly et al. (Connolly et al., 1984) studying unique sesquiterpene carbon structures isolated from liverworts. Conversely, **9**'s biogenic carbon skeleton arises from the initial C1 to C10 bond formation from the all trans-farnesyl carbocation (**1**). This is subsequently followed by concomitant deprotonation at C1 of the germacrene cation intermediate (**3**) leading to bond formation between C1 and C11 and yielding the bicyclogermacrene (**9**) intermediate (**Figure 2.1**) (S. Garms et al., 2010). According to the mechanistic model of Paknikar et al. (Paknikar et al., 2013), **17** can form from the bicyclogermacrene intermediate via an energetically unfavorable cyclopropylcarbinylation- cyclopropylcarbinylation rearrangement (CCR), a mechanism utilized by eukaryotes in the biosynthesis of triterpenoids, and useful in medicinal and industrial applications (Blagg et al., 2002; Kempinski & Chappell, 2019; Kempinski et al., 2019; Niehaus et al., 2011). This model is also consistent with the  $^{13}\text{C}$  labeling studies of Yeo et al. (Yeo et al., 2013) (**Figure 2.13**). Taken all together, VDS appears to be a

promiscuous enzyme which generates multiple reaction products, a precedent reported for many other terpene synthases (S. Garms et al., 2010; Vattekkatte et al., 2017; Yoshikuni, Ferrin, et al., 2006). And, the results from the Y535F mutation suggest that Y535 might indeed be responsible for initiating proton donation to the bicyclogermacrene intermediate, leading to the CCR (Poulter & Rilling, 1978) and formation of **17** as the final reaction product. Also arguing for the germacreanyl cation pathway for the biosynthesis of **17** is that no mutants yielding significant amounts of alpha-humulene (**5**) or beta-caryophyllene (**11**) were uncovered. While such a negative result cannot be taken as conclusive evidence that the humulyl cation pathway for the biosynthesis of **17** doesn't exist in VDS, the Y535F mutant is fully consistent with the importance of the germacreanyl cation in the biosynthesis of VLD (**17**).

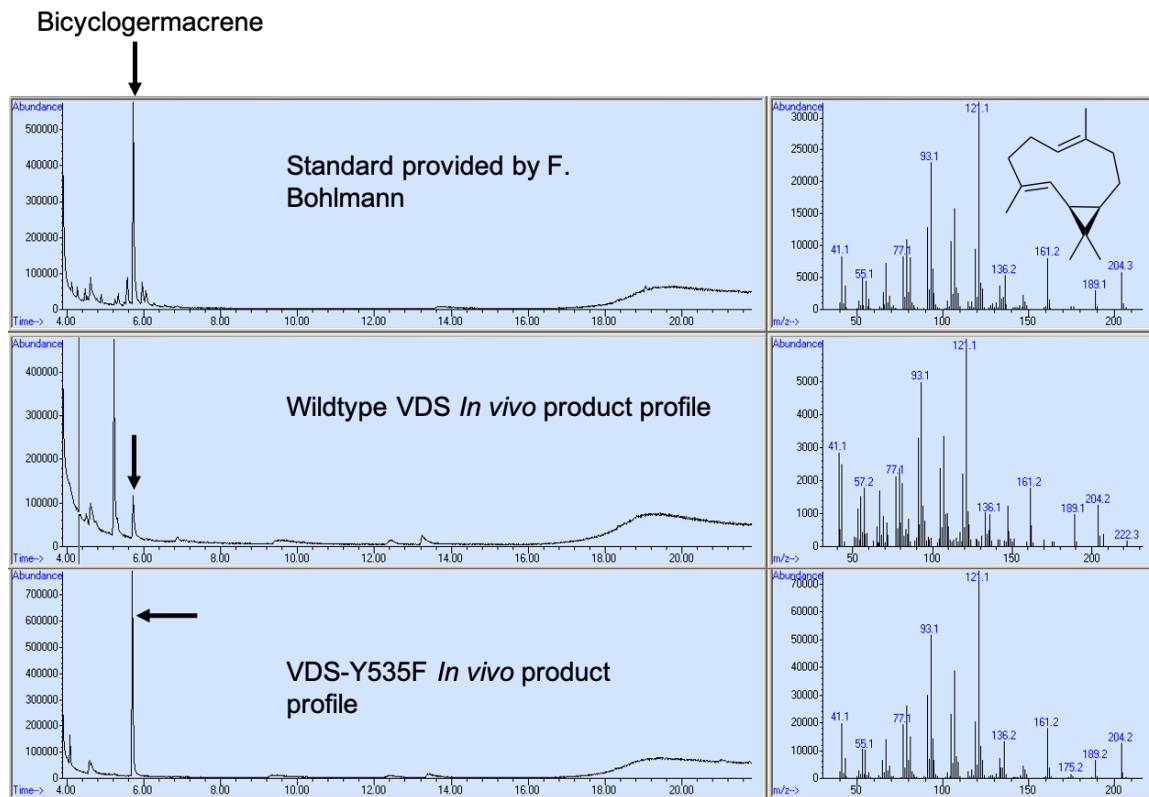


**Figure 2.11** GC-MS comparisons of bicyclogermacrene (9) standard from Jakupovic et. al. (Jakupovic et al., 1987) with the extracted chemistries from *E. coli* transformed with the Y535F mutant.

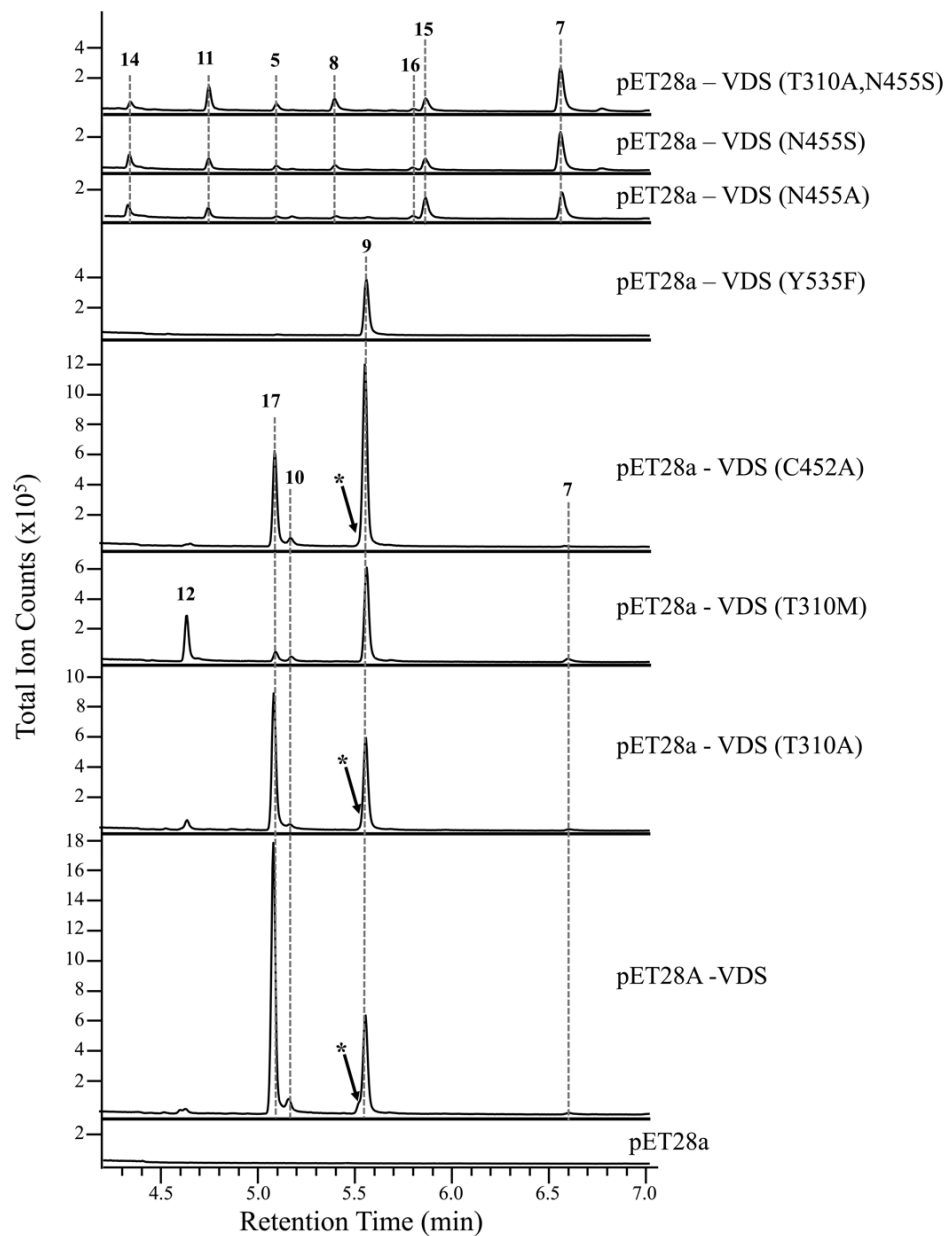


**Figure 2.12** Metabolite comparisons of *E. coli* cells expressing either wildtype VDS, mutant, or empty vector plasmids. Aliquots of a dodecane overlay are compared by GC. Gray dashed lines indicate products that accumulate in common amongst bacterial lines. Peak numbers correspond to the assigned reaction products in **Figure 2.1**. \*Peak of an unknown sesquiterpene alcohol that co-elutes with 9.

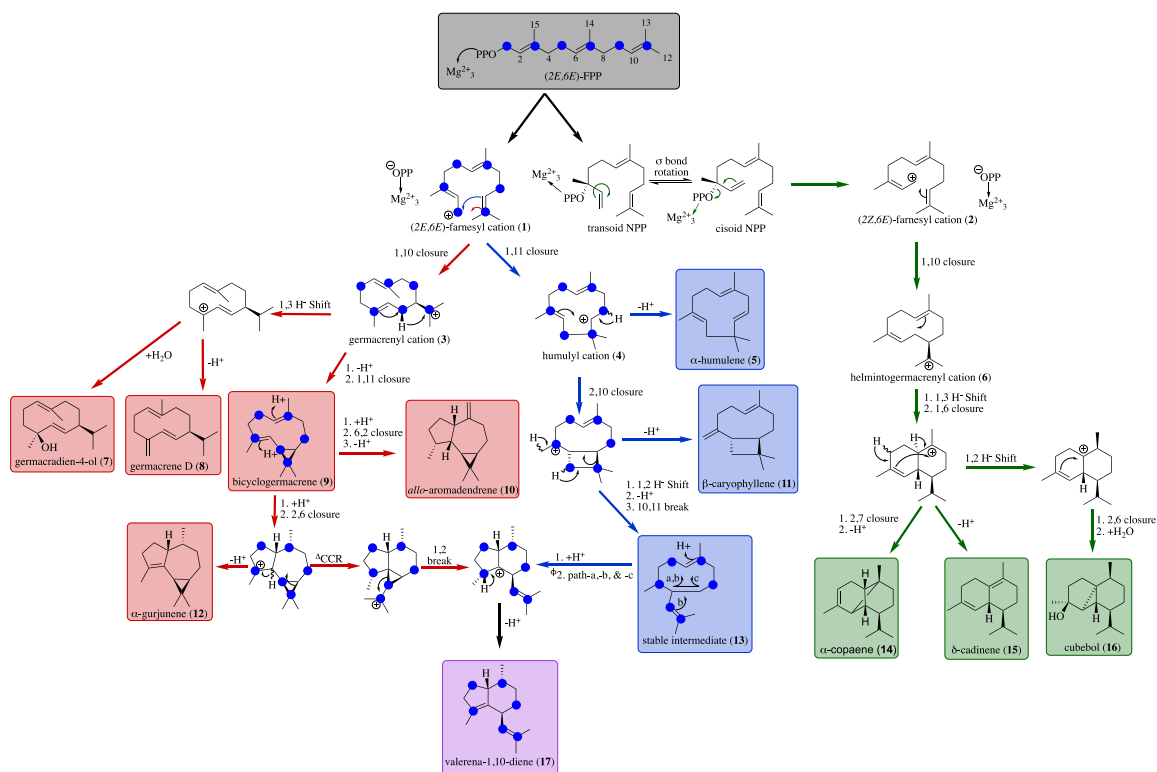


**Figure 2.13** Overlay of the observed and predicted  $^{13}\text{C}$  labeling pattern (blue spheres) from Yeo et. al. onto the revised catalytic cascades of **Figure 2.1**. The labeling pattern documented for **17** arising from the cyclization of  $^{13}\text{C}$ -labeled FPP (**1**) by VDS is consistent with either the humulyl (blue) or germacrenyl (red) pathways.

### 2.3.5 Probing the role of Cys415 and Cys452

From our previous efforts to alter product specificity of terpene synthases (Greenhagen et al., 2006), we hypothesized that if a TPS reaction cascade is truncated at a stable intermediate, then its catalytic turnover rate and efficiency should be at least comparable to (if not greater than) the wildtype enzyme such as we observed with the C440A mutant from EAS (Greenhagen, 2003; Greenhagen et al., 2003). We combed the active site residues of VDS from our constructed contact map, searching for a cysteinyl sulfhydryl positioned to interact with the  $\beta$  isoprene unit of FPP and discovered Cys415, located within the G1/G2 Helix break region (**Figure 2.5, Panel B**). Baer et al. (Baer et al., 2014) identified and characterized the G1/G2 Helix Break “effector triad” - a conserved structural motif comprised of three amino acids among all bacteria, fungi, and plant class I terpene synthases responsible for the induced fit between the synthase and substrate aiding in the transition from the open to the closed conformation. In the VDS homology model, Cys415’s carbonyl group is structurally positioned in the “effector” position (3.7 Å from C3 on FPP) could be responsible for triggering the cleavage and release of the diphosphate of FPP to form the delocalized allylic carbocation (**1**), while residues Ser414 (linker) and Arg456 (pyrophosphate sensor) comprise the rest of the effector triad (**Figure 2.5, Panel C**). To explore the catalytic role of Cys415, we substituted the thiol containing residue for an alanine and serine residue and profiled the reaction products *in vivo* (**Table 2.2**). Both mutations exhibited a dramatic decrease in total productivity with an approximate 50 % diversion of the catalytic specificity from **17** to **9**. Because neither C415A, nor C415S eliminated the production of the primary reaction products found with

the wildtype enzyme, it is unlikely Cys415 is directly involved in the active site acid-base chemistry.

From the homology model, Cys283(C Helix) and Cys452 (H Helix) are positioned 11.9 and 10.5 Å from C7 on **9** and **13**, respectively (**Figure 2.5, Panel C**). However, we narrowed our focus to Cys452 instead of Cys283, since it is positioned similarly to Cys270 in EAS (PDB: 5EAT) and appears to be involved in the formation of an active site hydrogen bond network with Tyr541 and the creation of an essential structural feature in VDS (Starks et al., 1997). We removed the proton donor capabilities of Cys452 by an alanine mutation and characterized the reaction products both *in vivo* and *in vitro*. The *in vivo* analysis detected a product distribution for C452A of 31 % valerenadiene (**17**), 65 % bicyclogermacrene (**9**) and 4 % *allo*-aromadendrene (**10**), similar to the product profile shift of the C415A and C415S mutants (**Table 2.2**). However, the  $K_M$  for the C452A mutant (20.7  $\mu\text{M}$ ) is identical to VDS (20.1  $\mu\text{M}$ ), but its  $k_{\text{cat}}$  of 0.038  $\text{s}^{-1}$  is double that for VDS (0.018  $\text{s}^{-1}$ ) which translates to a doubling in the catalytic efficiency ( $k_{\text{cat}}/K_M$ ) of C452A (**Table 2.3**).

The failure of C452A to completely shift the product specificity of VDS towards **9** is not consistent with its role as the Lewis acid in donating a proton to intermediate **13** in the VDS catalytic cascade (**Figure 2.1**). An alternative is that a water molecule may be trapped in the active site serving as the requisite proton donor, a hypothesis that cannot be ruled out for VDS (Christianson, 2017; Felicetti & Cane, 2004; S. Garms et al., 2010; Grundy et al., 2016; Rynkiewicz et al., 2002; Yoshikuni, Martin, et al., 2006). Perhaps Cys452 is contributing more to active site topology guiding catalytic outcomes. The analogous position within the previously characterized bicyclogermacrene synthase (Attia

et al., 2012) (**Figure 2.7**) is occupied by a leucine residue, located just outside the active site on Helix H (**Figure 2.5, Panel B & C**), which may offer sufficient influence on the active site contour to steer the catalytic activity more specifically towards **9**. A logical inference from this interpretation would be to evaluate a C452L mutation in VDS for its product specificity and catalytic efficiency.

### 2.3.6 Contributions of residues proximal to a metal binding domain

. Several research groups have demonstrated that residues surrounding the metal binding domains found within amorpho-4,11-diene synthase (ADS), can contribute to both the initial and subsequent ring closures of ionized FPP in the formation of the amorphenylation, directly impacting product specificity and catalytic activity (Abdallah et al., 2018; Fang et al., 2017; Li et al., 2016). Hence, we investigated Ile307, Thr310 and Ser311, the analogous residues proximal to the DDXXD metal binding domain in VDS (**Figure 2.7**).

To begin evaluating the contribution of the hydrophobic surface comprised of these residues to the catalytic activity, Ile307 associated with the D Helix was substituted with a leucine. This position resides within the hydrophobic core deep within the VDS' active site along with Trp286, Tyr417, and Leu420 (**Figure 2.5, Panel D**). Interestingly, an I307L mutation, a mutation of a conserved residue, resulted in almost a 60 % decline in relative activity without any change in overall product specificity other than a shift in the ratio of products, greater than 35 % increase in the amount of **9** accumulating and concomitant decrease in **17** (**Table 2.2**). Due to the buried nature of this residue within the active site, the loss of activity with a highly conserved mutation and the conserved nature of the Ile at



this position amongst terpene synthase (**Figure 2.7**), no further mutations at this site were investigated.

Thr310 and Ser311 are situated above the first aspartate residue of the DDXXD motif oriented towards the active site pocket and juxtaposed relative to the  $\gamma$ -isoprene unit of FPP, potentially poised to influence orientation of the initial farnesyl carbocation and control of the ensuing catalytic cascade (**Figure 2.5, Panel B**). Consistent with the essential nature of these particular residues (**Figure 2.7**), all attempts to mutate Ser311 with hydrophobic (alanine and isoleucine), polar (threonine), or aromatic (phenylalanine) mutations lead to inactive VDS mutants (**Table 2.2**). However, substitution mutants of Thr310 with alanine, isoleucine or methionine residues yielded catalytically active enzymes with alterations in the proportion of valerenadiene (**17**), bicyclogermacrene (**9**) and allo-aromadendrene (**10**) (**Table 2.2 & Table 2.3**), except that the methionine mutant (T310M) also generated a new product,  $\alpha$ -gurjunene (**12**) in 27 % abundance. While this particular mutant maintained a  $K_M$  (22.8  $\mu$ M) for FPP comparable to the wildtype enzyme, its catalytic turnover rate ( $k_{cat}$ ) was only about 1/10<sup>th</sup> of the wild type VDS (**Table 2.3**).

The Thr310 mutations are consistent with the germacreanyl cation pathway as the dominate pathway for the biosynthesis of VLD (**17**). Other than the T310S mutant, which was largely inactive, mutations to non-polar residues like alanine, isoleucine or methionine shifted the product profile to greater proportions of bicyclogermacrene (**9**), consistent with Thr310 being a gateway residue for the conversion of bicyclogermacrene (**9**) onto VLD (**17**). The extra bulk contributed by the T310M mutant would also be consistent with this mutant allowing the bicyclogermacrene (**9**) intermediate to initially proceed down the catalytic cascade, but to be diverted to a novel product,  $\alpha$ -gurjunene (**12**), because the

active site was constrained from performing the CCR. Schrepfer et al. (Schrepfer et al., 2016) used a similar logic in mapping functionally plasticity residues within taxadiene synthase, a type I diterpene synthase.

### 2.3.7 Asn455 suppress a dormant cyclization cascade in VDS

Based on the report of Nguyen et al. (Nguyen et al., 2016) that a valine to glycine mutation within a  $\beta$ -farnesene synthase was sufficient to convert product specificity from linear to complete cyclized products, we examined the possible role of the analogous position within VDS, 455 (**Figure 2.7**), to contribute to possible intermediate formation in the VLD cascade. When Asn455 was substituted for alanine, cysteine, serine or threonine, the resulting mutant enzymes possessed only 12 to 25 % of the wildtype enzyme activity and produced greater than 40 % of germacradien-4-ol (**7**) as the majority product. This is in contrast to VDS, or the other mutants mentioned above which only yield a small percentage of **7**. However, more surprising was that much of the remaining products resulting from these mutants were  $\alpha$ -copaene (**14**),  $\delta$ -cadinene (**15**), cubebol (**16**), products that can only arise for an all trans to cisoid confirmation change of FPP to nerolidyl diphosphate, NPP (**Figure 2.1**, green arrow route). Moreover, these mutants also lost their ability to produce **9** and **17**. While none of the Asn455 mutants accumulated products that could be interpreted as intermediates for either of the possible catalytic pathways to **17**, these mutants appear to be confirming an important evolutionary role for this position in the cyclization pathways of type 1 sesquiterpene synthases as suggested by Salmon et al. (Salmon et al., 2015).

## 2.4 Conclusions

While the experimental aim of this work was to find mutants of VDS that produced cyclic derivatives with alternative configurations of the iso-butenyl side chain or more structurally constrained analogs of the valerenadiene scaffold, the work has established a map of residues impacting catalytic outcomes, including a mutant producing exclusively bicyclogermacrene (Y535F) and identified Asn455 as serving as a gatekeeper for sesquiterpene products requiring a configurational isomerization of FPP to the cisoid precursor NPP. These results help focus future efforts in creating more constrained scaffolds for building analogs to test for their modulatory activity of the human GABA<sub>A</sub> receptor and anxiolytic activities in animal models.

## CHAPTER 3. TOWARDS BUILDING A VALERENIC ACID ANALOG BIOSYNTHESIS PLATFORM IN YEAST

### 3.1 Introduction

Our second objective was to produce at least three to four structurally constrained, carboxylated valerenadiene analogs for evaluation of their human GABA<sub>A</sub> receptor biological activity in a mammalian cell based GABA<sub>A</sub> receptor host system with a voltage sensitive fluorescent dye (**CHAPTER 4**). However, given our unsuccessful attempts to uncover VDS mutants which derail to more structurally constrained intermediates (**CHAPTER 2**), we shifted forward towards establishing a robust *S. cerevisiae* host platform capable of producing VA (**Figure 3.1**). It should be noted, a synthetic route to VA has been established and was considered as an alternative to obtaining the structurally constrained oxidized compounds; however, this strategy suffers from arduous reactions, costly reagents, and low substrate to product conversion rates (Ramharter & Mulzer, 2009). Therefore, we conducted our work in our ZXB yeast line (Zhuang & Chappell, 2015), as opposed to our current *E. coli* chassis for the following reasons: 1) ZXB contained a dispensable FPP substrate pool (Zhuang & Chappell, 2015) - the acyclic carbon backbone of all sesquiterpenes (Cane, 1990), 2) it possessed an endoplasmic reticulum (ER), the cellular organelle which anchors the N-terminal transmembrane domain of terpene modifying cytochrome P450 enzymes (Pateraki et al., 2015; Williams et al., 2000), and 3) ZXB's parental yeast strain, 178-08 (Chappell et al., 2021; Zhuang & Chappell, 2015), produced over 500 mg/L of a kaurenoic acid (Zhuang, 2013) - a successively oxidized terpene involved in the gibberellin biosynthetic pathway (Helliwell et al., 1998) – from episomal expression of kaurene synthase (a diterpene synthase (Yamaguchi et al., 1996; Yamaguchi et al., 1998)), kaurene oxidase (a cytochrome P450 responsible for the

successive oxidation at C19 (Helliwell et al., 1999)), and a NADPH dependent cytochrome P450 reductase (Takahashi, Yeo, Greenhagen, et al., 2007).

Recently Chappell and company investigated the tailoring enzyme(s) involved in VA's biosynthetic pathway using an *Agrobacterium rhizogenes* transformed hairy root culture system developed from valerian leaf explants (Ricigliano et al., 2016). CYP71D442, a putative terpene specific cytochrome P450 with an approximately 4-fold higher mRNA expression level in mature roots versus leaf and stem regions of wildtype *V. officinalis*, was hypothesized to play a significant role in VA biosynthesis. However, it was ruled out after its mRNA expression levels decreased, while mRNA levels increased for FPP and VDS in valerian hairy root cultures challenged with methyl jasmonate (Ricigliano et al., 2016). Despite the recent heroic efforts from the Chappell group, the native valerian enzyme(s) responsible for the oxidation of VA remain unknown.

To circumvent the arduous and labor-intensive task of functionally identifying the endogenous tailoring enzymes involved in VA biosynthesis, we explored an alternative strategy reported by the Ro group. Nguyen and company initially probed the substrate promiscuity of a germacrene A oxidase (GAO) cloned from lettuce (*Lactuca sativa*) and spiny barnadesia (*Barnadesia spinosa*) for subsequent oxidation at carbon atoms trans to double bonds on seven different sesquiterpenes containing a two-ring core structure (Nguyen et al., 2019). These investigators reported that both isoforms of the GAO enzyme successively oxidized the terminal methyl substituent on VLD's isobutenyl side chain to form the bona fide VA chemical structure (Nguyen et al., 2010; Nguyen et al., 2016; Nguyen et al., 2019). Hence, their discovery provided an approach for adding the

carboxylic acid functionality to carbon atom 12 or 13 (**Figure 2.1, Structure #17**) in the trans position on VLD's isobutenyl sidechain without reliance upon re-capitulation of the native VA biosynthetic pathway from *V. officinalis*. A hypothetical reaction scheme for successive oxidation of a desired constrained sesquiterpene scaffold, synthesized from the cyclization of FPP, involving a single cytochrome P450 enzyme or an assembly of tailoring enzymes, is shown in greater detail in **Figure 3.2**.

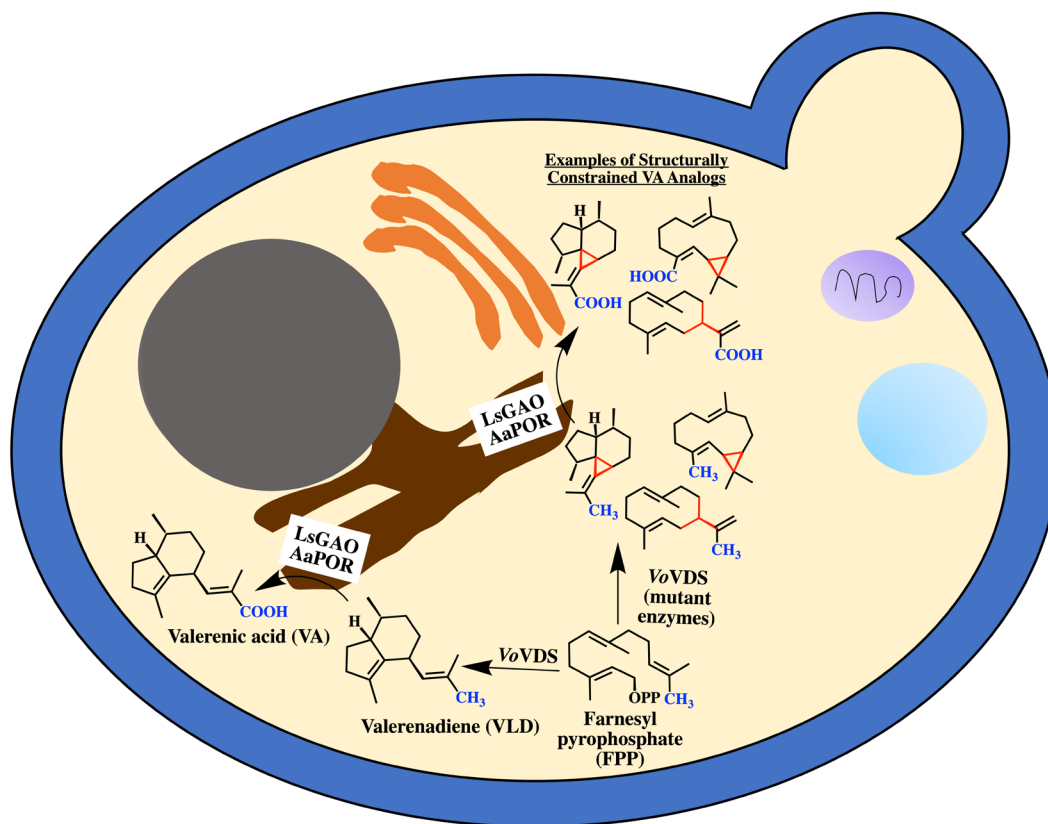


**Figure 3.1** VA and VA analog factory in our ZXB yeast host system. (Bottom pathway) The ZXB yeast host platform was utilized to constitutively express extrachromosomal copies of VDS from the xLEU – GPDp(VoVDS);TEFp(VoVDS) plasmid for de novo synthesis of VLD from FPP, the acyclic carbon precursor. VLD was then successively oxidized to a carboxylic acid at its terminal methyl group (colored in blue) located on its isobutenyl side chain by the endomembrane-bound (brown shape) catalytically promiscuous germacrene A oxidase from lettuce (LsGAO). Electrons are transferred from NADPH to LsGAO through the cytochrome P450 reductase from sweet wormwood (AaPOR). (Upper pathway) Once in hand, our goal is to co-transform separate plasmids encoding for the desired VDS mutant enzymes in our ZXB host system with the xHIS-GPDp(LsGAO);TEFp(AaPOR) plasmid for successive oxidation at one of the VLD constrained analog's terminal methyl groups (colored in blue) to form the carboxylic acid. The red highlighted C-C bonds show the location of structural constraint from either cyclization or a reduction in rotatable bonds in comparison with VLD's flexible isobutenyl side chain.

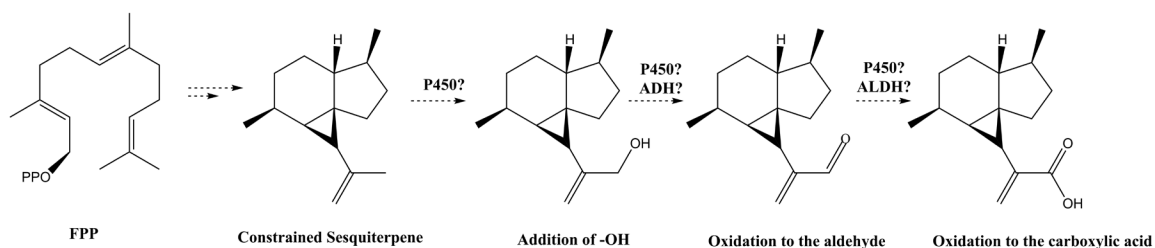


**Figure 3.2** In this hypothetical reaction oxidation scheme, the linear substrate FPP is first cyclized into the desired constrained sesquiterpene intermediate. Then, the hydrocarbon intermediate is trafficked to an endomembrane-bound cytochrome P450, where molecular oxygen is inserted at an allylic carbon atom to form the primary alcohol. The oxygenated intermediate is either oxidized to the aldehyde by the same P450 or through an alcohol dehydrogenase (ADH). Finally, the aldehyde intermediate is oxidized for the second time to the carboxylic acid by either the initial P450 or by an aldehyde dehydrogenase (ALDH) enzyme complex. For VA formation, both routes (successive oxidation by a single cytochrome P450 enzyme or by a set of tailoring enzymes) have been posited, but none proven to date (Ricigliano et al., 2016; Wong et al., 2018).



## 3.2 Materials and Methods

### 3.2.1 Chemicals and reagents

Acetone, n-dodecane, n-hexanes, and ethyl acetate were of ACS reagent grade and purchased through Fisher Scientific (Waltham, MA). Yeast synthetic drop-out medium lacking histidine, leucine, tryptophan, and uracil, hereafter referred to as SC (Cat # Y2001), and D-glucose (Cat # G8270) were all purchased from Sigma Aldrich (St. Louis, MO). Ergosterol (Cat #117810050) was purchased from Acros Organics (Fair Lawn, NJ). N-Methyl-N-(trimethylsilyl)trifluoroacetamide (MSTFA) + 1% Trimethylchlorosilane (TMCS) (Cat# RMB1204) was purchased from Ricca Chemical Company (Arlington, TX). TRI Reagent® (Cat # TR 118) was purchased from Molecular Research Center and kept at 4° C as instructed. Superscript III First-Strand Synthesis System for RT-PCR by Invitrogen (Cat # 18080-051) was purchased through Fisher Scientific and kept at -20° C as recommended.

### 3.2.2 VoVDS cloning and amplification

The xLEU-GPDp;TEFp expression plasmid, described in Zhuang's dissertation work (Zhuang, 2013), was employed to express multiple extrachromosomal copies of the VDS gene for constitutive VLD production. The VoVDS gene was first amplified by PCR from the pET28(a)-VoVDS vector (Yeo et al., 2013) with a gene specific forward and reverse primer (Integrated DNA Technologies) flanked with unique restriction sites at the 5' and 3' ends (**Table 3.1, primer #'s 1 & 2; 3 & 4**) using PrimeSTAR HS DNA polymerase (Takara Bio), according to the manufacturer's recommendations. Additionally,

the forward primer harbored the partial Kozak sequence “AAAACA” between the 5’ restriction site and the start methionine. The amplified VoVDS gene was verified by sizing via gel electrophoresis and the appropriate band was purified using the QIAquick Gel Extraction Kit (Qiagen) according to the manufacturer’s recommendations. The purified VDS insert, and the empty xLEU- GPDp();TEFp() vector were subjected to double restriction digestion with the appropriate restriction enzymes (**Figure 3.3, A**), ligated into the appropriate expression vectors using T4 DNA Ligase (Promega), followed by transformation into the *E. coli* DH5 $\alpha$  cell line. Positive transformants were selected on growth media plates containing 50-100 $\mu$ g/mL of ampicillin. Individual colonies were subsequently screened for recombinant plasmids using restriction digestion followed by DNA termination sequencing.

### 3.2.3 LsGAO amplification and cloning

Wildtype lettuce (*Lactuca sativa*) plants were grown in ProMix BX (Premier Tech) soil under a 16hr light/ 8hr dark cycle using Sylvania OCTRON 6500K bulbs in a greenhouse. To prevent bolting, plants were grown in a laboratory setting with minimal temperature and humidity fluctuations. After 4-5 weeks of growth, 2-3 leaves were harvested and immediately flash frozen in liquid nitrogen. The harvested leaf tissue was homogenized, and total RNA was isolated with Tri Reagent® (Molecular Research Center), following the manufacturer’s protocol. Quality of the isolated RNA was evaluated by agarose gel electrophoresis and the concentration estimated by a nanodrop spectrophotometer (Thermo 2000c). cDNA first-strand synthesis was carried using oligo dT’s and Superscript III Reverse Transcriptase (Invitrogen), per the manufacturer’s instructions. The LsGAO cDNA was PCR amplified with primers “5” and “6” in **Table**

**3.1.** The amplified DNA of 1400-1500bp was gel purified for subsequent ligation in the into the xHIS-GPDp();TEFp(AaPOR) vector (Zhuang, 2013) at the 5'-EcoRI & 3'-NotI cloning sites (**Figure 3.3, B**). The DNA constructs was verified by DNA termination sequencing.

**Table 3.1** List of VoVDS and LsGAO forward and reverse cloning primers

<b>Primer</b>	<b>Sequence (5' to 3')</b>	<b>Name</b>
1	GCGGCCGCAAAACAATGGAGAGTTGCCTTAGTTTTTCAAG	NotI-Kozak-VoVDS (Fwd)
2	ACTAGTTTAATACGGAACACTTTCTACTAGAAG	VoVDS-SpeI (Rev)
3	GGATCCAAAACAATGGAGAGTTGCCTTAGTTTTTCAAG	BamHI-Kozak-VoVDS (Fwd)
4	GTCGACTTAATACGGAACACTTTCTACTAGAAG	VoVDS-SalI (Rev)
5	GGAATTCAAAACAATGGAGCTTTCAATAACCACCTCCATTGCT	EcoRI-Kozak-LsGAO (Fwd)
6	ATAGTTTAGCGGCCCTAAAACTCGGTACGAGTAACAACCTCAGTC	LsGAO-NotI (Rev)

### A. VDS Expression Construct



### B.

### LsGAO/AaPOR Expression Construct

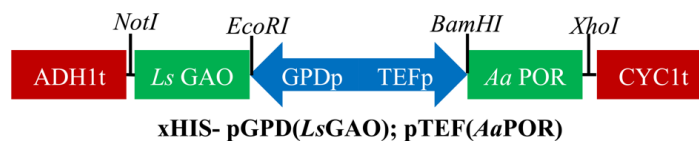


**Figure 3.3** Molecular constructs co-transformed into the ZXB yeast line for *de novo* synthesis of valerenic acid. (A) The valerenadiene synthase (*VoVDS*) gene were amplified off of the pET28(a)-VDS construct (Yeo et al., 2013) with a forward and reverse primer listed in **Table 3.1** and subcloned into a modified pescLeu backbone (Zhuang, 2013) under the glyceraldehyde-3-phosphate (GPDp) and the translational elongation factor EF-1 alpha (TEFp) independent, divergent promoters for constitutive VLD production. (B) The promiscuous germacrene A oxidase from lettuce (*LsGAO*) was amplified from an isolated *L. sativa* cDNA pool and ligated into xHIS backbone (Zhuang, 2013) under the GPDp promoter using primer #'s 5 & 6 **Table 3.1**. To transfer electrons from NADPH to *LsGAO*, the cytochrome P450 reductase from the artemisinin acid biosynthetic pathway (Ro et al., 2006) (*AaPOR*) was previously amplified from isolated *A. annua* cDNA pool and ligated into xHIS backbone under the TEF promoter (Zhuang, 2013).

### 3.2.4 *S. pyogenes* Cas9-NLS amplification and cloning

To construct the xLEU-GPDp(Cas9-NLS)ADH1t plasmid (**Figure 3.4, A**) the human codon-optimized version DNA coding sequence of Cas9 fused at its carboxy terminus to the simian virus 40 nuclear localization signal (SV40 NLS), originally isolated from *Streptococcus pyogenes* (Jinek et al., 2012; Mali et al., 2013), was amplified from the p414-TEF1p-Cas9-CYC1t vector with primers “7” and “8” listed in **Table 3.2**. The p414-TEF1p-Cas9-CYC1t plasmid (DiCarlo et al., 2013) was a gift from George Church obtained from Addgene (plasmid #43802). Using standard restriction enzyme cloning (RE cloning) procedures described previously, the Cas9-NLS gene was positioned under the GPD (TDH3) promoter by ligation at the 5'-NotI, 3'-SpeI restriction sites within the xLEU-GPDp;TEFp empty vector (Zhuang, 2013). Verification of correct insertion of the Cas9-NLS gene was confirmed by single-pass nucleotide sequencing analyzed at the UK HealthCare Genomics Core Laboratory.

### 3.2.5 BTS1, Rox1, YPL062W, & YJL064W gRNA cassettes

Synthetic DNA sequences coding for the entire guide RNA (gRNA) expression cassette including the promoter, target sequence, gRNA structural components, and terminator (**Table 3.3**) were synthesized as gene fragments (gBlocks<sup>®</sup>) by Integrated DNA Technologies (Coralville, IA). The nucleotide sequences for the tRNA<sup>Tyr</sup> promoter, gRNA scaffold, and SNR52 terminator, were taken directly from Ryan et. al. (Ryan et al., 2014) (**Table 3.3**). The target gRNA sequences for the *Saccharomyces cerevisiae* *BTS1*(YPL069C), *Rox1*(YPR065W), *YPL062W*, and *YJL064W* genomic sites were copied

directly from Jakociunas et. al. (Jakociunas et al., 2015). For constitutive, high-level expression in yeast, the gRNA cassettes were amplified with primers 9 & 10 (**Table 3.2**) and cloned in at the BamHI/HindIII restriction sites within the xURA-GPDp();TEFp() empty vector (Zhuang, 2013)

### 3.2.6 Homology-armed VDS DNA oligo

The dsDNA repair template was constructed from standard molecular techniques of PCR and SOE (splicing by overlap extension) PCR (Heckman & Pease, 2007). Using a two-step PrimeSTAR HS DNA Polymerase PCR (Takara) protocol, the 500bp homologous regions upstream and downstream of the yeast *BTS1*, *Rox1*, *YPL062W*, and *YJL064W* genomic loci, were attached to appropriate ends of the GPDp(VDS)ADH1t gene blocks (**Figure 3.4, C**). Primer #'s 11-16, 17-22, 23-28, and 29-34 (**Table 3.2**) were used to attach the *BTS1*, *Rox1*, *YPL062W*, and *YJL064W* 500bp homology arms to the GPDp(VDS)ADH1t gene block, respectively. ZXB genomic DNA, isolated following the protocol described within (Harju et al., 2004), served as the PCR template for cloning the 500bp homologous DNA strands up- and down-stream of the four targeted yeast loci. The *BTS1*, *Rox1*, *YPL062W*, and *YJL064W* yeast genomic sequences were copied directly from [www.yeastgenome.org](http://www.yeastgenome.org).

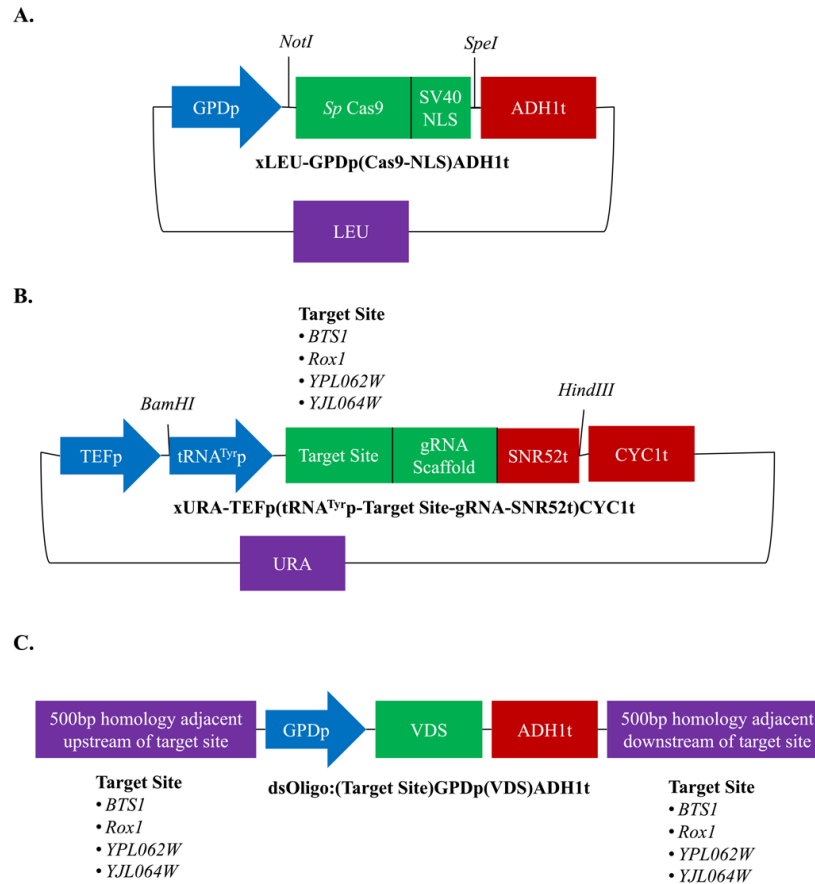


**Figure 3.4** Molecular constructs used to knock out specific yeast genomic loci and replace with single copies of a constitutive VDS expression construct. (A) A yeast codon optimized version of the *S. pyogenes* Cas9 gene (*SpCas9*) fused at its C terminus to the SV40 nuclear localization signal (SV40 NLS) (Jinek et al., 2012) was amplified from the p414-TEF1p-Cas9-CYC1t vector (DiCarlo et al., 2013) with primer #'s 7&8 (**Table 3.2**) and positioned under the GPD promoter (GPDp) in the xLEU-GPDp(ADH1t) empty vector (Zhuang, 2013) using RE cloning. (B) The *BTS1*, *Rox1*, *YPL062W*, & *YJL064W* gRNA structural cassettes were constructed as double-stranded DNA gene blocks (Integrated DNA Technologies) and RE cloned into the xURA-GPDp(ADH1t) empty backbone (Zhuang, 2013) with primer #'s 9&10 (**Table 3.2**). (C) The GPDp(VDS)ADH1t DNA oligo (minus the homology arms) was amplified from the xLEU-GPDp(VoVDS);TEFp(VoVDS) vector (**Figure 3.3, A**) with the primer #'s 11&13, 14&16 - *BTS1*; 17&19, 20&22 - *Rox1*; 23&25, 26&28 - *YPL062W*; 29&31, 32&34 - *YJL064W* (**Table 3.2**) and subsequently, gel purified. The 500bp up- and downstream homology arms were amplified from ZXB genomic DNA with the primer #'s 11&13, 14&16 - *BTS1*; 17&19, 20&22 - *Rox1*; 23&25, 26&28 - *YPL062W*; 29&31, 32&34 - *YJL064W* (**Table 3.2**), then purified by gel electrophoresis. The flanking homology arms were subsequently sown onto the GPDp(VDS)ADH1t amplicon using the primer pair #'s 11&16 - *BTS1*; 17&22 - *Rox1*; 23&28 - *YPL062W*; 29&34 - *YJL064W* (**Table 3.2**) in a two-step PCR protocol.



**Table 3.2** List of CRISPR/Cas9 cloning primers

<b>Primer</b>	<b>Sequence (5' to 3')</b>	<b>Comment</b>
7	ATGCGGCCGCAAAACAATGGACAAGAAGTACTCCATTGGGC	NotI-Kozak-pCas9 (Fwd)
8	ATACTAGTTCACACCTTCTCTTCTTCTGGGG	pCas9-SpeI (Rev)
9	ATTGGATCCGTATACTCTTCTTCAACAA	BamHI-tRNATyr-prom (Fwd)
10	TAAAAGCTTTATCCACTAGACAGAAGTTT	HindIII-SNR52-term (Rev)
11	AGCATTATCAAAAAGCTTGACAAGC	BTS1 upstream (Fwd)
12	GGAGCCAAGATAGATGAGCAGTTTATCATTATCAATACT	BTS1 upstream GPDp (Fwd)
13	AGTATTGATAATGATAAACTGCTCATCTATCTTGGCCTCC	BTS1 upstream GPDp (Rev)
14	GGTATAGCATGAGGTCGCTCTGGTCCAGCCAAAATGAAAAG	BTS1 downstream ADH1t (Fwd)
15	CTTTCATTTGGCTGGACCAGAGCGACCTCATGCTATAACC	BTS1 downstream ADH1t (Rev)
16	ATGAGTCTCAACGTTAATCTGAAAAGG	BTS1 downstream (Rev)
17	ACTTGCGATTGCTGACAAAAGAAGAAAAG	Rox1 upstream (Fwd)
18	TCTGTTTACAGACAGCACTACCAGTTTATCATTATCAATACT	Rox1 upstream GPDp (Fwd)
19	AGTATTGATAATGATAAACTGGTAGTGTCTGAACAGA	Rox1 upstream GPDp (Rev)
20	GGTATAGCATGAGGTCGCTCTGGACCGCTCAAGGTGTGGA	Rox1 downstream ADH1t (Fwd)
21	TCCACACCTTGAGCGGTCCAGAGCGACCTCATGCTATAACC	Rox1 downstream ADH1t (Rev)
22	AGTTGAGATGACAGCTGTGGTAGGTC	Rox1 downstream (Rev)
23	TCATTTTGTACTGTATGTAATAAACTTATG	YPL062W upstream (Fwd)
24	TACCATTGTAGAAGCAACCAAGTTTATCATTATCAATACT	YPL062W upstream GPDp (Fwd)
25	AGTATTGATAATGATAAACTGGTTGCTTCTACAATGGTA	YPL062W upstream GPDp (Rev)
26	GGTATAGCATGAGGTCGCTCAGGTCTCTTGGCCGGGC	YPL062W downstream ADH1t (Fwd)
27	GCCCGGGCAAGAGGAGACCTGAGCGACCTCATGCTATAACC	YPL062W downstream ADH1t (Rev)
28	ATTTATATATGATATCAAGAAGTTGTTAAACACGCC	YPL062W downstream (Rev)
29	TTGATATATTTGTCATTAATGCCTTGG	YJL064W upstream (Fwd)
30	TGCGGCAGAGATGTCATCGTAGTTTATCATTATCAATACT	YJL064W upstream GPDp (Fwd)
31	AGTATTGATAATGATAAACTACGATGACATCTTGCCGCA	YJL064W upstream GPDp (Rev)
32	GGTATAGCATGAGGTCGCTCGGGAGCGGGTACCTGTTG	YJL064W downstream ADH1t (Fwd)
33	CAACAGGTACCGCCGCTCCCGAGCGACCTCATGCTATAACC	YJL064W downstream ADH1t (Rev)
34	GTCTACTCTTCGTCATTGCCAAAAGAAG	YJL064W downstream (Rev)
35	CGGTAGGTATTGATTGTAATTCTG	GPDp sequencing promoter (Fwd)
36	GAGTCACTTTAAAATTTGTATACAC	ALDH1t sequencing promoter (Rev)

**Table 3.3** BTS1, Rox1, YPL062W, & YJL064W gRNA cassette nucleotide sequences

<u>gBlock</u>	<u>Sequence (5' to 3')</u>	<u>Name</u>
1	GTATACTCTTTCTTCAACAATTAATACTCTCGGTA GCCAAGTTGGTTTAAGGCGCAAGACTGTAATTTAT CACTACGAAATCTTGAGATCGGGCGTTCGACTCGC CCCC <del>GGG</del> GAGAGCAC <del>GT</del> CGCCGTGGCTGATGGTTTT AGAGCTAGAAAATAGCAAGTTAAAATAAGGCTAGTC CGTTATCAACTTGAAAAAGTGGCACCGAGTCGGTG CTTTTTTTATTTTTTGTCACTATTGTTATGTAAAATG CCACCTCTGACAGTATGGAACGCAAACCTTCTGTCT AGTGGATA	tRNA <sup>tyr</sup> Prom-BTS1gRNA-SNR52t
2	GTATACTCTTTCTTCAACAATTAATACTCTCGGTA GCCAAGTTGGTTTAAGGCGCAAGACTGTAATTTAT CACTACGAAATCTTGAGATCGGGCGTTCGACTCGC CCCC <del>GGG</del> GAGAACAGGATCTTAATAGACGAAGTTTT AGAGCTAGAAAATAGCAAGTTAAAATAAGGCTAGTC CGTTATCAACTTGAAAAAGTGGCACCGAGTCGGTG CTTTTTTTATTTTTTGTCACTATTGTTATGTAAAATG CCACCTCTGACAGTATGGAACGCAAACCTTCTGTCT AGTGGATA	tRNA <sup>tyr</sup> Prom-Rox1gRNA-SNR52t
3	GTATACTCTTTCTTCAACAATTAATACTCTCGGTA GCCAAGTTGGTTTAAGGCGCAAGACTGTAATTTAT CACTACGAAATCTTGAGATCGGGCGTTCGACTCGC CCCC <del>GGG</del> GAGATGATCAATAATGATCCTGTTGTTTTA GAGCTAGAAAATAGCAAGTTAAAATAAGGCTAGTCC GTTATCAACTTGAAAAAGTGGCACCGAGTCGGTG TTTTTTTTATTTTTTGTCACTATTGTTATGTAAAATG CACCTCTGACAGTATGGAACGCAAACCTTCTGTCTA GTGGATA	tRNA <sup>tyr</sup> Prom-YPL062WgRNA-SNR52t
4	GTATACTCTTTCTTCAACAATTAATACTCTCGGTA GCCAAGTTGGTTTAAGGCGCAAGACTGTAATTTAT CACTACGAAATCTTGAGATCGGGCGTTCGACTCGC CCCC <del>GGG</del> GAGAACGACAGCGTGAGTTCATCTGTTTT AGAGCTAGAAAATAGCAAGTTAAAATAAGGCTAGTC CGTTATCAACTTGAAAAAGTGGCACCGAGTCGGTG CTTTTTTTATTTTTTGTCACTATTGTTATGTAAAATG CCACCTCTGACAGTATGGAACGCAAACCTTCTGTCT AGTGGATA	tRNA <sup>tyr</sup> Prom-YJL064WgRNA-SNR52t

The tRNA tyrosine promoter (tRNA<sup>tyr</sup>Prom), BTS1, Rox1, YPL062W, and YJL064W target sequences, gRNA structural scaffold, and the SNR52 terminator (SNR52t) coding nucleotide sequences are colored in red, blue, green, and black, respectively.

### 3.3 Construction and maintenance of utilized yeast lines

#### 3.3.1 ZXB yeast line

Details on how the ZXB yeast line (**Table 3.4**) was generated can be found in (Chappell et al., 2021; Zhuang & Chappell, 2015). Briefly, the BY4741 parental yeast line was first subjected to unbiased ethyl methanesulfonate mutagenesis, then subsequently grown on media containing nystatin, squalastatin, and exogenous cholesterol to select for yeast lines having a dispensable mevalonate biosynthetic pathway and an ability to take up exogenous sterols to meet their metabolic needs under aerobic condition. Further genetic modifications included gene knockout of Erg9 (squalene synthase) and the replacement of Erg1 (squalene epoxidase) with a catalytically improved version of 3-hydroxy-3-methylglutaryl-CoA reductase (HMGR), the rate-limiting step in the sterol biosynthetic pathway (Chappell et al., 1995).

For routine culturing, wildtype ZXB colonies were grown on YPG-E solid agar plates (10g/L Yeast extract, 10g/L Peptone, and 20g/L Glucose, supplemented with 4mL/L of a 10mg/mL Ergosterol stock solution – 0.5g ergosterol dissolved in 50mL of a 1:1 ethanol:triton-x-100 solution) (Zhuang & Chappell, 2015). The VoVDS and LsGAO :AaPOR expression constructs (**Figure 3.3, A & B**) were co-transformed into ZXB using the standard lithium acetate method (Gietz & Woods, 2002; Liu et al., 2017), described in detail below:

A single,  $\leq 5$ -day old, ZXB colony was inoculated into 3-5 mL of YPG-E liquid media (10 g/L Yeast extract, 10 g/L Peptone, and 20 g/L Glucose, supplemented with 0.5mL/L of a 10mg/mL Ergosterol stock solution, pH 5.3-5.5) in a 14mL centrifugation

tube and incubated at 28°C, while shaking at 230 RPM for 24-48 hrs. The next morning, the culture's optical density at 600nm was measured and subsequently diluted down to a  $OD_{600}$  0.1-0.3 in 2xYPG-E. The culture was incubated in the 28°C with shaking for two growth cycles, which took six to eight hours. Once the culture density reached an  $OD_{600}$  of 0.4 – 1.2, cells were pelleted by centrifugation at 3000xg for 5min at room temperature. The cell pellet was washed with sorbitol wash buffer (1.2M sorbitol solution buffered with potassium phosphate (pH 7.5)) by pipetting up and down with a 1mL pipet. The cells were pelleted again, then gently washed with 100 mM lithium acetate (1 mL) and pelleted for a third time. The lithium acetate layer was carefully removed, and the yeast cells carefully resuspended in 3.55 mL of the pre-filtered transformation buffer – 100 $\mu$ L of 10mg/mL denatured salmon sperm DNA stock, 360 $\mu$ L of a 1M lithium acetate, 690 $\mu$ L of distilled water, and 2400 $\mu$ L of a 50% PEG 4000 (w/v) stock solution. 200  $\mu$ L of the competent yeast cell resuspension was mixed with 0.5-1.0  $\mu$ g of the yeast expression constructs from **(Figure 3.3, A&B)**, followed by heat-shocking at 42°C for 15-60min. Afterwards, the cells were pelleted by centrifugation (6000xg, 15min, room temperature), resuspended in 200 $\mu$ L of filter-sterilized, double-distilled water, then dispersed across SCG-E (SC+ 20g/L Glucose + 4mL/L of the Ergosterol stock solution) solid media plates with the omission of one or two auxotrophic markers – L-leucine (leu), L-histidine (his). The plates were kept at 28°C until colony formation (typically three to four days). Colonies selected for chemical analysis were re-streaked onto fresh SCG-E selection plates every five days. Note: all wash buffers and reagents, except for the 10mg/ml denatured salmon sperm DNA, were prepared fresh weekly, then filtered through a sterile 0.25 $\mu$ m PES membrane and kept at 4°C or on ice prior to the yeast transformations. Double-stranded salmon sperm DNA (Invitrogen)

(10 mg/ml) was denatured in a 96°C water bath for 5min and aliquots stored at -20°C until needed for transformations.

### 3.3.2 CRISPR/Cas9 engineered yeast lines from ZXB

The GZyBTS1, GZyRox1, GZyYJL064W , and GZyYPL062W yeast lines (Table 3.4) were generated by co-transforming 1µg of the xLEU-GPDp(Cas9-NLS)ADH1t plasmid (**Figure 3.4, A**), with 1µg of xURA-TEFp(tRNA<sup>tyr</sup>p-(Target Site-gRNA-SNR52t)CYCt (**Figure 3.4, B**), onboarded with 0.4-0.6µg of the GPDp(VDS)ADH1t DNA oligo template (**Figure 3.4, C**) into the ZXB parental yeast line following a standard lithium acetate protocol previously described (**Figure 3.5**). The transformed yeast cells were dispersed across SCG-E solid media plates with omission of leucine and uracil amino acids and stored at 28°C until colonies appeared, typically three to four days later. Colonies selected for chemical analysis were re-streaked onto fresh SCG-E selection plates every five days.

**Table 3.4** Genotypes of yeast lines used in this study

<u>Strain</u>	<u>Parent (+ additional genetic changes)</u>	<u>Reference</u>
BY4741	MATa;his3 $\Delta$ 1;leu2 $\Delta$ 0; met15 $\Delta$ 0; ura3 $\Delta$ 0	(Brachmann et al., 1998)
ZXB	BY4741 (SUE;HPH: $\Delta$ erg9;tHMGR-KanMX4: $\Delta$ erg1)	(Zhuang & Chappell, 2015)
GZyBTS1	ZXB (GPDp-VDS-ADH1t: $\Delta$ BTS1)	This study
GZyRox1	ZXB (GPDp-VDS-ADH1t: $\Delta$ Rox1)	This study
GZyYPL062W	ZXB (GPDp-VDS-ADH1t: $\Delta$ YPL062W)	This study
GZyYJL064W	ZXB (GPDp-VDS-ADH1t: $\Delta$ YJL064W)	This study

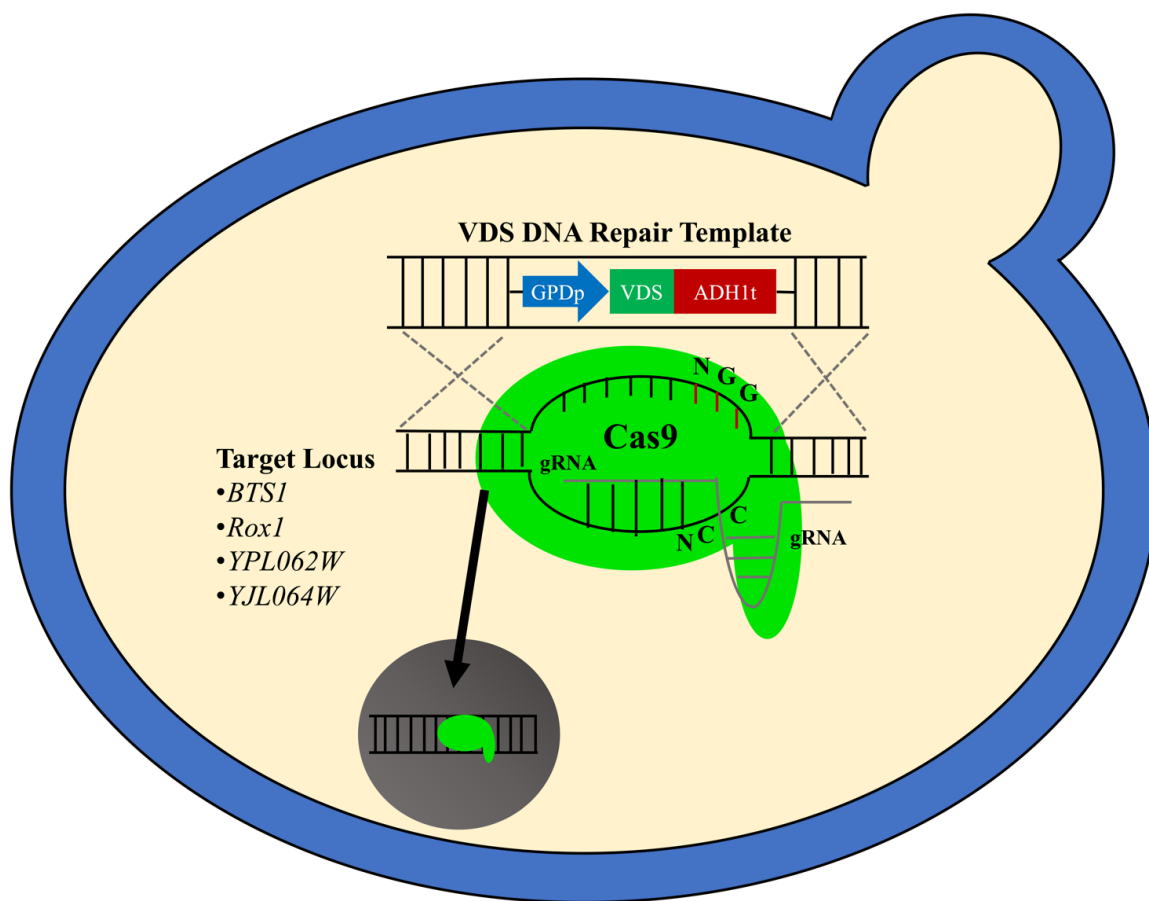


**Figure 3.5** CRISPR/Cas9-DNA Repair System was used to perform simultaneous genomic knock out and knock in with VDS expression construct in yeast. The Cas9 gene and gRNA expression cassettes (for the four target loci) were cloned into and expressed from auxotrophic vectors (**Figure 3.4, A & B**), respectively. The VDS DNA repair template (**Figure 3.4, C**) was constructed from the primers listed in **Table 3.2**, then co-transformed with the Cas9 and gRNA expression cassette plasmids at equal molar ratios into chemically competent ZXB cells.

### 3.4 Detection of VLD and VA from engineered yeast lines

#### 3.4.1 Plasmid-based expression system

Yeast co-transformed with the xLEU-GPDp(VoVDS);TEFp(VoVDS) (**Figure 3.3, A**) and xHIS-GPDp(LsGAO);TEFp(AaPOR) (**Figure 3.3, B**) plasmids were auxotrophically selected on SCG-E (-leu, -his) agar plates, then subsequently cultured in 3mL of liquid SCG-E (-leu, -his) media buffered with 100mM HEPES pH 7.5 (sterile filtered) for seven days at room temperature with vigorous orbital shaking. Nguyen et al. (Nguyen et al., 2010) discovered that when the yeast growth media was buffered between pH 6-7, acid-induced structural rearrangements, such as hydration and allylic rearrangements, are minimized leading to increased titers of desired carboxylated sesquiterpenes (Nguyen et al., 2010; Nguyen et al., 2019), which we mimic in our culturing methods as well.

After 7 days, 1 mL of the yeast cultures were lysed with 1mL of acetone, and the culture's hydrophobic constituents partitioned into 80% ethyl acetate and 20% n-hexanes spiked with a known amount of (-) cedrene. The glass vials were subsequently vortexed, then left on the benchtop for 10 – 20 min. Further phase separation was obtained with a low-speed centrifugation protocol (300xg, 10min, room temperature). Aliquots (1 $\mu$ L) of the dodecane or organic layer were then injected onto a Agilent 7890 GC programed with the following parameters: splitless injection; HP-5MS column, 30m x 0.25mm, 0.25 $\mu$ m film, 250°C inlet temperature; oven temperature was 100°C initially, then increased to 140°C (10°C/min), then increased to 200°C (5°C/min), and finally increased to 300°C (120°C/min) and held for 5min; 0.9 mL/min He flow rate) connected to a 5975C Agilent mass spectrometer (run in positive ionization mode, 70 eV, scanning 40-500 amu). VLD



yields were estimated from a hexadecane standard. Aliquots of the organic layer were also dried down under nitrogen prior to derivatization MSTFA + 1% TMCS, described below.

To increase the GC-MS sensitivity for detection of VA, we replaced the H atom of the carboxylic acid group with a trimethyl silane handle using N-Methyl-N-(trimethylsilyl)trifluoroacetamide (MSTFA) + 1% Trimethyl chlorosilane (TMCS). Briefly, an aliquot (100 $\mu$ L) of the organic layer was evaporated off by a low, steady stream of nitrogen. 30 $\mu$ L of MSTFA + 1% TMCS (Ricca Chemical Company) was added by a clean glass syringe, vial re-capped, vortexed for 5sec, and then placed in a 50 $^{\circ}$ C heating block for 1hr. The vial was removed from the heating block and 70 $\mu$ L of ethyl acetate to maintain the original sample volume. Then, 1 $\mu$ L of the derivatized sample was analyzed by GC-MS (method described above). VA yields were estimated with derivatized VA standard.

#### 3.4.2 CRISPR/Cas9 VDS knock in yeast line system

For confirmation of VDS genomic insertion and subsequent VLD production from chemically competent ZXB cells co-transformed with the CRISPR/Cas9 molecular constructs (**Figure 3.4 A, B & C**), four to five colonies were randomly selected from the SCG-E growth plates. Then, subjected to colony PCR with primers designed to only amplify the upstream and downstream homology arms flanking each of the integration sites (**Table 3.2, primer pair #'s - 11 & 16 (BTS1), 17 & 22 (Rox1), 23 & 28 (YPL062W), and 29 & 34 (YJL064W)**) (Figure 3.6). Only PCR-confirmed colonies were then inoculated into 3mL of YPD-E media with a 10% dodecane overlay in 14mL test tubes. After 7 days, 1 $\mu$ L of the dodecane layer was subjected to GC-MS chemical analysis and

VLD titers (mg/L) were estimated with an external hexadecane standard curve, as described previously.

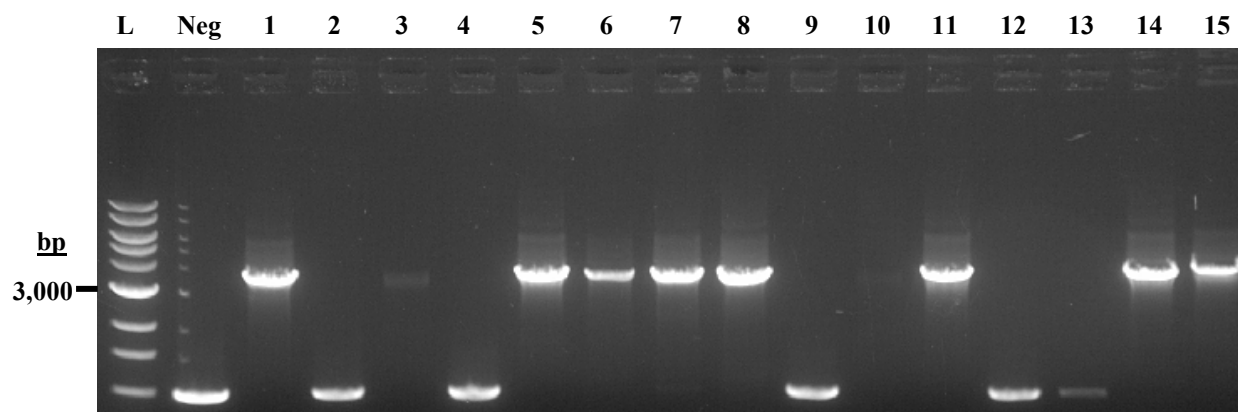


**Figure 3.6** The VDS DNA expression oligo (Figure 3.4, C) was integrated through the highly favored HR DNA repair pathway at Cas9 mediated double-strand DNA break sites within the BTS1, Rox1, YPL062W, and YJL064W genomic loci. Primers which annealed to the flanking homology arms (**Table 3.2**, primer pair #'s: 11&16-BTS1, 17&22-Rox1, 23&28-YPL062W, and 29&34-YJL064W) were used to confirm insertion of the GPDp(VDS)ADH1t DNA oligo by colony PCR. VDS expression DNA oligo + 500bp homology arms  $\approx$  3700bp. L, DNA ladder (GeneRuler 1kB Plus, Thermo Fisher); Neg, amplification from the 500bp upstream to the 500bp downstream homology arms of BTS1 =1000bp; Lanes 1-4, VDS insertion at the BTS1 site; Lanes 5-7, VDS insertion at the Rox1 site; Lanes 8-11, VDS insertion at the YPL062W site; Lanes 12-15, insertion at the YJL064W site.

## 3.5 Results and Discussions

### 3.5.1 Successive oxidation of valerenadiene to valerenic acid

To confirm the results of Nguyen et al. (Nguyen et al., 2019), we co-transformed the LsGAO1;AaPOR (**Figure 3.3, B**) and the VoVDS;VoVDS (**Figure 3.3, A**) vectors into chemically competent ZXB yeast cells, generating yeast lines that accumulated 11mg/L VLD and 1.7mg/L VA, as detected by GC-MS analysis (**Table 3.5**). For VA structural confirmation, we compared the EI mass spectra of an authentic, MSTFA + 1% TMCS derivatized 3ng VA standard (**Figure 3.7, Panel A**) with a derivatized organic extract (**Figure 3.7, Panel B**) from yeast co-transformed with the VDS and GAO vectors (**Figure 3.3, A&B**). Although our VA titers were nearly two times lower than reported by Nguyen et al. (Nguyen et al., 2019), our 16-18% conversion of VLD to VA was three to four times higher than the recently reported 2.9% to 3.6% within yeast microbial host systems (Nguyen et al., 2019; Wong et al., 2018), but slightly below 25% *in planta* (detected within Ricigliano et al.'s "VoVDS-1" hairy root line (Ricigliano et al., 2016)). Given the low titers of VLD and VA, but respectable VLD to VA conversion efficiency in the ZXB host system, we sought to compare the titers in yeast who had VDS expression cassettes inserted into their genomes at transcriptional safe loci using the CRISPR/Cas9-DNA repair model (**Figure 3.5**). We surmised if we could improve the VLD's titers to 50-60mg/L, then the concomitant VA titers would fall into the range of 9-11mg/L. Hence, a production platform for VA analogs yielding sufficient amounts (~10 mg) of constrained acid analogs for subsequent biological testing might be realized (**Figure 3.1**).

**Table 3.5** Valerenadiene (VLD) and valerenic acid (VA) titers from plasmids transformed into ZXB

Yeast Line	Transformed Plasmids	VLD Titers <sup>a</sup>	VA Titers <sup>a</sup>	% VLD Converted
ZXB	xLEU:VDS;VDS xHIS:GAO;POR	11.1 ± 1.8	1.7 ± 0.2	15.3 ± 0.2

<sup>a</sup>Titers represent the averages from four independent yeast colonies, mg/L ± SEM.

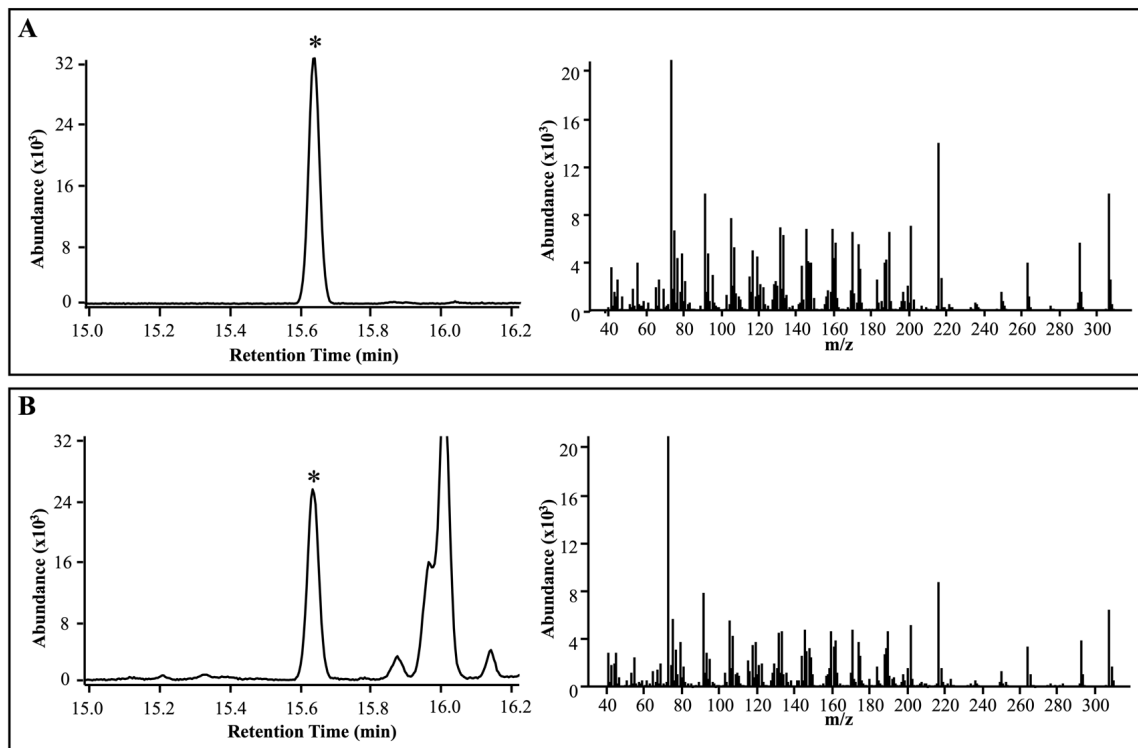


**Figure 3.7** Retention time and EI mass spectral validation of bona fide valerenic acid (VA) (Panel B) produced within ZXB transformed with the constructs shown in Figure 3.3, A&B compared to the 3ng of a valerenic acid standard (Panel A). \*Denotes the VA peak. Both samples were dried completely under nitrogen and subjected to MSTFA + 1% TMCS derivatization for 60min at 50°C. 1 $\mu$ L aliquots were then injected on a 7890 Agilent GC tandem arrayed to a 5975C EI-MS for separation (left panels) and detection (right panels).

### 3.5.2 Improvement in valerenadiene yeast titers using CRISPR/Cas9

The Chappell lab recently adopted the re-purposed CRISPR (Clustered Interspaced Palindromic Repeats)/Cas9 (Crispr-associated protein 9) bacteriophage defense system (Cong et al., 2013; DiCarlo et al., 2013; Jinek et al., 2012) optimized for yeast genome editing (DiCarlo et al., 2013; Jakociunas et al., 2015; Ryan & Cate, 2014; Ryan et al., 2014) to produce upwards of 500mg/L of triterpenes (Tateno et al., 2020) within our ZX strain (Zhuang & Chappell, 2015). Following the work of Tateno et. al. (Tateno et al., 2020), we simultaneously knocked out and inserted single copies of a GPD promoter driven VDS expression cassettes (**Figure 3.4, C**) at four unique genomic loci: *BTS1* (Verwaal et al., 2007), *Rox1* (Henry et al., 2002), *YPL062W* (Chen et al., 2019), and *YJL064W* (Jakociunas et al., 2015). Jakočiūnas et. al (Jakociunas et al., 2015) previously reported these genes encode for proteins which perturb the carbon flux through the mevalonate pathway. For example, Özyaydın et. al. discovered a *YJL064W* yeast knockout line increased their terpene titers 40-fold in shake flasks compared to the wildtype strain (Özyaydın et al., 2013). The GZyBTS1, GZyRox1, GZyYPL062W, & GZyYJL064W yeast lines were generated by inserting single copies of a GPDp-VDS-ADH1t DNA oligo into the *BTS1*, *Rox1*, *YPL062W*, & *YPL064W* loci found within the ZXB parental line using a multiplexed CRISPR/Cas9- DNA repair template method as described by Jakociunas et. al. (Jakociunas et al., 2015). Colonies, with correct insertion of the VDS expression construct (**Figure 3.6**), were subjected to chemical analysis and VLD titers estimated from a hexadecane standard. The GzyRox1 (18mg/L), GZyYJL064W (19mg/L), and GZyYPL062W (23mg/L) yeast lines nearly doubled the VLD titers achieved using the plasmid based VDS expression system (11mg/L) (**Table 3.6**). On the other hand, when we integrated a single copy of the

GPDp-VDS-ADH1t oligo into the *BTS1* genomic locus, we observed similar VLD titers compared with yeast transformed with a plasmid harboring two copies of the VDS gene (**Figure 3.3, A**) expressed from distinct independent promoters (10mg/L vs. 11mg/L, respectively) (**Table 3.6**). These results may suggest, deletion of yeast loci that encode for proteins which negatively repress gene expression of enzymes involved in the MVA pathway or inversely regulate the available acetyl-CoA substrate pool (i.e., *YPL062W*) is a productive metabolic engineering strategy for increasing VLD titers in yeast.



**Table 3.6** VLD titers from plasmid expression of VDS vs. chromosomal insertion within ZXB

Yeast Line	VDS cDNA Expression	VLD Titers <sup>a</sup>	Statistical Significance
ZXB	plasmid	11.1 ± 1.8 <sup>b</sup>	-
GZyBTS1	integrated	10.1 ± 2.3 <sup>c</sup>	No
GZyRox1	integrated	17.7 ± 0.2 <sup>c</sup>	No
GZyYPL062W	integrated	22.6 ± 1.5 <sup>c</sup>	Yes**
GZyYJL064W	integrated	19.0 ± 0.7 <sup>c</sup>	Yes*

<sup>a</sup>Titers represent the averages from either 2<sup>c</sup> or 4<sup>b</sup> independent yeast colonies, mg/L ± SEM. A one-way ANOVA was performed using the Dunnett's multiple comparison between the VLD titers from plasmid expression of the VDS gene under divergent, independent promoters vs. single-copy chromosomal integration. \*P value = 0.0472; \*\*P value = 0.0079.

### 3.6 Conclusions

Recently, Wong et. al. (Wong et al., 2018) reported achieving 140mg/L of VLD, the highest titers to date produced within a genetically modified yeast line with four copies of a galactose inducible VDS expression construct inserted into transcriptionally active chromosomal loci (Reider Apel et al., 2017). Yet, their VLD to VA conversion percentage was less than 3% after combinatorially pairing a candidate cytochrome P450 cloned from *V. officinalis* with the alcohol and aldehyde dehydrogenases from the artemisinin biosynthetic pathway (Paddon et al., 2013). Wong et. al.'s results would suggest simply increasing VLD concentrations in the cytosol may not correlate to enhanced cytochrome P450-mediated VLD to VA conversion efficiencies. An alternative interpretation to Wong et. al.'s low VLD to VA conversion efficiency may be the overexpressed candidate P450's kinetic parameters were submaximal (i.e., poor substrate affinity for VLD and/or low catalytic turnover rate), a theory which cannot be ruled out. Hence, a three-pronged metabolic engineering strategy should be highly considered to increase the downstream titers of VA – improving cytosolic VLD concentrations by increasing VDS expression levels, exploring ways to improve the protein-protein coupling efficiency between VDS and its endomembrane-bound tailoring enzyme(s), while considering ways to enhance the paired P450s' substrate affinity and turnover rate (i.e., using directed evolution (Hammer et al., 2017; Takahashi, Yeo, Zhao, et al., 2007))

## CHAPTER 4. ESTABLISHING & VALIDATING A HUMAN CELL LINE-BASED FLUORESCENCE ASSAY FOR MODULATION OF THE HUMAN GABA<sub>A</sub> $\alpha 1\beta 3\gamma 2L$ RECEPTOR

### 4.1 Introduction

Developed in 1976 by Neher and Sakmann, single channel recordings of cellular membranes expressing ionic channels revolutionized the field of neurophysiology, allowing researchers to understand and characterize functional excitable neurons (Hamill et al., 1981; Neher & Sakmann, 1976; Neher et al., 1978). This technology was applied to transiently expressed GABA<sub>A</sub> receptors in 1987 by Schofield et al., who proposed GABA<sub>A</sub> receptors are part of the ligand-ion superfamily with each subunit containing four transmembrane domains, forming a selective pore for chloride ions to passively pass through (Pritchett et al., 1988; Schofield et al., 1987). Schofield and company pioneered the patch-clamp technique establishing it as the “gold standard” for future work in functionally characterizing GABA<sub>A</sub> receptors’ role(s) as the fundamental inhibitory pathway in the central nervous system (Angelotti et al., 1993; Benke et al., 2009; Jacob et al., 2005; Jurd et al., 2003; Karim et al., 2013; Klausberger et al., 2001; Low et al., 2000; Luger et al., 2015; Miller & Aricescu, 2014; Succol et al., 2012; Tretter et al., 1997). Though patch-clamping is a useful research tool to the field of drug discovery, it naturally doesn’t bode well for screening libraries of chemistries for their potential neuropharmacological activities in an expedient manner (i.e. – less than two weeks) (Obergrussberger et al., 2021). Hence, to streamline ion channel drug discovery, researchers have optimized fluorescent probes as a way to measure the activity level of membrane-bound ion channels (Baxter et al., 2002; Fiala et al., 2020; Joesch et al., 2008). This has afforded pharmaceutical drug researchers the opportunity to screen through

libraries of compounds within a matter of weeks, as opposed to months associated the more traditional screening methodologies, such as patch-clamping (Neher & Sakmann, 1976). The class of molecules are typically grouped together based upon their reporting mechanisms, however; all fall under the more broad category as voltage-sensitive dyes (VSDs) (Cohen & Salzberg, 1978). One fluorescent dye in particular, DiSBAC<sub>13</sub> (**Figure 4.1, Structure G**), naturally partitions across a living cell's semi-permeable membrane in a voltage dependent manner (Baxter et al., 2002; Joesch et al., 2008). When a living cell's membrane is depolarized due to flux of chloride ions through a recombinant GABA<sub>A</sub> receptor, the DiSBAC<sub>13</sub> molecules separate from the membrane impermeable quencher and move into the phospholipid bilayer, thus becoming available for excitation under visible light at  $\lambda_{525\text{nm}}$ , capturable with an emission filter set to  $\lambda_{595\text{nm}}$  on a fluorescent plate reader (**Figure 4.2, B**). The net change in fluorescence reflects the level of affinity (or potency) and stimulation (or efficacy) of a given compound in a concentration-dependent manner for a recombinantly expressed ion channel at the cell surface (Figure 4.2, C).

In the following body of work, the FMP Red dye assay was assessed for its utility to detect the varying levels of potencies and efficacies from chemistries with known and unknown activity for the human GABA<sub>A</sub> receptor (**Figure 4.1, Structures A - F**). Such an assay, if suitably validated, would afford investigators the ability to have a rapid and selective screening tool for combing through libraries of compounds in search of novel chemistries with potentiation activity for the human GABA<sub>A</sub> ( $\alpha 1\beta 3\gamma 2L$ ) receptor. More specifically, we aimed to evaluate the FMP Red dye assay as a screening paradigm for the evaluation of chemically constrained VA analogs, which we hope can be produced and

purified from the yeast production platform described in Chapter 3 (**CHAPTER 3**) of this dissertation.

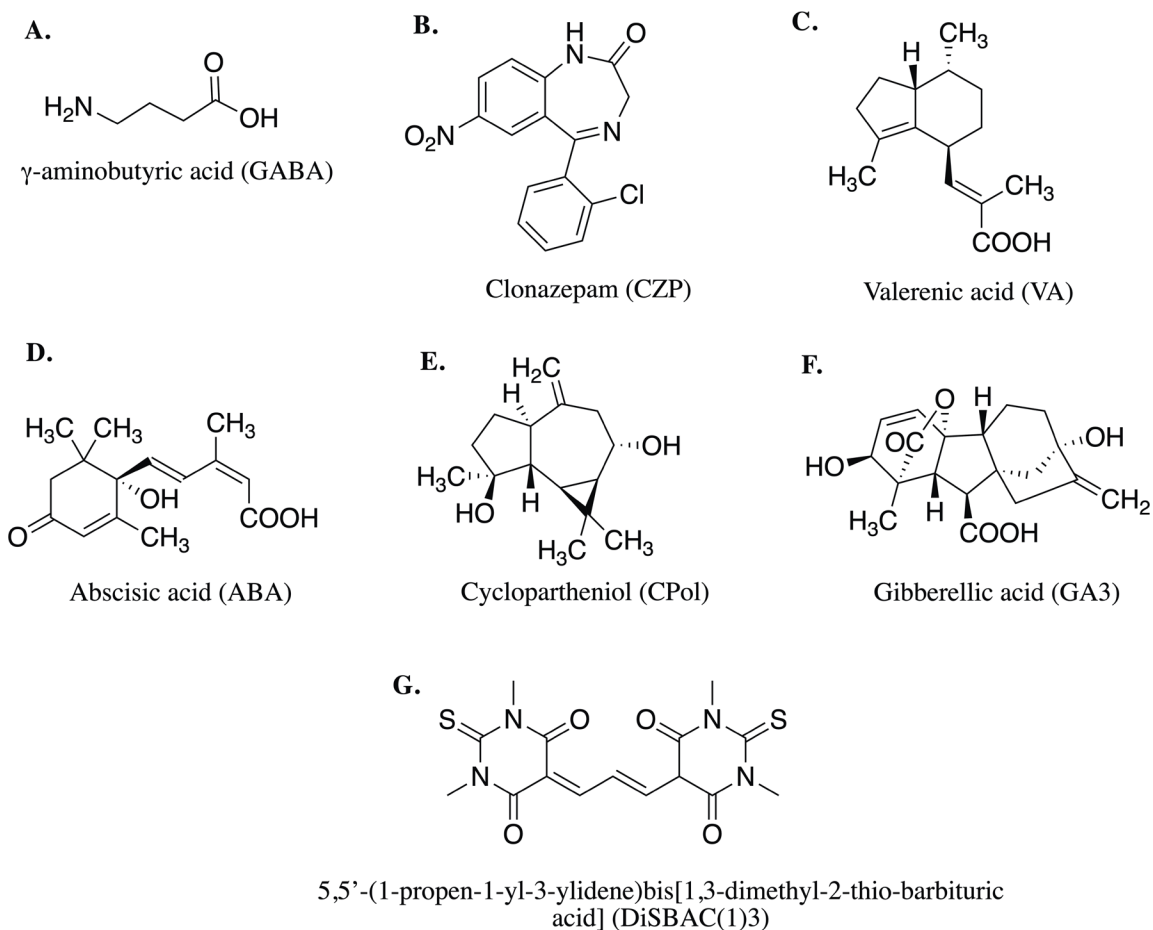


**Figure 4.1** Compounds A-C were used to validate the FMP Red Dye assay for its sensitive and high-throughput capabilities as a drug discovery screening tool for novel GABA<sub>A</sub> receptor (allosteric) modulators (Nik et al., 2017). Compounds D-F were included as experimental controls to evaluate the structural specificity at VA's putative binding site(s) on the TM2 domain within the  $\beta_3$  subunit of the human GABA<sub>A</sub> receptor (Benke et al., 2009; Luger et al., 2015). Compound G is the elucidated structure of the fluorescent probe commercially sold as FMP-Red dye by Molecular Devices (Nik et al., 2017).

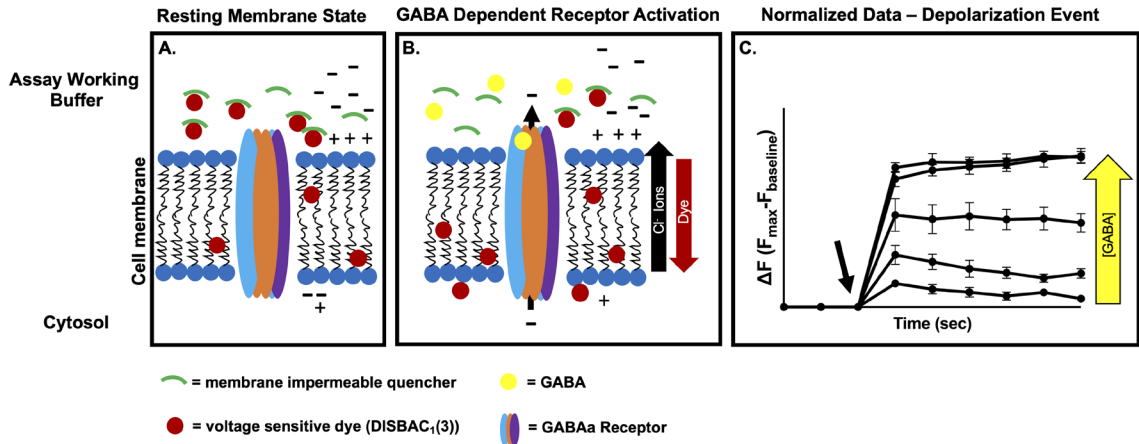


**Figure 4.2** Conceptualization of the FMP Red Dye assay used to identify novel modulators of the human GABA<sub>A</sub> receptor. A) When the FMP red dye (DiSBAC<sub>1</sub>(3)(Nik et al., 2017), red filled circles) is added to the outside of living cell's, a portion (approximately 25%) of the DiSBAC<sub>1</sub>(3) molecules separate from the membrane impermeable quencher (green arcs, masking dye meant to block the excitation of the DiSBAC<sub>1</sub>(3) molecules without interfering with the cell's biological processes) and intercalate into the phospholipid bilayer in a voltage dependent manner (Baxter et al., 2002). Only unquenched DISBAC<sub>1</sub>(3) molecules are excitable under visible light at  $\lambda_{525\text{nm}}$ , capturable with an emission filter set to  $\lambda_{595\text{nm}}$ . B) In the presence of FMP Red dye molecules, exogenously added GABA (yellow filled circles) binds at the interface of the  $\alpha$  &  $\beta$  subunits (orange & blue ovals, respectively), shifting the GABA<sub>A</sub> receptor from a "closed" to an "open" state (Karim et al., 2013; Miller & Aricescu, 2014), concomitantly permitting chloride ions to efflux out of the cytosol, against their concentration gradient, depolarizing the cell membrane. At the same time, partially negative DISBAC<sub>1</sub>(3) molecules separate from the membrane impermeable quencher and move into (or even through) the plasma membrane, increasing the fluorescence signal detected from inside the cell (Joesch et al., 2008; Nik et al., 2017). C) The net change in fluorescence ( $\Delta F$ ) is linear with respect to the concentration of bound GABA molecules and follows the typical dose-response behavior, eventually reaching the maximal effect once all surface-expressing GABA<sub>A</sub> receptors are occupied by GABA (Goodman et al., 2011). Normalized fluorescent traces were calculated from subtracting the average of three baseline readings taken prior to the addition of GABA (indicated by the black arrow) from the raw fluorescent values after the addition of GABA.

## 4.2 Materials and Methods

### 4.2.1 Chemicals and reagents

Cyclopartheniol (CPol) was originally synthesized by Dr. Michel Crevoisier at the University of Berne (Berne, Switzerland) (Crevoisier et al., 1984) and was a gift from Dr. Robert Coates at the University of Illinois (Urbana, IL). Gamma aminobutyric acid (GABA) (Cat# A2129), clonazepam (CZP) (Cat# C1277), 2-cis,4-trans-abscisic acid (ABA) (Cat# 862169), gibberellic acid (GA3) (Cat# 48880), and molecular biology grade HEPES (Cat# H4034) were purchased through Sigma Aldrich (St. Louis, MO). Valerenic acid (VA) (Cat# 3801S) was purchased as lyophilized powder through Extrasynthese (Genay, France) and kept at -20°C upon receipt. High-purity dimethyl sulfoxide (DMSO) (Cat# 97063-136) was purchased through the third-party supplier Avantor (Radnor, PA). The FLIPR Membrane Potential (FMP red dye), which included the membrane impermeable quencher, was purchased through Molecular Devices (San Jose, CA) (Cat # R8126) as a freeze-dried powder and kept in the dark at -20°C upon receipt.

### 4.2.2 Culturing wildtype HEK293 cells

HEK293 cells (ATCC# CRL-1573) were a gift from Dr. Daniel Pack (University of Kentucky). Frozen vials of cells were thawed and expanded in Dulbecco's modified Eagle's medium (Corning) and 5% fetal bovine serum (Corning or VWR) at 37°C in 5% CO<sub>2</sub>. When cells reached 70-80% confluency, they were harvested using 0.05% trypsin-EDTA and 1.0-2.0 x 10<sup>6</sup> cells were placed into a new, sterile T-75 flask. Passage numbers



used in this study were from 10-20. Twenty-four hours prior to the FMP RED Dye assay, naïve HEK293 cells were harvested, counted, and seeded in a 96-well black well, clear bottom imaging plates (Falcon) at 50,000-60,000 cells/well in 100 $\mu$ L of growth media. The cells were allowed to adhere for 24hrs.

#### 4.2.3 Culturing transfected HEK293 cells

On day zero, 2,500,000 naïve HEK293 cells were seeded into a 10 cm<sup>2</sup> sterile, cell culture treated dish in Dulbecco's modified media (DMEM) + 5% fetal bovine serum (FBS) (growth media). The following day (day one), the cells were transfected using Lipofectamine 3000 (Invitrogen) with equal amounts (4.8 $\mu$ g/plasmid) of the pcDNA3.1(+)-bovine GABA<sub>A</sub> ( $\alpha$ 1), pcDNA3.1(+)-human GABAA ( $\beta$ 3), and pcDNA3.1(+)-human GABAA ( $\gamma$ 2L) plasmids, following the manufacturer's recommendations. It should be noted, the bovine GABAA  $\alpha$ 1 subunit differs only in the signal peptide with the human GABAA  $\alpha$ 1 subunit, the mature peptides are identical (Dostalova et al., 2014). The cells were placed back at 37°C in 5% CO<sub>2</sub> to recover for twenty-four hours. The following day (day 2), the transfected cells were harvested, counted, and seeded into a 96-well black well, clear bottom imaging plate (Falcon) at 50,000-60,000 cells/well in 100 $\mu$ L in growth media. The cells were allowed to attach for 24hrs. Passages used in this study were 11-20. The bovine and human GABA<sub>A</sub> receptor plasmids were a generous gift from Dr. Stuart Forman, Massachusetts General Hospital. Before transfection experiments, the GABA<sub>A</sub> -  $\alpha$ 1 /  $\beta$ 3 /  $\gamma$ 2L subunit sequences were verified by sanger sequencing (UK HealthCare Genomics Core Laboratory) using a CMV promoter forward and a bGH poly-A termination signal

reverse sequencing primer. The DNA coding sequences matched the NCBI GenBank references: CAA29189.1 (bovine GABRA1); NP\_068712.1 (human GABRB3 mRNA transcript 2); NP\_944494.1 (human GABRG2 mRNA transcript 1).

For experiments examining the statistical reliability of the HEK 293 cells expressing the three expression vectors, three 10cm dishes were seeded with wildtype HEK293 cells, then transfected the next day with three separate preparations of the Lipofectamine 3000 (Invitrogen) mixed with 4.8 $\mu$ g of each  $\alpha_1$ ,  $\beta_3$ , &  $\gamma_{2L}$  human GABA<sub>A</sub> receptor expression vectors. Care was taken to ensure the three, independently transfected HEK293 cell lines were kept separated to preserve their biological heterogeneity. Similar experimental design was used to examine the reliability of independently prepared expression vector DNA and for experiments examining the ratios of the 3 vectors used in the transfections. The vector ratios tested included 1:1:1, 2:2:1 and 1:1:10 with the amount of each vector DNA being adjusted to not exceed the total DNA amount of 14.4  $\mu$ g.

#### 4.2.4 Culturing HEK293 cells stably expressing human GABA<sub>A</sub> receptors

HEK293 cells stably expressing the human GABA<sub>A</sub>  $\alpha_1\beta_3\gamma_2$  subunits (CYL3053 PrecISION hGABA-A  $\alpha_1/\beta_3/\gamma_2$ -HEK Recombinant Cell Line) was a generous gift from Dr. Isaac Pessah (University of California). Upon arrival, cells were expanded in Dulbecco's modified Eagle's medium, 10% fetal bovine serum, and 1% penicillin-streptomycin at 37°C in 5% CO<sub>2</sub>. To maintain pressure for cells that only express the human GABA<sub>A</sub>  $\alpha_1\beta_3\gamma_2$  subunits, 400  $\mu$ g/mL G418, 100  $\mu$ g/mL hygromycin B, 0.625 $\mu$ g/mL puromycin was added to the growth media. When cells reached 70-80%

confluency, they were harvested using 0.05% trypsin-EDTA and  $1.0\text{-}2.0 \times 10^6$  cells were placed into a new, sterile T-75 flask. Passage numbers used in this study were 10-15. Twenty-four hours prior to the FMP RED Dye Assay, the cells were trypsinized, collected by centrifugation, counted by trypan blue exclusion, and seeded in a 96-well black well, clear bottom imaging plate (Falcon) at 50,000-60,000 cells/well in  $100\mu\text{L}$  of growth media. The plate was placed back in the incubator for an additional 24hrs.

#### 4.2.5 FMP RED dye assay 96 well plate preparation

The morning of the assay, a single 96-well imaging plate was removed from the incubator and the growth media was removed by a swift, jerking-motion. The media replaced with  $100\mu\text{L}$  of the Assay Working Buffer #2 (Hank's Balanced Salt Solution buffered with 20mM HEPES pH 7.2-7.4 + 0.05% DMSO), hereafter referred to as AWB #2. Cells were incubated for an additional 3-5min to allow for equilibration. Afterwards, 1 vial of the red membrane potential dye was thoroughly reconstituted with 10.4 mL AWB #2.  $100\mu\text{L}$  of the FMP-Red-Dye solution was added to each well by an 8-well multichannel pipet. The plate was then transferred to a CLARIOstar multimode plate reader (BMG Labtech) and allowed to incubate for 30-40 min to allow for dye penetration and to minimize the potential photodynamic effects of the voltage-sensitive dye (Mennerick et al., 2010).

#### 4.2.6 CLARIOstar optical settings and run mode

Before the assay began, the bottom optic eye was calibrated its optimal positioning. This ranged from 3.6 to 3.8 for each plate. The gain on the photomultiplier tube was set to 1450 for each study. Each well's response was recorded via orbital averaging (2mm); the dye was excited at 510-540nm, and fluorescent signals were recorded at an emission wavelength window of 566-625nm. Baseline recordings were acquired for eight wells successively over 15sec (3 cycles total, 35 flashes/well, 5 sec total cycle time) in plate kinetic mode. The plate was ejected and 50  $\mu$ L of the either the AWB #2 (vehicle control) or a 5x experimental compound was simultaneously added to eight wells using an 8-channel pipettor. Responses were recorded within 14 sec of the addition to the well (instrument delay time in positioning plate) for a total of 60 sec (12 cycles total, 35 flashes/well, 5 sec total cycle time). Individual well responses were calculated as follows:  $\Delta F = F_{\max} - F_{\text{baseline}}$ , where the  $F_{\max}$  was the maximum response in arbitrary fluorescence units (AFU's) observed after addition of the AWB #2 or a 5x stock of the experimental compound and  $F_{\text{baseline}}$  was the average fluorescence before the AWB #2 or a 5x stock of the experimental compound was added. For comparison of each compound's ability to directly activate the recombinant hGABA<sub>A</sub> receptors, dose-response curves were generated by plotting the observed  $\Delta F$  for each compound vs. the final compound concentration (nM) in the well.

#### 4.2.7 Immunoblot confirmation of the $\alpha_1$ , $\beta_3$ , & $\gamma_{2L}$ human GABA<sub>A</sub> subunit total expression in transfected naïve HEK293 whole cell lysates

2.5-3.0 x10<sup>6</sup> naïve HEK293 cells were seeded in two, sterile 10cm tissue culture treated petri dishes and transfected with plasmids harboring the cDNA of the human GABA<sub>A</sub> receptor  $\alpha_1$ ,  $\beta_3$ , and  $\gamma_{2L}$  subunits under the cytomegalovirus promoter (CMV) using Lipofectamine 3000 (Invitrogen), as described above. Forty-eight hours after transfection, the cells were washed twice with 5 mL of PBS (4°C) and subsequently, lysed with 0.5 -1.0 mL of 4°C RIPA Buffer (Thermo Fisher) for 5min on ice. The lysed cellular debris was collected into a sterile, 1.5 mL Eppendorf tube and pelleted by centrifugation (16,000 x g in a 4°C cold room). The supernatant was transferred to a new, sterile 1.5 mL Eppendorf tube and total protein amounts was estimated using a bovine serum albumin standard curve with the Pierce BCA Protein Assay kit (Thermo Fisher). 1, 5 & 15  $\mu$ g of the total protein from the transfected hGABAAR ( $\alpha_1$   $\beta_3$   $\gamma_{2L}$ ) HEK293 cells were diluted in 4X SDS-PAGE Loading Buffer (250mM Tris-HCl (pH 6.8), 8% SDS, 0.2% bromophenol blue, 40% glycerol, 20%  $\beta$ -mercaptoethanol), denatured in a water bath at 95°C for 5min, centrifuged at 10,000 xg for 5min at 23°C, then loaded and separated on an 8% SDS-PAGE gel. Proteins were transferred to a methanol pre-soaked PVDF membrane at 4°C for one hour. The membrane was subsequently blocked with a 5% dry milk buffer (TBST (20mM Tris-HCl (pH 7.6), 150mM NaCl + 0.1% Tween 20) for one hour at 23°C, then incubated with the appropriate primary antibody overnight, shaking at 4°C. The following day, the unbound primary antibody solution was discarded, and the membrane was washed three times in five-minute intervals with TBST. Secondary antibodies conjugated to HRP diluted in blocking buffer were then added to the appropriate

membranes and incubated while rocking at 23°C for one hour. The blots were washed again as described above with TBST. For chemiluminescent detection, blots were incubated for 5-10min with the working solution from the SuperSignal West Pico Plus Chemiluminescent Substrate kit (Thermo Fisher) and developed on x-ray film in a dark room (**Figure 4.3**).

For whole-cell lysate analysis of expression of the hGABA<sub>A</sub> receptor, we used an anti- $\alpha_1$  (1:500, Invitrogen, Cat# PA563170, rabbit), anti- $\beta_3$  (1:2000, BioLegend, Cat# 818501, mouse), anti- $\gamma_{2L}$  (1:1000, Abnova, Cat# PAB18556, goat), anti-GAPDH (1:10000, Invitrogen, Cat# TAB1001, rabbit). The goat anti-rabbit (IgG) horseradish peroxidase (HRP) conjugated secondary antibody used to identify the  $\alpha_1$  and GAPDH proteins (1:20000, Invitrogen, Cat#31460). A goat anti – mouse (IgG) conjugated to an HRP tag was used to identify the  $\beta_3$  human GABA<sub>A</sub> subunit (1:20000, KPL, Cat# 5450-0011). The  $\gamma_2$  GABA<sub>A</sub> subunit long isoform was detected with a rabbit anti-goat(IgG)-HRP secondary antibody (1:20000, Invitrogen, Cat# A27014).

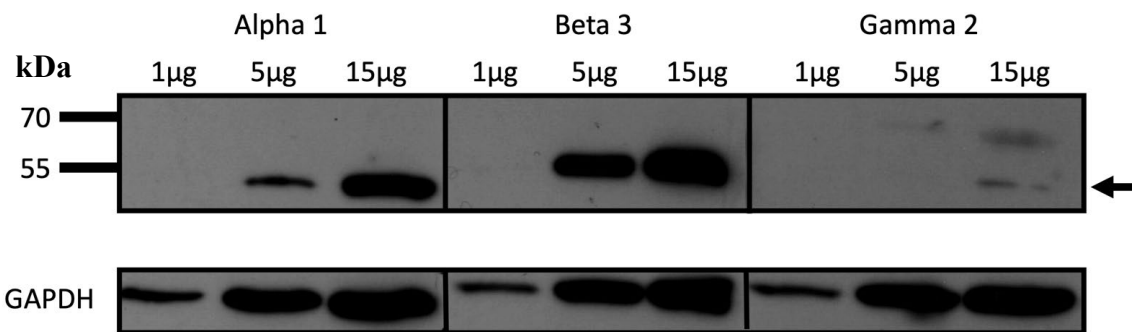


**Figure 4.3** Chemiluminescent blot showing immunodetection of the  $\alpha_1$ ,  $\beta_3$ ,  $\gamma_{2L}$  human GABA<sub>A</sub> receptor subunits from whole cell lysates of HEK293 (ATCC# CRL-1573) cells transfected with Lipofectamine 3000 and equal amounts (4.8  $\mu$ g/plasmid) of the pcDNA3.1- bovine alpha 1, human beta 3, and human gamma 2L expression vectors. Antibodies used for detection were  $\alpha_1$ , anti- $\alpha_1$ ;  $\beta_3$ , anti- $\beta_3$ ;  $\gamma_{2L}$ , anti- $\gamma_{2L}$ . The black arrow (top right panel) corresponds to the correct  $\gamma_{2L}$  band size at  $\approx 54$  kDa. Loading control: GAPDH, glyceraldehyde-3-phosphate dehydrogenase.

#### 4.2.8 Data analysis parameters

Log(concentration)-dependent response curves were generated (**Figure 4.4**) and statistical analyzed using the GraphPad Prism software v.9. The potency, or EC<sub>50</sub>, values were determined using the nonlinear regression mathematical formula with a four-parameter logistic equation within GraphPad Prism (**Equation 4.1**). Data are presented as the mean  $\pm$  SEM from three biological or technical triplicates (stable cell line only). Unpaired Student's t-tests were applied to look for statistical differences within the potency and efficacy means of GABA, CZP, and VA treatments between the transient and stable GABA<sub>A</sub> receptor cell lines. The uncorrected Fisher's Least Significant Differences (LSD) tests were applied to evaluate the statistical differences between the potency and efficacy means of GABA, CZP, and VA treatments across HEK293 cells transfected with variable ratios of the plasmids encoding the  $\alpha_1$ ,  $\beta_3$ , &  $\gamma_{2L}$  subunits, 1:1:1, 2:2:1 and 1:1:10.



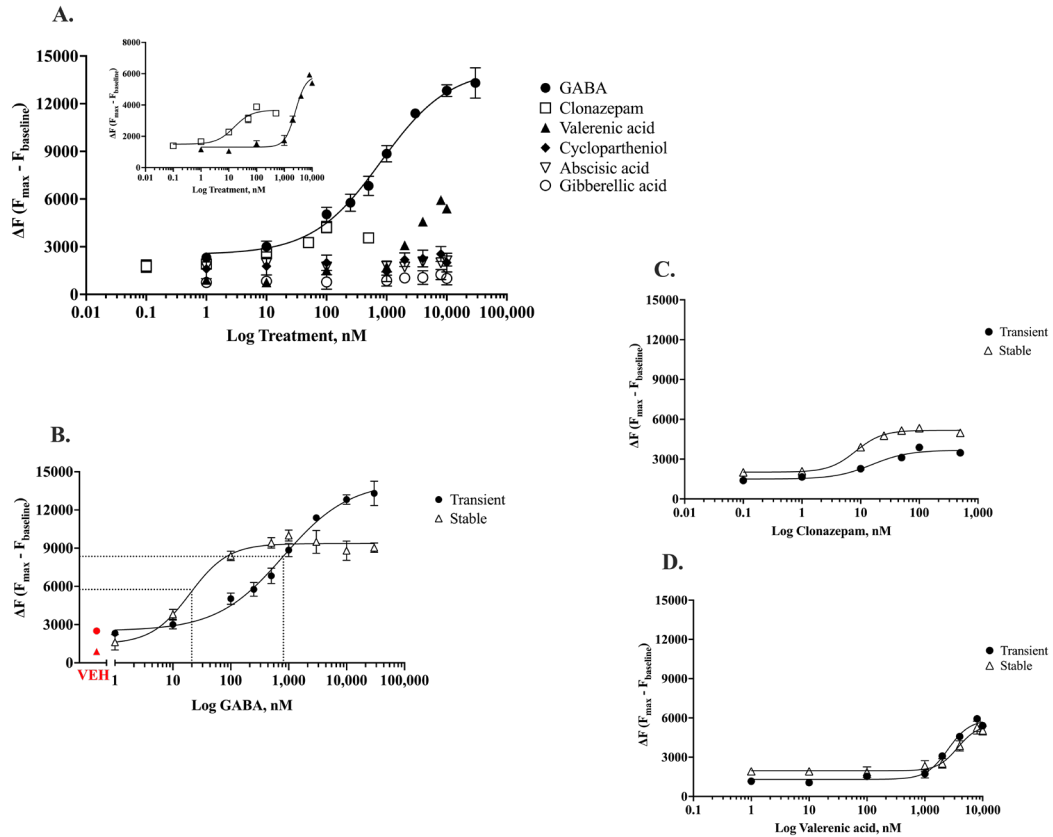


**Figure 4.4.** A) Transiently expressing human GABA<sub>A</sub> ( $\alpha_1$ ,  $\beta_3$ ,  $\gamma_{2L}$ ) receptor HEK293 cells were challenged separately with 0.1 to 30,000nM of GABA, Clonazepam (CZP), Valerenic acid (VA), Cyclopartheniol (CPol), Absciscic acid (ABA), and Gibberellic acid (GA3). The net change in fluorescence ( $\Delta F = F_{max} - F_{baseline}$ ) from three independently transfected wells were averaged and plotted against the final in-well concentration for each drug/compound treatment. The fitted sigmoidal curve (solid black line) is shown for the (●) GABA concentration-dependent response. (inset) Besides GABA, only (□) CZP and (▲)VA generated measurable responses above baseline. B) GABA was 40-fold more potent (19.6 nM vs. 808 nM), but 1.5 times less efficacious in HEK293 cells (Δ) stably vs. (●) transiently expressing the hGABA<sub>A</sub> ( $\alpha_1$ ,  $\beta_3$ , &  $\gamma_{2L}$ ) receptors. The intersection of the black dotted lines denotes the calculated potency ( $EC_{50}$ ) value for each cell line. Exposure to the vehicle control (VEH, AWB#2) resulted in  $\Delta F$ 's equivalent or below 1nM of GABA for the (●) transient and (▲) stable GABA<sub>A</sub> receptor cell lines. C) For CZP, potency (8.2nM vs.15.6nM) and efficacy (5332 AFUs vs. 3880 AFUs) were nearly two times and 1.4 times greater for (Δ) stably vs. (●) transiently expressing hGABA<sub>A</sub> receptor HEK293 cell lines, respectively. D) The (Δ) stably vs. (●) transiently expressing hGABA<sub>A</sub> receptor HEK293 cell lines exhibited non-statistically different potencies (3687nM vs. 2502nM) and efficacies (5255AFUs vs. 5935AFUs) to VA challenge.

$$Response = bottom + \frac{(top - bottom)}{1 + 10^{(LogEC_{50} - x)n}}$$

**Equation 4.1** The four parameter, non-linear regression formula was used to fit concentration-dependent response curves through the normalized fluorescent responses of the transient and stable HEK293 cell lines treated with 0.1 – 30,000nM of GABA, CZP, VA, ABA, CPol, & GA3 (**Figure 4.4**) for estimating the average potency and efficacy values of the “active” treatments. Where the response refers to the measured output from a perturbed biological system; bottom, the lowest observed response; top, the greatest observed response; EC<sub>50</sub>, the agonist (drug) concentration which elicits 50% of the response between the top and bottom boundaries; x, concentration of the drug/compound; *n*, hill slope – steepness of the sigmoidal-shaped log (concentration) response curve, standard value is 1.0.

## 4.3 Results and Discussion

### 4.3.1 Validating heterologously expressed human GABA<sub>A</sub> ( $\alpha_1$ , $\beta_3$ , $\gamma_{2L}$ ) receptors display GABA concentration-dependance within the confines of the FMP Red Dye activity assay

The initial set of experiments were designed to validate the construction of the fluorescence-based drug discovery platform within HEK293 cells (**Figure 4.4**), which would allow corollary evidence to the more laborious patch-clamping studies considered the gold-standard for measuring perturbations to an ion channel's physiology (Neher & Sakmann, 1976) and allow for more rapid screening of chemical libraries for novel allosteric modulators of the human GABA<sub>A</sub> ( $\alpha_1$ ,  $\beta_3$ ,  $\gamma_{2L}$ ) receptor. To substantiate our experimental protocol and ensure the CLARIOstar's optical settings were optimized for the DiSBAC<sub>1</sub>(3)'s 525nm excitation and 595nm emission wavelengths, we treated the stably expressing human GABA<sub>A</sub> receptor HEK293 cell line cells with eight concentrations of GABA (1-30,000nM). In parallel, naïve HEK293 cells were treated with 1000nM of GABA and exhibited minimal net increases in their fluorescent responses (less than 1000 AFUs), which were within the background or baseline recordings of the instrument (**Figure 4.5**). When the average normalized responses from three biologically equivalent wells are plotted on a log (concentration)-response curve and a graded dose-response curve, using the four parameter, non-linear regression equation (**Equation 4.1**), fitted through all of the data points, a classical, sigmodal-shaped dose response curve (**Figure 4.4., B**) (Goodman et al., 2011) was observed. The GABA EC<sub>50</sub> determination is reported in **Table 4.1**. When the GABA's EC<sub>50</sub> value determined here is compared to that of the Pessah research groups (Nik et al., 2017), the GABA potency was two times greater

in our hands (19.6nM vs. 40.0nM, respectively) (**Table 4.1**). Interestingly, the GABA potencies difference were statistically significant by the unpaired Student's t-test ( $p < 0.05$ ); however, this didn't account for outside sources of variation such as the quality of the reagents, differences in detectors' fluorescent dye sensitivity, and the overall fitness of cell line. All of which are imperative parameters to consider while interpreting results from validated mammalian cell-based drug discovery high-throughput assays, as specifically outlined by the *Assay Guidance Manual* (Markossian et al., 2004). Therefore, up to 20% variation between the reported results from two independent research groups is acceptable within the context of validating a high-throughput cell-based *in vitro* assay.

GABA's 30nM<sup>3</sup> average potency (determined using the FMP Red Dye) was 300 – 1200 fold greater than the potencies reported through patch-clamping of HEK293 cells recombinantly expressing the same GABA<sub>A</sub> subunits ( $\alpha_1$ ,  $\beta_3$ , &  $\gamma_{2L}$ ) (6,670nM (Nik et al., 2017); 36,000nM (Dostalova et al., 2014)). This may likely suggest the voltage-sensitive DiSBAC<sub>1</sub>(3) dye within the FMP assay is intrinsically more sensitive in detecting small voltage changes across the cell's plasma membrane in comparison with whole-cell patch-clamping techniques. An alternative and more widely discussed explanation in the scientific literature is that the DiSBAC<sub>1</sub>(3) structure (**Figure 4.1, Structure G**), along with the other members of the bis-oxonol slow response dye family, may bind directly at or near one or more of barbiturate's two binding sites (located at the interface of the  $\alpha - \beta$  &  $\gamma - \beta$  subunits (Kim et al., 2020)) allosterically potentiating the GABA<sub>A</sub> receptor (Mennerick et al., 2010; Nik et al., 2017; Wang et al., 2020). Consistent with this suggestion is the dual-

---

<sup>3</sup> Average of the EC<sub>50</sub> values from Chappell (19.6nM) and Pessah (40nM)

barbituric acid ring core structure (Nik et al., 2017). This anecdotal theory could rationally explain the greater GABA potencies observed by us and the Pessah research groups. A critical experiment to help resolve this theory would be to remove or perturb the barbiturate binding site(s) and re-evaluate GABA's potency. This could be accomplished by recombinant expression of the wildtype  $\beta_3$  subunit paired with the  $\alpha$ S270M &  $\gamma$ S280M mutated subunits, observed by Kim et.al. (Kim et al., 2020) to significantly lower phenobarbital's allosteric potentiation of the GABA<sub>A</sub> receptor.

Hence, GABA<sub>A</sub> receptor potentiation from novel allosteric modulators may also be masked by or arbitrarily inflated in the presence of the DiSBAC<sub>1</sub>(3) molecules, without proper control experiments in place such as, evaluating a range of the candidate concentrations in the presence and absence of a submaximal concentration of GABA. This was conducted by Nik et. al. (Nik et al., 2017), who demonstrated a panel of known PAM neurosteroids and benzodiazepines directly potentiate human GABA<sub>A</sub> receptors in the absence of GABA using the FMP Red Dye assay.

Fluorescent Responses of Naïve (gray) vs. HEK293 cells  
Transiently Expressing the Human GABA<sub>A</sub> receptor  $\alpha 1\beta 3\gamma 2L$   
subunits (orange) Exposed to 1000 nM of GABA

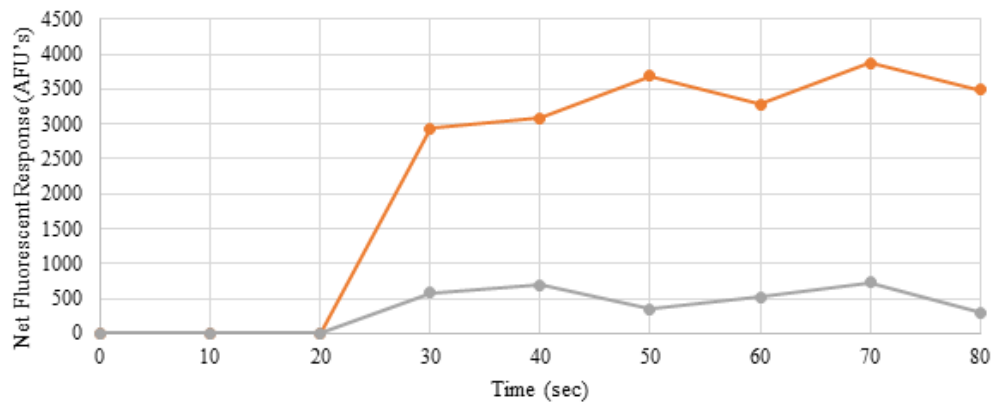


**Figure 4.5** Wildtype naïve HEK293 cells (gray line) were seeded at 50,000 – 60,000 cells/well in a 96 black well, clear bottom plate twenty-four hours prior measuring their responses to 1000 nM of exogenously supplied GABA using the FMP Red Dye assay. The maximum change in fluorescence of the naïve HEK293 cells (800 AFU at 70 sec) was about eight times less than HEK293 cells transfected with the human GABA<sub>A</sub>  $\alpha 1\beta 3\gamma 2L$  receptor (4000 AFUs at 70 sec). The response of both naïve and transfected HEK293 cells to the vehicle control (AWB #2) mirrored the response of the naïve HEK293 cells treated with 1000 nM GABA (not shown).

**Table 4.1** GABA potency for the CYL3053 PreciSION hGABA-A  $\alpha 1/\beta 3/\gamma 2$ -HEK Recombinant Cell Line independently observed by the Chappell and Pessah research groups using the FMP Red Dye assay.

<u>Treatment</u>	<u>Chappell lab</u> <sup>a</sup>	<u>Pessah lab</u> <sup>a,b</sup>
GABA	19.6 ± 6.1	40.0 ± 3.5

<sup>a</sup>Potencies are expressed as nM ± SEM; <sup>b</sup>The potency standard error the mean (SEM) was derived by dividing the reported standard deviation (11nM) by the square root of the sample size (10) (Nik et al., 2017)

#### 4.3.2 Recombinantly expressed GABA<sub>A</sub> ( $\alpha_1$ , $\beta_3$ , $\gamma_{2L}$ ) receptors are directly potentiated by GABA, CZP, & VA in a concentration dependent manner in the absence of GABA and in the presence of the FMP Red Dye

Having established a reproducible, transient human GABA<sub>A</sub> ( $\alpha_1$ ,  $\beta_3$ ,  $\gamma_{2L}$ ) receptor expression system in naïve HEK293 cells responsive to GABA potentiation, the next objective was to characterize the activities of chemistries with known mechanisms of action: clonazepam (CZP, an FDA-approved benzodiazepine approved to treat PD (Nardi et al., 2013)) and valerianic acid ((VA), a putative allosteric modulator of the human GABA<sub>A</sub> receptors (Benke et al., 2009; Khom et al., 2007; Khom et al., 2010) from *V. officinalis*' root system (Ricigliano et al., 2016; Yeo et al., 2013)). Equal amounts (4.8  $\mu$ g) of each plasmid DNA harboring the genes encoding for the  $\alpha_1$ ,  $\beta_3$ ,  $\gamma_{2L}$  subunits were transfected into naïve HEK393 cells (ATCC # CRL-1573), as described in **Section 4.2.3**, and qualitatively verified for the presence of the mature  $\alpha_1$ ,  $\beta_3$ ,  $\gamma_{2L}$  peptides in whole cell lysates 48 h post-transfection by western blotting (**Figure 4.3**). We hypothesized the protein expression levels for the  $\alpha_1$ : $\beta_3$ : $\gamma_{2L}$  subunits would align with the canonical 2:2:1 subunit composition ratio, an established observation made for heterologous expression of synaptic GABA<sub>A</sub> receptors (Angelotti et al., 1993; Baumann et al., 2003; Jacob et al., 2008). However, a ratio closer to 5:5:1 of  $\alpha_1$ : $\beta_3$ : $\gamma_{2L}$  was observed (15  $\mu$ g total protein, **Figure 4.3**). The lower  $\gamma_{2L}$  protein expression levels, compared with the  $\alpha_1$ : $\beta_3$  subunits, could suggest a lower transfection or transcription/translation efficiency for the  $\gamma_{2L}$  subunit, something previously noted by others (Botzolakis et al., 2016; Hinkle & Macdonald, 2003) and remedied by attaching the 5' end of an 11-residue flexible linker to  $\gamma_{2L}$ 's carboxy terminus with the linker's 3' end connected to a 1D4 epitope tag (Dostalova et al., 2014).



The potency and efficacy of GABA, CZP, and VA were measured for the transient and stably expressing GABA<sub>A</sub> receptor cell lines using the FMP Red Dye assay (**Table 4.2**). With the HEK293 cell line transiently expressing the GABA receptor, we observed a 40-fold decrease in GABA potency, but nearly a 50% increase in efficacy (maximum stimulation) compared to the HEK293 cell harboring and expressing stably integrated GABA<sub>A</sub> receptor subunit genes (808 nM vs. 19.6 nM; 13,309 AFUs vs. 9998 AFUs, respectively). This might suggest a differential expression profile of GABA<sub>A</sub> receptor isoforms lacking one or both of GABA's orthosteric binding sites, but capable of forming functional ligand-gated ion channels at the cell's surface (the  $\beta_3$ , the  $\alpha_1:\beta_3$ , or the  $\alpha_1:\beta_3:\gamma_{2L}$  subunits) (Botzolakis et al., 2016; Masiulis et al., 2019; Miller & Aricescu, 2014; Yip et al., 2013). This hypothesis awaits additional experimental evidence in the form of protein expression analysis of the plasma membrane fraction.

Both the transient and stable cell lines expressing the GABA<sub>A</sub> receptor genes displayed BZD sensitivity as evident by CZP concentration-dependent observations (**Figure 4.4**), thus affirming successful incorporation of the  $\gamma_{2L}$  subunit into the GABA<sub>A</sub> receptor pseudopentameric structure because the BZD binding site resides on the extracellular domain of the  $\alpha - \gamma$  interface (Han et al., 2019; Masiulis et al., 2019). CZP's potency, determined in the absence of GABA, was slightly lower in the HEK293 cell line transiently expressing the GABA<sub>A</sub> receptor genes, though not statistically significant in comparison to the HEK293 cell line stably expressing the GABA<sub>A</sub> receptor genes ( $EC_{50}$ :15.6nM vs. 8.2nM, respectively) (**Table 4.2**). The efficacy, however, was almost 30% lower in the transient expressing cells compared to the stably expressing HEK293 cell line (3880AFU vs. 5332AFU, respectively;  $p < 0.05$ ). As alluded to previously, the FMP

Red Dye (and quite possibly the masking dye) partially agonizes the GABA<sub>A</sub> receptor, therefore lowering the maximal threshold for desensitization.

We were not able to confirm the widely reported positive modulatory activity of CZP on GABA sensitivity using the FMP Red Dye. In numerous attempts, we were not able to reproducibly document an enhanced CZP dose response at suboptimal concentrations of GABA (from 5 to 30 % of the GABA concentration necessary for maximal efficacy measurements). Nonetheless, a reliable and reproducible dose dependent CZP potentiation response in both cells transiently and stably expressing the GABA receptor subunit genes was documented (**Figure 4.4**). The results appear to confirm the presence of an accessible BZD binding site, which would be necessary for validating the exact binding site on the GABA<sub>A</sub> receptor of novel chemistries with PAM activity.

Furthermore, we also confirmed the presence of at least one VA binding site within both our transient and stable HEK293 cell lines. Once VA's concentration-dependent responses were plotted on a log(concentration)-response graph (**Figure 4.4, A & D**), VA's potency and efficacy for the human GABA<sub>A</sub> receptor transiently and stably expressed in HEK293 cells using the FMP Red Dye assay without the presence of GABA could be calculated (Potency: 2502nM (Transient) vs. 3687nM (Stable); Efficacy 5,935AFUs (Transient) vs. 5,255AFUs (Stable)) (**Table 4.2**).

We were unable to confirm the seminal work of Hering et al. (Khom et al., 2007) and Mohler et al. (Benke et al., 2009) establishing VA's primary mechanism of actions as a positive allosteric modulator of GABA<sub>A</sub> receptor PAM. As already noted elsewhere, we suspect this is because the FMP Red Dye itself can induce a partial potentiation of the GABA<sub>A</sub> receptor via the barbiturate binding site (Mennerick et al., 2010; Nik et al., 2017),

thus short-circuiting the potential to observe the action of other PAM molecules. Regardless, the FMP Red Dye assay was sufficient to document potentiation of the GABA<sub>A</sub> receptor by VA, encouraging further screening of VA constrained analogs and other novel chemistries for their level of direct potentiation of the human GABA<sub>A</sub> ( $\alpha_1$ ,  $\beta_3$ ,  $\gamma_{2L}$ ) receptor genes expressed transiently and in stably transformed HEK293 cells.

**Table 4.2** GABA, CZP, & VA potency (nM) and efficacy (AFUs) of transiently vs. stably expressed human GABA<sub>A</sub> receptors in HEK293 cells

<u>Treatment</u>	<u>Potency<sup>a</sup></u>		<u>Efficacy<sup>b</sup></u>		<u>Hill Slope<sup>c</sup></u>	
	<u>Transient</u>	<u>Stable</u>	<u>Transient</u>	<u>Stable</u>	<u>Transient</u>	<u>Stable</u>
GABA	808 ± 206	19.6 ± 6.1*	13309 ± 953	9998 ± 430	0.8 ± 0.1	1.3 ± 0.4
CZP	15.6 ± 5.5	8.2 ± 1.1	3880 ± 72	5332 ± 17*	1.4 ± 0.6	1.9 ± 0.6
VA	2502 ± 278	3687 ± 901	5935 ± 104	5255 ± 495	2.3 ± 0.5	2.5 ± 1.3
ABA	not active	not tested				
CPol	not active	not tested				
GA3	not active	not tested				

<sup>a</sup>Potency values are in nM ± SEM; <sup>b</sup>Efficacy values are AFUs ± SEM; <sup>c</sup>slope ± SEM; Means of transient and stable cell lines were compared using the Student's t-test (unpaired), \*p < 0.05.

#### 4.3.3 The sesquiterpenoids ABA & CPol along with diterpenoid GA3 showed no detectable level of potentiation for transiently expressed human GABA<sub>A</sub> ( $\alpha_1$ , $\beta_3$ , $\gamma_{2L}$ ) receptors

Although unsuccessful in efforts to create biosynthetically constrained, rigid analogs of VLD (**CHAPTER 2**) oxidized to their carboxylic acid form (**CHAPTER 3**), we were able to screen and evaluate three decorated terpenoids with varying degrees of structural rigidity (**Figure 4.1, Structures D-F**) in our FMP Red Dye assay. Abscisic acid (ABA) (**Figure 4.1, Structure D**) is a 15-carbon breakdown product from the carotenoid zeaxanthin, and contains one oxygenated (ketone and tertiary alcohol) with a six-membered ring connected to a flexible, isopentyl side chain successively oxidized at the terminal methyl substituent (Finkelstein & Rock, 2002; Izquierdo-Bueno et al., 2018). To date, ABA's biological role as a plant growth regulator, controlling stomatal closure, cuticular wax accumulation, leaf senescence, bud dormancy, seed germination, osmotic regulation, and growth inhibition is well documented (Chen et al., 2020). Cyclopartheniol (CPol) (**Figure 4.1, Structure E**) is a C15 sesquiterpenoid first extracted from the defoliated twigs of *Parthenium argentatum* (Crevoisier et al., 1984) closely resembling *allo*-aromadendrene's structure (**Figure 2.1, Structure #10**). CPol's gem-dimethylcycopropyl unit was hypothesized to contribute to the biosynthetic origins of many aristolane's, including aromadendrane's, secoaromadendrane's, cycloaromadendrane's, and lepidozane's and documented for their anti-viral, antimicrobial, and antifeedant activities (Durán-Peña et al., 2015). Gibberellic acid (GA3) (**Figure 4.1, Structure F**) is a pentacyclic oxygenated diterpenoid which functions as plant phytohormone involved in cell growth processes such as, stem elongation (Nagai et al., 2020)). Unfortunately, no concentration dependent GABA<sub>A</sub> potentiation responses in the

FMP RED dye assay were observed up to 10,000 nM for ABA, CPol, or GA3 (**Figure 4.6, Graph A**). Thus, we concluded these molecules lack an ability to either bind to or modulate the GABA<sub>A</sub> receptor (**Table 4.2**). It is also conceivable the differences in the water solubility of ABA (3.2 g/L), CPol ( $\approx 0.012$  g/L)<sup>4</sup>, and GA3 (5 g/L) may have negatively influenced any potential GABA<sub>A</sub> receptor- ligand binding interactions. In either scenario, the FMP Red Dye assay independently identified CZP and VA as “active” GABA receptor chemistries – previously well-characterized positive allosteric GABA<sub>A</sub> receptor allosteric modulators by several other groups (Benke et al., 2009; Khom et al., 2007; Louiset et al., 2000).

This is the first report, to our knowledge, of ABA, CPol, and GA3 evaluated for their potential allosteric modulation of the human GABA<sub>A</sub> ( $\alpha_1$ ,  $\beta_3$ ,  $\gamma_{2L}$ ) receptors. Though ABA, CPol, nor GA3 displayed detectable levels of activity (up to the 10,000nM<sup>5</sup>), they did help strengthen the specificity within our cell-based fluorescence biological assay to, without bias, correctly identify known biologically active chemistries, while eliminating “inactive” compounds.

---

<sup>4</sup> This is the estimated water solubility of a spathulenol (a tri-cyclic monooxygenated sesquiterpene with a gem-dimethyl ring structure) reported by the Good Scents Company

<sup>5</sup> Final in-well concentration was limited by the compound’s solubility (in DMSO) and the maximum DMSO percentage tolerated by the HEK293 cells (0.05%)

#### 4.3.4 Varying the $\alpha_1$ , $\beta_3$ , & $\gamma_{2L}$ subunits' availability directly impacts GABA's, CZP's, & VA's potency and efficacy for transiently expressed GABA<sub>A</sub> receptor in naive HEK293 cells

In a last set of experiments, we envisioned having a malleable, recombinant GABA<sub>A</sub> receptor transient expression system to further investigate the subunit specific binding sites of those chemistries screened and found to have a modulatory activity above the vehicle control using the FMP Red Dye assay. As noted by the MacDonald research group and others (Angelotti et al., 1993; Botzolakis et al., 2016; Schofield et al., 1987; Tretter et al., 1997), varying the DNA concentration for the genes encoding for the  $\alpha(1-6)$ ,  $\beta(1-3)$ , and  $\gamma(1-3)$  subunits (the mature peptide expression ratio for GABA<sub>A</sub> receptor subunit subtypes commonly found within the central nervous system (Olsen & Sieghart, 2009)) should translate to directly influencing the subunit stoichiometry of the multimeric GABA<sub>A</sub> receptor, directly impacting the receptor's channel kinetics, neuropharmacology, and subcellular localization.

We therefore varied the transfected DNA concentrations from 1:1:1 to 2:2:1 and 1:1:10 for the  $\alpha_1$ ,  $\beta_3$ , and  $\gamma_{2L}$  subunits and noted the impacts to the GABA, CZP and VA GABA<sub>A</sub> receptor pharmacology (**Table 4.3, Figure 4.6**). Transfection of the  $\gamma_{2L}$  plasmid DNA at 50% of the individual  $\alpha_1$  &  $\beta_3$  subunit plasmid DNA amounts (2.9  $\mu\text{g}$  vs. 5.8  $\mu\text{g}$ ), increased GABA's potency 2-fold (though not statistically significant), with a concomitant decrease of 1.5 times ( $p < 0.001$ ) to the maximum channel stimulation (efficacy) in reference to the transfection ratio (T.R.) of 1:1:1 (260nM vs. 808nM; 8284 AFUs vs. 13,309 AFUs, respectively). Conversely, when cells were transfected with 12 $\mu\text{g}$  of the  $\gamma_{2L}$  plasmid DNA and 1.25  $\mu\text{g}$  for each of the  $\alpha_1$  &  $\beta_3$  subunits (T.R. 1:1:10), we observed a 2.5-fold decrease in potency and a 1.2 time in increase in efficacy ( $P < 0.003$ ), compared

to the T.R. of 1:1:1 (2033nM vs. 808nM; 15,730 AFUs vs. 13,309 AFUs, respectively). Altogether, these results suggest that transfecting in the  $\alpha_1$ ,  $\beta_3$ , &  $\gamma_{2L}$  subunits at a 2:2:1 ratio may reduce alternative GABA<sub>A</sub> conformations and support the canonical  $\beta - \alpha - \beta - \alpha - \gamma$  subunit GABA<sub>A</sub> receptor formation.

Interestingly, we observed little to no change in CZP's potency and efficacy across the 1:1:1, 2:2:1, and 1:1:10 transient cell lines (**Table 4.3, Figure 4.6**). This would suggest the canonical BZD binding site was preserved and functioning properly, regardless of the  $\gamma_{2L}$  subunit availability. Finally, in the 2:2:1 and 1:1:10 cell lines, we observed a significant increase in VA's potency, which was indetermined given the concentration-dependent response curves kept rising and never plateaued at 10,000nM (the maximum tested concentration). VA efficacies for 2:2:1 and 1:1:10 transfected cells slightly decreased ( $P < 0.003$ ) or nearly doubled ( $P < 0.003$ ) compared with the T.R. 1:1:1 cell line (3982 AFUs vs. 9048 AFUs vs. 5935 AFUs, respectively). Therefore, increasing the transfection  $\beta_3$  subunit concentration by 50% or decreasing it approximately 8-fold with respect to the  $\gamma_{2L}$ , has bifurcating effects on VA's efficacy, while shifting VA's potency further right on the concentration-response curve. Taken together, additional transfection permutations, such as strictly only transfection of the  $\beta_3$  subunit and  $\alpha_1 + \beta_3$  subunits are warranted to grasp a more comprehensive understanding of the impact on GABA<sub>A</sub> receptor's pharmacology to provide the necessary benchmarks for comparing the novel chemistries across a diverse recombinantly expressed GABA<sub>A</sub> receptor subunit conformers.



**Table 4.3** Potency and efficacy of GABA, CZP, & VA for transiently expressed human GABA<sub>A</sub> receptors with varying  $\alpha_1$ ,  $\beta_3$ , &  $\gamma_{2L}$  subunit availability

<b>T.R.<sup>a</sup></b>	<b>GABA</b>		<b>CZP</b>		<b>VA</b>	
	<b>Potency<sup>b</sup></b>	<b>Efficacy<sup>c</sup></b>	<b>Potency<sup>b</sup></b>	<b>Efficacy<sup>c</sup></b>	<b>Potency<sup>b</sup></b>	<b>Efficacy<sup>c</sup></b>
1:1:1	808 ± 206	13309 ± 953	16 ± 6	3880 ± 72	2502 ± 278	5935 ± 104
2:2:1	260 ± 76	8284 ± 243***	12	2588 ± 375*	>10,000 <sup>d</sup>	3982 ± 72**
1:1:10	2033 ± 431	15730 ± 947**	23 ± 3	3960 ± 84	>10,000 <sup>d</sup>	9048**

<sup>a</sup>T.R, transfection DNA ratio of expression vectors harboring the  $\alpha_1$ ,  $\beta_3$ , &  $\gamma_{2L}$  GABA<sub>A</sub> receptor subunit coding DNA, respectively;  
<sup>b</sup>Potency values are nM ± SEM; <sup>c</sup>Efficacy values are AFUs ± SEM; <sup>d</sup>Accurate statistical difference not definable given sample size was n=2; Comparison of individual means for 1:1:1 to 2:2:1 and 1:1:10 cell lines by Fishers Least Significant Difference test (uncorrected), \*p < 0.05, \*\*p < 0.003, \*\*\*p < 0.001.

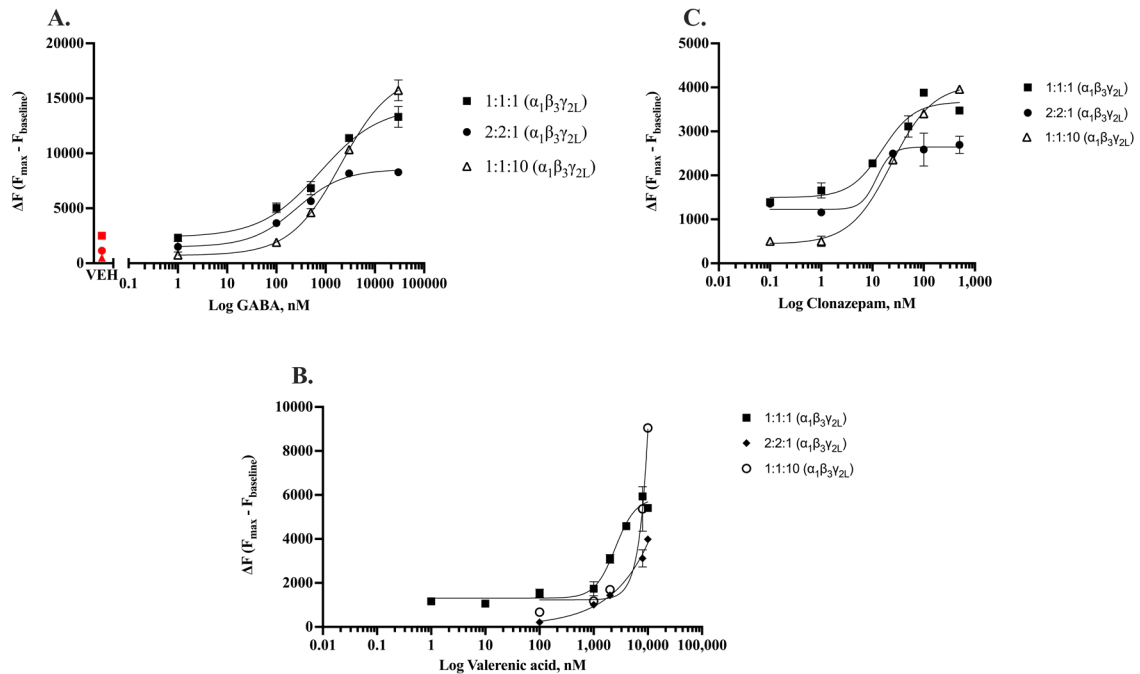


**Figure 4.6** GABA (A), VA (B), and CZP (C) for HEK293 concentration-dependent response curves for naïve HEK293 cells transfected at (■) 1:1:1, (●) 2:2:1, (△) 1:1:10 with the  $\alpha 1$ ,  $\beta 3$ ,  $\gamma 2L$  the human GABA<sub>A</sub> receptor subunits, respectively. (A) HEK293 cells transfected at 2:2:1 exhibited two-to-seven-fold greater GABA potencies, than cells transfected at 1:1:1 and 1:1:10. VEH; vehicle control (red filled in shapes) (B) The 1:1:1 HEK293 transfected cells demonstrated the typical concentration-dependent response, reaching saturation prior to 10,000nM of VA, the maximum tested dose. Potencies and efficacies were unable to be calculated for the 2:2:1 and 1:1:10 transfected cells, given that a saturation response was not observed. (C) All three transfected HEK293 cells demonstrated relatively the same level of potency and efficacy for CZP. This would indicate both the alpha and gamma subunits were correctly assembled in the ER and trafficked to the cell surface for functional expression of the benzodiazepine binding site (Dostalova et al., 2014; Masiulis et al., 2019).

#### 4.4 Conclusions

In conclusion, this work establishes a cell-based fluorescence bioassay for the detection of novel direct activators of the human GABA<sub>A</sub> ( $\alpha$ 1,  $\beta$ 3,  $\gamma$ 2L) receptor in both transiently and stably expressed. Albeit, the DiSBAC<sub>1</sub>(3) dye may have a partial agonistic effect on the recombinantly expressed human GABA<sub>A</sub> ( $\alpha$ 1,  $\beta$ 3,  $\gamma$ 2L) receptors, the FMP Red Dye assay provides a facile, sensitive tool to indirectly measure and quantify specific binding interaction at the GABA<sub>A</sub> receptor. Thus, allowing for additional ways to conduct drug discovery structure-activity relationship studies. It is not the goal for the such tools to replace the gold-standard patch-clamp electrophysiology techniques, but merely provide a method for pre-screening through a large chemical library for reduction in the more labor intensive and costly patch-clamp type of experimentation.

## CHAPTER 5. CONCLUSIONS AND PERSPECTIVES

### 5.1 Conclusions and perspectives

The intent of this dissertation was to develop a biosynthetic platform for the generation of structural analogs that could be tested in a facile bioassay for their potentiation of the GABA<sub>A</sub> receptor. Though the full embodiment of this vision might not have been realized, the construction of a platform to evaluate microbially synthesized VA analogs from engineered VDS mutant enzymes in a “plug-in-play” type manner was developed. One of the next steps that should be undertaken is the development of a greater diverse VDS mutant library with an enhanced high-throughput chemical screening analysis (O'Maille et al., 2008). In parallel, an engineered ZXB yeast line, or possibly another high terpene yielding yeast host, should be genetically engineered to contain with multiple copies of the GAO and its P450 reductase at various and previously uncharacterized genomic loci near ARS sites to improve the yield of biosynthetically oxidized sesquiterpenes. These efforts would afford a stream-lined and more productive route for obtaining the necessary VDS mutant enzymes, which then could be expressed in a yeast host extrachromosomally or chromosomally inserted, yielding higher conversion efficiencies of structurally constrained VLD analogs to their final carboxylated forms at titers of 10-20mg/L. Once purified (purity >90%), by preparative TLC or HPLC, the structurally constrained analogs can immediately into the FMP Red Dye assay for screening in both the stably and transiently (1:1:1) expressing human GABA<sub>A</sub> ( $\alpha 1$ ,  $\beta 3$ ,  $\gamma 2L$ ) receptor cell lines for preliminary pharmacological characterization. Analogs which demonstrate at least the same level of potentiation to VA, should then be rescreened in a

transiently expressing human GABA<sub>A</sub> ( $\beta$ 3 only) receptor cell line for probing its putative receptor binding site, which may or may not be the same as VA (TM2 domain on the  $\beta$ <sub>2,3</sub>). If the compound(s) show greater than 2-fold better potency to VA and equivalent or greater efficacy, they could be targeted as “ready to test by patch-clamping.” At which time, it would be necessary to seek out additional support to setup the patch-clamping studies, while continuing to screen structural conformers of VA for enhance potencies and efficacies for allosteric modulation of the human GABA<sub>A</sub> ( $\alpha$ 1,  $\beta$ 3,  $\gamma$ 2L) receptor. Furthermore, adopting additional GABA<sub>A</sub> receptor subunit subtypes into the transient expression system, would significantly improve one’s ability to uncover potentiation selectivity for GABA<sub>A</sub> receptor specific subunit subtype. Ultimately aiding to focusing on generating potentially novel anxiolytic chemistries that would have reduced adverse effects and low abuse potential of the currently FDA-approved anti-anxiety treatments.

## REFERENCES

- Aaron, J. A., & Christianson, D. W. (2010). Trinuclear metal clusters in catalysis by terpenoid synthases. *Pure Applied Chemistry*, 82(8), 1585-1597. <https://doi.org/10.1351/PAC-CON-09-09-37>
- Abdallah, II, van Merkerk, R., Klumpenaar, E., & Quax, W. J. (2018). Catalysis of amorpho-4,11-diene synthase unraveled and improved by mutability landscape guided engineering. *Scientific Reports*, 8(1), 9961. <https://doi.org/10.1038/s41598-018-28177-4>
- Allen, S. E., Dokholyan, N. V., & Bowers, A. A. (2016). Dynamic docking of conformationally constrained macrocycles: Methods and applications. *ACS Chemical Biology*, 11(1), 10-24. <https://doi.org/10.1021/acscchembio.5b00663>
- Althaus, A. L., Ackley, M. A., Belfort, G. M., Gee, S. M., Dai, J., Nguyen, D. P., Kazdoba, T. M., Modgil, A., Davies, P. A., Moss, S. J., Salituro, F. G., Hoffmann, E., Hammond, R. S., Robichaud, A. J., Quirk, M. C., & Doherty, J. J. (2020). Preclinical characterization of zuranolone (sage-217), a selective neuroactive steroid gaba(a) receptor positive allosteric modulator. *Neuropharmacology*, 181, 108333-108333. <https://doi.org/10.1016/j.neuropharm.2020.108333>
- American Psychiatric, A. (2013). *Diagnostic and statistical manual of mental disorders* (5th ed.). <https://doi.org/https://doi.org/10.1176/>
- Angelotti, T. P., Uhler, M. D., & Macdonald, R. L. (1993). Assembly of gabaa receptor subunits: Analysis of transient single-cell expression utilizing a fluorescent substrate/marker gene technique. *Journal Neuroscience*, 13(4), 1418-1428. <https://www.ncbi.nlm.nih.gov/pubmed/7681869>
- Attia, M., Kim, S. U., & Ro, D. K. (2012). Molecular cloning and characterization of (+)-epi-alpha-bisabolol synthase, catalyzing the first step in the biosynthesis of the natural sweetener, hernandulcin, in lippia dulcis. *Archives of Biochemistry & Biophysics*, 527(1), 37-44. <https://doi.org/10.1016/j.abb.2012.07.010>
- Baer, P., Rabe, P., Fischer, K., Citron, C. A., Klapschinski, T. A., Groll, M., & Dickschat, J. S. (2014). Induced-fit mechanism in class i terpene cyclases. *Angewandte Chemie International* 53(29), 7652-7656. <https://doi.org/10.1002/anie.201403648>
- Bandelow, B., Lichte, T., Rudolf, S., Wiltink, J., & Beutel, M. E. (2015). The german guidelines for the treatment of anxiety disorders. *European Archives of Psychiatry and Clinical Neuroscience*, 265(5), 363-373. <https://doi.org/10.1007/s00406-014-0563-z>
- Bannai, H., Niwa, F., Sherwood, M. W., Shrivastava, A. N., Arizono, M., Miyamoto, A., Sugiura, K., Levi, S., Triller, A., & Mikoshiba, K. (2015). Bidirectional control of synaptic gabaar clustering by glutamate and calcium. *Cell Reports*, 13(12), 2768-2780. <https://doi.org/10.1016/j.celrep.2015.12.002>

- Barrett, B., Kiefer, D., & Rabago, D. (1999). Assessing the risks and benefits of herbal medicine: An overview of scientific evidence. *Alternative Therapies in Health Medicine*, 5(4), 40-49. <http://www.ncbi.nlm.nih.gov/pubmed/10394673>
- Baumann, S. W., Baur, R., & Sigel, E. (2003). Individual properties of the two functional agonist sites in gaba(a) receptors. *Journal of Neuroscience*, 23(35), 11158-11166. <https://www.ncbi.nlm.nih.gov/pubmed/14657175>
- Baxter, D. F., Kirk, M., Garcia, A. F., Raimondi, A., Holmqvist, M. H., Flint, K. K., Bojanic, D., Distefano, P. S., Curtis, R., & Xie, Y. (2002). A novel membrane potential-sensitive fluorescent dye improves cell-based assays for ion channels. *Journal of Biomolecular Screening*, 7(1), 79-85. <https://doi.org/10.1177/108705710200700110>
- Bell, S. A., Niehaus, T. D., Nybo, S. E., & Chappell, J. (2014). Structure-function mapping of key determinants for hydrocarbon biosynthesis by squalene and squalene synthase-like enzymes from the green alga *botryococcus braunii* race b. *Biochemistry*, 53(48), 7570-7581. <https://doi.org/10.1021/bi501264s>
- Benke, D., Barberis, A., Kopp, S., Altmann, K. H., Schubiger, M., Vogt, K. E., Rudolph, U., & Mohler, H. (2009). Gaba a receptors as in vivo substrate for the anxiolytic action of valerianic acid, a major constituent of valerian root extracts. *Neuropharmacology*, 56(1), 174-181. <https://doi.org/10.1016/j.neuropharm.2008.06.013>
- Bennett, M. H., Mansfield, J. W., Lewis, M. J., & Beale, M. H. (2002). Cloning and expression of sesquiterpene synthase genes from lettuce (*lactuca sativa* l.). *Phytochemistry*, 60(3), 255-261. <https://www.ncbi.nlm.nih.gov/pubmed/12031443>
- Bent, S., Padula, A., Moore, D., Patterson, M., & Mehling, W. (2006). Valerian for sleep: A systematic review and meta-analysis. *American Journal of Medicine*, 119(12), 1005-1012. <https://doi.org/10.1016/j.amjmed.2006.02.026>
- Blagg, B. S., Jarstfer, M. B., Rogers, D. H., & Poulter, C. D. (2002). Recombinant squalene synthase. A mechanism for the rearrangement of presqualene diphosphate to squalene. *Journal of American Chemical Society*, 124(30), 8846-8853. <https://www.ncbi.nlm.nih.gov/pubmed/12137537>
- Bos, R., Woerdenbag, H. J., Hendriks, H., Zwaving, J. H., De Smet, P. A. G. M., Tittel, G., Wikström, H. V., & Scheffer, J. J. C. (1996). Analytical aspects of phytotherapeutic valerian preparations. *Phytochemical Analysis*, 7(3), 143-151. [https://doi.org/doi:10.1002/\(SICI\)1099-1565\(199605\)7:3<143::AID-PCA284>3.0.CO;2-1](https://doi.org/doi:10.1002/(SICI)1099-1565(199605)7:3<143::AID-PCA284>3.0.CO;2-1)
- Botzolakis, E. J., Gurba, K. N., Lagrange, A. H., Feng, H.-J., Stanic, A. K., Hu, N., & Macdonald, R. L. (2016). Comparison of  $\gamma$ -aminobutyric acid, type a (gaba<sub>a</sub>), receptor  $\alpha\beta\gamma$  and  $\alpha\beta\delta$  expression using flow cytometry and electrophysiology: Evidence for alternative subunit stoichiometries and arrangements. *The Journal of Biological Chemistry*, 291(39), 20440-20461. <https://doi.org/10.1074/jbc.M115.698860>

- Bouwmeester, H. J., Kodde, J., Verstappen, F. W., Altug, I. G., de Kraker, J. W., & Wallaart, T. E. (2002). Isolation and characterization of two germacrene synthase cDNA clones from chicory. *Plant Physiology*, *129*(1), 134-144.  
<https://doi.org/10.1104/pp.001024>
- Brachmann, C. B., Davies, A., Cost, G. J., Caputo, E., Li, J., Hieter, P., & Boeke, J. D. (1998). Designer deletion strains derived from *Saccharomyces cerevisiae* s288c: A useful set of strains and plasmids for PCR-mediated gene disruption and other applications. *Yeast*, *14*(2), 115-132. [https://doi.org/10.1002/\(sici\)1097-0061\(19980130\)14:2<115::Aid-yea204>3.0.Co;2-2](https://doi.org/10.1002/(sici)1097-0061(19980130)14:2<115::Aid-yea204>3.0.Co;2-2)
- Bystritsky, A. (2006). Treatment-resistant anxiety disorders. *Molecular Psychiatry*, *11*(9), 805-814. <https://doi.org/10.1038/sj.mp.4001852>
- Cai, Y., Jia, J. W., Crock, J., Lin, Z. X., Chen, X. Y., & Croteau, R. (2002). A cDNA clone for beta-caryophyllene synthase from *Artemisia annua*. *Phytochemistry*, *61*(5), 523-529.  
<https://www.ncbi.nlm.nih.gov/pubmed/12409018>
- Calhoun, G. G., & Tye, K. M. (2015). Resolving the neural circuits of anxiety. *Nature Reviews Neuroscience*, *18*(10), 1394-1404. <https://doi.org/10.1038/nrn.4101>
- Cane, D. E. (1990). Enzymic formation of sesquiterpenes. *ACS Chemical Reviews*, *90*(7), 1089-1103. <https://doi.org/10.1021/cr00105a002>
- Chappell, J., Wolf, F., Proulx, J., Cuellar, R., & Saunders, C. (1995). Is the reaction catalyzed by 3-hydroxy-3-methylglutaryl coenzyme A reductase a rate-limiting step for isoprenoid biosynthesis in plants? *Plant Physiology*, *109*(4), 1337-1343.  
<https://doi.org/10.1104/pp.109.4.1337>
- Chappell, J., Zhuang, X., & Wu, S. (2021). Method and system for terpene production platforms in yeast. In: Google Patents.
- Chen, K., Li, G. J., Bressan, R. A., Song, C. P., Zhu, J. K., & Zhao, Y. (2020). Abscisic acid dynamics, signaling, and functions in plants. *Journal of Integrative Plant Biology*, *62*(1), 25-54. <https://doi.org/10.1111/jipb.12899>
- Chen, X. Y., Wang, M., Chen, Y., Davisson, V. J., & Heinstein, P. (1996). Cloning and heterologous expression of a second (+)-delta-cadinene synthase from *Gossypium arboreum*. *Journal of Natural Products*, *59*(10), 944-951.  
<https://doi.org/10.1021/np960344w>
- Chen, Y., Wang, Y., Liu, M., Qu, J., Yao, M., Li, B., Ding, M., Liu, H., Xiao, W., Yuan, Y., & Cann, I. (2019). Primary and secondary metabolic effects of a key gene deletion (*deltaYp1062w*) in metabolically engineered terpenoid-producing *Saccharomyces cerevisiae*. *Applied and Environmental Microbiology*, *85*(7), e01990-01918.  
<https://doi.org/doi:10.1128/AEM.01990-18>



- Christianson, D. W. (2017). Structural and chemical biology of terpenoid cyclases. *ACS Chemical Reviews*, 117(17), 11570-11648. <https://doi.org/10.1021/acs.chemrev.7b00287>
- Christine, A. R., & Phan, K. L. (2014). Cannabinoid modulation of fear extinction brain circuits: A novel target to advance anxiety treatment. *Current Pharmaceutical Design*, 20(13), 2212-2217. <https://doi.org/http://dx.doi.org/10.2174/13816128113199990437>
- Cohen, L. B., & Salzberg, B. M. (1978). Optical measurement of membrane potential. In *Reviews of physiology, biochemistry and pharmacology, volume 83: Volume: 83* (pp. 35-88). Springer Berlin Heidelberg. [https://doi.org/10.1007/3-540-08907-1\\_2](https://doi.org/10.1007/3-540-08907-1_2)
- Cong, L., Ran, F. A., Cox, D., Lin, S., Barretto, R., Habib, N., Hsu, P. D., Wu, X., Jiang, W., Marraffini, L. A., & Zhang, F. (2013). Multiplex genome engineering using crispr/cas systems. *Science*, 339(6121), 819-823. <https://doi.org/10.1126/science.1231143>
- Connolly, J. D., Harrison, L. J., & Rycroft, D. S. (1984). The structure of tamariscol, a new pacifigorgiane sesquiterpenoid alcohol from the liverwort *frullania tamarisci*. *Tetrahedron Letters*, 25(13), 1401-1402. [https://doi.org/https://doi.org/10.1016/S0040-4039\(01\)80169-6](https://doi.org/https://doi.org/10.1016/S0040-4039(01)80169-6)
- Cragg, G. M., & Newman, D. J. (2013). Natural products: A continuing source of novel drug leads. *Biochimica et Biophysica Acta*, 1830(6), 3670-3695. <https://doi.org/10.1016/j.bbagen.2013.02.008>
- Crevoisier, M., Stedule, K. C., & Buerger, H. B. (1984). 3,3,11-trimethyl-7-methylenetricyclo[6.3.0.0<sup>2,4</sup>]undecane-5,11-diol, C<sub>15</sub>H<sub>24</sub>O<sub>2</sub>. *Acta Crystallographica Section C*, 40(6), 979--980. <https://doi.org/10.1107/S010827018400648X>
- Cryan, J. F., & Sweeney, F. F. (2011). The age of anxiety: Role of animal models of anxiolytic action in drug discovery. *British Journal of Pharmacology*, 164(4), 1129-1161. <https://doi.org/10.1111/j.1476-5381.2011.01362.x>
- Davis, M., Walker, D. L., Miles, L., & Grillon, C. (2010). Phasic vs sustained fear in rats and humans: Role of the extended amygdala in fear vs anxiety. *Neuropsychopharmacology*, 35(1), 105-135. <https://doi.org/10.1038/npp.2009.109>
- Dias, D. A., Urban, S., & Roessner, U. (2012). A historical overview of natural products in drug discovery. *Metabolites*, 2(2), 303-336. <https://doi.org/10.3390/metabo2020303>
- DiCarlo, J. E., Norville, J. E., Mali, P., Rios, X., Aach, J., & Church, G. M. (2013). Genome engineering in *saccharomyces cerevisiae* using crispr-cas systems. *Nucleic Acids Res*, 41(7), 4336-4343. <https://doi.org/10.1093/nar/gkt135>
- Dixit, M., Weitman, M., Gao, J., & Major, D. T. (2017). Chemical control in the battle against fidelity in promiscuous natural product biosynthesis: The case of trichodiene synthase. *ACS Catalysis*, 7(1), 812-818. <https://doi.org/10.1021/acscatal.6b02584>
- Dostalova, Z., Zhou, X., Liu, A., Zhang, X., Zhang, Y., Desai, R., Forman, S. A., & Miller, K. W. (2014). Human alpha1beta3gamma21 gamma-aminobutyric acid type a

- receptors: High-level production and purification in a functional state. *Protein Science*, 23(2), 157-166. <https://doi.org/10.1002/pro.2401>
- Durán-Peña, M. J., Botubol Ares, J. M., Hanson, J. R., Collado, I. G., & Hernández-Galán, R. (2015). Biological activity of natural sesquiterpenoids containing a gem-dimethylcyclopropane unit. *Natural Product Reports*, 32(8), 1236-1248. <https://doi.org/10.1039/c5np00024f>
- Engin, E., Liu, J., & Rudolph, U. (2012). A2-containing gaba(a) receptors: A target for the development of novel treatment strategies for cns disorders. *Pharmacology & Therapeutics*, 136(2), 142-152. <https://doi.org/10.1016/j.pharmthera.2012.08.006>
- Eramian, D., Eswar, N., Shen, M. Y., & Sali, A. (2008). How well can the accuracy of comparative protein structure models be predicted? *Protein Science*, 17(11), 1881-1893. <https://doi.org/10.1110/ps.036061.108>
- Fang, X., Li, J. X., Huang, J. Q., Xiao, Y. L., Zhang, P., & Chen, X. Y. (2017). Systematic identification of functional residues of artemisia annua amorpho-4,11-diene synthase. *Biochemical Journal*, 474(13), 2191-2202. <https://doi.org/10.1042/BCJ20170060>
- Felicetti, B., & Cane, D. E. (2004). Aristolochene synthase: Mechanistic analysis of active site residues by site-directed mutagenesis. *Journal of American Chemical Society*, 126(23), 7212-7221. <https://doi.org/10.1021/ja0499593>
- Ferguson, J. M. (2001). Ssri antidepressant medications: Adverse effects and tolerability. *Primary Care Companion to the Journal of Clinical Psychiatry*, 3(1), 22-27. <http://www.ncbi.nlm.nih.gov/pubmed/15014625>
- Fiala, T., Wang, J., Dunn, M., Šebej, P., Choi, S. J., Nwadiibia, E. C., Fialova, E., Martinez, D. M., Cheetham, C. E., Fogle, K. J., Palladino, M. J., Freyberg, Z., Sulzer, D., & Sames, D. (2020). Chemical targeting of voltage sensitive dyes to specific cells and molecules in the brain. *Journal of the American Chemical Society*, 142(20), 9285-9301. <https://doi.org/10.1021/jacs.0c00861>
- Finkelstein, R. R., & Rock, C. D. (2002). Abscisic acid biosynthesis and response. *The Arabidopsis Book*, 2002(1). <https://doi.org/10.1199/tab.0058>
- Garakani, A., Murrough, J. W., Freire, R. C., Thom, R. P., Larkin, K., Buono, F. D., & Iosifescu, D. V. (2020). Pharmacotherapy of anxiety disorders: Current and emerging treatment options. *Frontiers in Psychiatry*, 11, 595584. <https://doi.org/10.3389/fpsy.2020.595584>
- Garms, S., Kollner, T. G., & Boland, W. (2010). A multiproduct terpene synthase from medicago truncatula generates cadalane sesquiterpenes via two different mechanisms. *J Org Chem*, 75(16), 5590-5600. <https://doi.org/10.1021/jo100917c>

- Garms, S., Köllner, T. G., & Boland, W. (2010). A multiproduct terpene synthase from *Medicago truncatula* generates cadalane sesquiterpenes via two different mechanisms. *The Journal of Organic Chemistry*, 75(16), 5590-5600. <https://doi.org/10.1021/jo100917c>
- Gietz, R. D., & Woods, R. A. (2002). Transformation of yeast by lithium acetate/single-stranded carrier DNA/polyethylene glycol method. *Methods in Enzymology*, 350, 87-96. [https://doi.org/10.1016/s0076-6879\(02\)50957-5](https://doi.org/10.1016/s0076-6879(02)50957-5)
- Goodman, L. S., Brunton, L. L., Chabner, B., & Knollmann, B. r. C. (2011). *Goodman & Gilman's pharmacological basis of therapeutics* (12th ed.). McGraw-Hill.
- Greenberg, P. E., Sisitsky, T., Kessler, R. C., Finkelstein, S. N., Berndt, E. R., Davidson, J. R., Ballenger, J. C., & Fyer, A. J. (1999). The economic burden of anxiety disorders in the 1990s. *Journal of Clinical Psychiatry*, 60(7), 427-435. <https://doi.org/10.4088/jcp.v60n0702>
- Greenhagen, B. T. (2003). *Origins of isoprenoid diversity: A study of structure-function relationships in sesquiterpene synthases* [University of Kentucky]. [https://uknowledge.uky.edu/gradschool\\_diss/440](https://uknowledge.uky.edu/gradschool_diss/440)
- Greenhagen, B. T., Griggs, P., Takahashi, S., Ralston, L., & Chappell, J. (2003). Probing sesquiterpene hydroxylase activities in a coupled assay with terpene synthases. *Archives of Biochemistry & Biophysics*, 409(2), 385-394. <https://www.ncbi.nlm.nih.gov/pubmed/12504906>
- Greenhagen, B. T., O'Maille, P. E., Noel, J. P., & Chappell, J. (2006). Identifying and manipulating structural determinates linking catalytic specificities in terpene synthases. *Proceedings of the National Academy of Sciences of the United States of America*, 103(26), 9826-9831. <https://doi.org/10.1073/pnas.0601605103>
- Griebel, G., & Holmes, A. (2013). 50 years of hurdles and hope in anxiolytic drug discovery. *Nature Reviews Drug Discovery*, 12(9), 667-687. <https://doi.org/10.1038/nrd4075>
- Grundy, D. J., Chen, M., Gonzalez, V., Leoni, S., Miller, D. J., Christianson, D. W., & Allemann, R. K. (2016). Mechanism of germacradien-4-ol synthase-controlled water capture. *Biochemistry*, 55(14), 2112-2121. <https://doi.org/10.1021/acs.biochem.6b00115>
- Hamill, O. P., Marty, A., Neher, E., Sakmann, B., & Sigworth, F. J. (1981). Improved patch-clamp techniques for high-resolution current recording from cells and cell-free membrane patches. *Pflugers Arch*, 391(2), 85-100. <https://www.ncbi.nlm.nih.gov/pubmed/6270629>
- Hammer, S. C., Kubik, G., Watkins, E., Huang, S., Mingos, H., & Arnold, F. H. (2017). Anti-markovnikov alkene oxidation by metal-oxo-mediated enzyme catalysis. *Science*, 358(6360), 215-218. <https://doi.org/10.1126/science.aao1482>

- Han, W., Li, J., Pelkey, K. A., Pandey, S., Chen, X., Wang, Y.-X., Wu, K., Ge, L., Li, T., Castellano, D., Liu, C., Wu, L.-G., Petralia, R. S., Lynch, J. W., McBain, C. J., & Lu, W. (2019). Shisa7 is a gabaa receptor auxiliary subunit controlling benzodiazepine actions. *Science*, 366(6462), 246-250. <https://doi.org/10.1126/science.aax5719>
- Harju, S., Fedosyuk, H., & Peterson, K. R. (2004). Rapid isolation of yeast genomic DNA: Bust n' grab. *BMC Biotechnology*, 4, 8. <https://doi.org/10.1186/1472-6750-4-8>
- Heckman, K. L., & Pease, L. R. (2007). Gene splicing and mutagenesis by pcr-driven overlap extension. *Nature Protocols*, 2(4), 924-932. <https://doi.org/10.1038/nprot.2007.132>
- Helliwell, C. A., Poole, A., Peacock, W. J., & Dennis, E. S. (1999). Arabidopsis ent-kaurene oxidase catalyzes three steps of gibberellin biosynthesis. *Plant Physiology*, 119(2), 507-510. <https://doi.org/10.1104/pp.119.2.507>
- Helliwell, C. A., Sheldon, C. C., Olive, M. R., Walker, A. R., Zeevaart, J. A., Peacock, W. J., & Dennis, E. S. (1998). Cloning of the arabidopsis ent-kaurene oxidase gene ga3. *Proceedings of the National Academy of Sciences of the United States of America*, 95(15), 9019-9024. <https://doi.org/10.1073/pnas.95.15.9019>
- Henry, K. W., Nickels, J. T., & Edlind, T. D. (2002). Rox1 and erg regulation in *saccharomyces cerevisiae*: Implications for antifungal susceptibility. *Eukaryotic Cell*, 1(6), 1041-1044. <https://doi.org/doi:10.1128/EC.1.6.1041-1044.2002>
- Hinkle, D. J., & Macdonald, R. L. (2003). Beta subunit phosphorylation selectively increases fast desensitization and prolongs deactivation of alpha1beta1gamma21 and alpha1beta3gamma21 gaba(a) receptor currents. *Journal Neuroscience*, 23(37), 11698-11710. <https://doi.org/10.1523/jneurosci.23-37-11698.2003>
- Houghton, P. J. (1988). The biological activity of valerian and related plants. *Journal of Ethnopharmacology*, 22(2), 121-142. <https://www.ncbi.nlm.nih.gov/pubmed/3287008>
- Houghton, P. J. (1999). The scientific basis for the reputed activity of valerian. *Journal of Pharmacy and Pharmacology*, 51(5), 505-512. <https://www.ncbi.nlm.nih.gov/pubmed/10411208>
- Iijima, Y., Davidovich-Rikanati, R., Fridman, E., Gang, D. R., Bar, E., Lewinsohn, E., & Pichersky, E. (2004). The biochemical and molecular basis for the divergent patterns in the biosynthesis of terpenes and phenylpropenes in the peltate glands of three cultivars of basil. *Plant Physiology*, 136(3), 3724-3736. <https://doi.org/10.1104/pp.104.051318>
- Izquierdo-Bueno, I., González-Rodríguez, V. E., Simon, A., Dalmais, B., Pradier, J. M., Le Pêcheur, P., Mercier, A., Walker, A. S., Garrido, C., Collado, I. G., & Viaud, M. (2018). Biosynthesis of abscisic acid in fungi: Identification of a sesquiterpene cyclase as the key enzyme in *botrytis cinerea*. *Environmental Microbiology*, 20(7), 2469-2482. <https://doi.org/10.1111/1462-2920.14258>

- Jacob, T. C., Bogdanov, Y. D., Magnus, C., Saliba, R. S., Kittler, J. T., Haydon, P. G., & Moss, S. J. (2005). Gephyrin regulates the cell surface dynamics of synaptic gabaa receptors. *J Neurosci*, 25(45), 10469-10478. <https://doi.org/10.1523/JNEUROSCI.2267-05.2005>
- Jacob, T. C., Moss, S. J., & Jurd, R. (2008). Gabaa receptor trafficking and its role in the dynamic modulation of neuronal inhibition. *Nature Reviews Neuroscience*, 9(5), 331-343. <https://doi.org/10.1038/nrn2370>
- Jakociunas, T., Bonde, I., Herrgard, M., Harrison, S. J., Kristensen, M., Pedersen, L. E., Jensen, M. K., & Keasling, J. D. (2015). Multiplex metabolic pathway engineering using crispr/cas9 in *saccharomyces cerevisiae*. *Metabolic Engineering*, 28, 213-222. <https://doi.org/10.1016/j.ymben.2015.01.008>
- Jakubovski, E., Johnson, J. A., Nasir, M., Müller-Vahl, K., & Bloch, M. H. (2019). Systematic review and meta-analysis: Dose-response curve of ssris and snris in anxiety disorders. *Depression and Anxiety*, 36(3), 198-212. <https://doi.org/10.1002/da.22854>
- Jakupovic, J., Pathak, V. P., Grenz, M., Banerjee, S., Wolfrum, C., Baruah, R. N., & Bohlmann, F. (1987). Sesquiterpene derivatives from *othonna* and related species. *Phytochemistry*, 26(4), 1049-1052. [https://doi.org/https://doi.org/10.1016/S0031-9422\(00\)82348-1](https://doi.org/https://doi.org/10.1016/S0031-9422(00)82348-1)
- Jinek, M., Chylinski, K., Fonfara, I., Hauer, M., Doudna, J. A., & Charpentier, E. (2012). A programmable dual-rna-guided DNA endonuclease in adaptive bacterial immunity. *Science*, 337(6096), 816-821. <https://doi.org/10.1126/science.1225829>
- Joesch, C., Guevarra, E., Parel, S. P., Bergner, A., Zbinden, P., Konrad, D., & Albrecht, H. (2008). Use of flipr membrane potential dyes for validation of high-throughput screening with the flipr and microarcs technologies: Identification of ion channel modulators acting on the gaba(a) receptor. *Journal of Biomolecular Screening*, 13(3), 218-228. <https://doi.org/10.1177/1087057108315036>
- Jurd, R., Arras, M., Lambert, S., Drexler, B., Siegwart, R., Crestani, F., Zaugg, M., Vogt, K. E., Ledermann, B., Antkowiak, B., & Rudolph, U. (2003). General anesthetic actions in vivo strongly attenuated by a point mutation in the gaba(a) receptor beta3 subunit. *The FASEB Journal*, 17(2), 250-252. <https://doi.org/10.1096/fj.02-0611fje>
- Kaczurkin, A. N., & Foa, E. B. (2015). Cognitive-behavioral therapy for anxiety disorders: An update on the empirical evidence. *Dialogues in Clinical Neuroscience*, 17(3), 337-346. <https://doi.org/10.31887/DCNS.2015.17.3/akaczurkin>
- Karim, N., Wellendorph, P., Absalom, N., Johnston, G. A., Hanrahan, J. R., & Chebib, M. (2013). Potency of gaba at human recombinant gaba(a) receptors expressed in *xenopus oocytes*: A mini review. *Amino Acids*, 44(4), 1139-1149. <https://doi.org/10.1007/s00726-012-1456-y>

- Kempinski, C., & Chappell, J. (2019). Engineering triterpene metabolism in the oilseed of *arabidopsis thaliana*. *Plant Biotechnology Journal*, *17*(2), 386-396. <https://doi.org/10.1111/pbi.12984>
- Kempinski, C., Jiang, Z., Zinck, G., Sato, S. J., Ge, Z., Clemente, T. E., & Chappell, J. (2019). Engineering linear, branched-chain triterpene metabolism in monocots. *Plant Biotechnology Journal*, *17*(2), 373-385. <https://doi.org/10.1111/pbi.12983>
- Kersten, R. D., Diedrich, J. K., Yates, J. R., 3rd, & Noel, J. P. (2015). Mechanism-based post-translational modification and inactivation in terpene synthases. *ACS Chemical Biology*, *10*(11), 2501-2511. <https://doi.org/10.1021/acscchembio.5b00539>
- Kessler, R. C., Petukhova, M., Sampson, N. A., Zaslavsky, A. M., & Wittchen, H. U. (2012). Twelve-month and lifetime prevalence and lifetime morbid risk of anxiety and mood disorders in the united states. *International Journal of Methods in Psychiatric Research*, *21*(3), 169-184. <https://doi.org/10.1002/mpr.1359>
- Khom, S., Baburin, I., Timin, E., Hohaus, A., Trauner, G., Kopp, B., & Hering, S. (2007). Valerenic acid potentiates and inhibits gaba(a) receptors: Molecular mechanism and subunit specificity. *Neuropharmacology*, *53*(1), 178-187. <https://doi.org/10.1016/j.neuropharm.2007.04.018>
- Khom, S., Hintersteiner, J., Luger, D., Haider, M., Pototschnig, G., Mihovilovic, M. D., Schwarzer, C., & Hering, S. (2016). Analysis of beta-subunit-dependent gabaa receptor modulation and behavioral effects of valerenic acid derivatives. *Journal of Pharmacology & Experimental Therapeutics*, *357*(3), 580-590. <https://doi.org/10.1124/jpet.116.232983>
- Khom, S., Strommer, B., Ramharter, J., Schwarz, T., Schwarzer, C., Erker, T., Ecker, G. F., Mulzer, J., & Hering, S. (2010). Valerenic acid derivatives as novel subunit-selective gabaa receptor ligands - in vitro and in vivo characterization. *British Journal of Pharmacology*, *161*(1), 65-78. <https://doi.org/10.1111/j.1476-5381.2010.00865.x>
- Kim, J. J., Gharpure, A., Teng, J., Zhuang, Y., Howard, R. J., Zhu, S., Noviello, C. M., Walsh, R. M., Lindahl, E., & Hibbs, R. E. (2020). Shared structural mechanisms of general anaesthetics and benzodiazepines. *Nature*, *585*(7824), 303-308. <https://doi.org/10.1038/s41586-020-2654-5>
- Klausberger, T., Ehya, N., Fuchs, K., Fuchs, T., Ebert, V., Sarto, I., & Sieghart, W. (2001). Detection and binding properties of gabaa receptor assembly intermediates. *Journal of Biological Chemistry*, *276*(19), 16024-16032. <https://doi.org/10.1074/jbc.M009508200>
- Konnopka, A., & König, H. (2020). Economic burden of anxiety disorders: A systematic review and meta-analysis. *Pharmacoeconomics*, *38*(1), 25-37. <https://doi.org/10.1007/s40273-019-00849-7>



- Kopp, S., Baur, R., Sigel, E., Mohler, H., & Altmann, K. H. (2010). Highly potent modulation of gaba(a) receptors by valerenic acid derivatives. *ChemMedChem*, 5(5), 678-681. <https://doi.org/10.1002/cmdc.201000062>
- Kupfer, D. J. (2015). Anxiety and dsm-5. *Dialogues in Clinical Neuroscience*, 17(3), 245-246. <https://doi.org/10.31887/DCNS.2015.17.3/dkupfer>
- Lee, R., Coccaro, E., Cremers, H., McCarron, R., Lu, S.-f., Brownstein, M., & Simon, N. (2013). A novel v1a receptor antagonist blocks vasopressin-induced changes in the cns response to emotional stimuli: An fmri study [Original Research]. *Frontiers in Systems Neuroscience*, 7(100). <https://doi.org/10.3389/fnsys.2013.00100>
- Lefaucheur, J.-P., André-Obadia, N., Antal, A., Ayache, S. S., Baeken, C., Benninger, D. H., Cantello, R. M., Cincotta, M., de Carvalho, M., De Ridder, D., Devanne, H., Di Lazzaro, V., Filipović, S. R., Hummel, F. C., Jääskeläinen, S. K., Kimiskidis, V. K., Koch, G., Langguth, B., Nyffeler, T., . . . Garcia-Larrea, L. (2014). Evidence-based guidelines on the therapeutic use of repetitive transcranial magnetic stimulation (rtms). *Clinical Neurophysiology*, 125(11), 2150-2206. <https://doi.org/https://doi.org/10.1016/j.clinph.2014.05.021>
- Lesburg, C. A., Zhai, G., Cane, D. E., & Christianson, D. W. (1997). Crystal structure of pentalenene synthase: Mechanistic insights on terpenoid cyclization reactions in biology. *Science*, 277(5333), 1820-1824. <https://www.ncbi.nlm.nih.gov/pubmed/9295272>
- Li, Z., Gao, R., Hao, Q., Zhao, H., Cheng, L., He, F., Liu, L., Liu, X., Chou, W. K., Zhu, H., & Cane, D. E. (2016). The t296v mutant of amorpha-4,11-diene synthase is defective in allylic diphosphate isomerization but retains the ability to cyclize the intermediate (3r)-nerolidyl diphosphate to amorpha-4,11-diene. *Biochemistry*, 55(48), 6599-6604. <https://doi.org/10.1021/acs.biochem.6b01004>
- Licata, S. C., & Rowlett, J. K. (2008). Abuse and dependence liability of benzodiazepine-type drugs: Gaba(a) receptor modulation and beyond. *Pharmacology Biochemistry and Behavior*, 90(1), 74-89. <https://doi.org/10.1016/j.pbb.2008.01.001>
- Liu, G., Lanham, C., Buchan, J. R., & Kaplan, M. E. (2017). High-throughput transformation of *saccharomyces cerevisiae* using liquid handling robots. *PLoS One*, 12(3), e0174128. <https://doi.org/10.1371/journal.pone.0174128>
- Louiset, E., McKernan, R., Sieghart, W., & Vaudry, H. (2000). Subunit composition and pharmacological characterization of gamma-aminobutyric acid type a receptors in frog pituitary melanotrophs. *Endocrinology*, 141(3), 1083-1092. <https://doi.org/10.1210/endo.141.3.7397>
- Low, K., Crestani, F., Keist, R., Benke, D., Brunig, I., Benson, J. A., Fritschy, J. M., Rulicke, T., Bluethmann, H., Mohler, H., & Rudolph, U. (2000). Molecular and neuronal substrate for the selective attenuation of anxiety. *Science*, 290(5489), 131-134. <http://www.ncbi.nlm.nih.gov/pubmed/11021797>

- Luger, D., Poli, G., Wieder, M., Stadler, M., Ke, S., Ernst, M., Hohaus, A., Linder, T., Seidel, T., Langer, T., Khom, S., & Hering, S. (2015). Identification of the putative binding pocket of valerenic acid on gabaa receptors using docking studies and site-directed mutagenesis. *British Journal of Pharmacology*, *172*(22), 5403-5413. <https://doi.org/10.1111/bph.13329>
- Mali, P., Yang, L., Esvelt, K. M., Aach, J., Guell, M., DiCarlo, J. E., Norville, J. E., & Church, G. M. (2013). Rna-guided human genome engineering via cas9. *Science*, *339*(6121), 823-826. <https://doi.org/10.1126/science.1232033>
- Markossian, S., Grossman, A., Brimacombe, K., Arkin, M., Auld, D., Austin, C. P., Baell, J., Chung, T. D. Y., Coussens, N. P., Dahlin, J. L., Devanarayan, V., Foley, T. L., Glicksman, M., Hall, M. D., Haas, J. V., Hoare, S. R. J., Inglese, J., Iversen, P. W., Kales, S. C., . . . Xu, X. (2004). In *Assay guidance manual*. <https://www.ncbi.nlm.nih.gov/pubmed/22553861>
- Masiulis, S., Desai, R., Uchański, T., Serna Martin, I., Lavery, D., Karia, D., Malinauskas, T., Zivanov, J., Pardon, E., Kotecha, A., Steyaert, J., Miller, K. W., & Aricescu, A. R. (2019). Gabaa receptor signalling mechanisms revealed by structural pharmacology. *Nature*, *565*(7740), 454-459. <https://doi.org/10.1038/s41586-018-0832-5>
- Mejo, S. L. (1992). Anterograde amnesia linked to benzodiazepines. *Nurse Practitioner*, *17*(10), 44, 49-50. <http://www.ncbi.nlm.nih.gov/pubmed/1357612>
- Melo, F., Sanchez, R., & Sali, A. (2002). Statistical potentials for fold assessment. *Protein Science*, *11*(2), 430-448. <https://doi.org/10.1002/pro.110430>
- Mennerick, S., Chisari, M., Shu, H. J., Taylor, A., Vasek, M., Eisenman, L. N., & Zorumski, C. F. (2010). Diverse voltage-sensitive dyes modulate gabaa receptor function. *Journal of Neuroscience*, *30*(8), 2871-2879. <https://doi.org/10.1523/JNEUROSCI.5607-09.2010>
- Miller, P. S., & Aricescu, A. R. (2014). Crystal structure of a human gabaa receptor. *Nature*, *512*(7514), 270-275. <https://doi.org/10.1038/nature13293>
- Mohler, H., Fritschy, J. M., Vogt, K., Crestani, F., & Rudolph, U. (2005). Pathophysiology and pharmacology of gaba(a) receptors. *Handbook of Experimental Pharmacology*(169), 225-247. [https://doi.org/10.1007/3-540-28082-0\\_9](https://doi.org/10.1007/3-540-28082-0_9)
- Murphy, K., Kubin, Z. J., Shepherd, J. N., & Ettinger, R. H. (2010). Valeriana officinalis root extracts have potent anxiolytic effects in laboratory rats. *Phytomedicine*, *17*(8-9), 674-678. <https://doi.org/10.1016/j.phymed.2009.10.020>
- Nagai, K., Mori, Y., Ishikawa, S., Furuta, T., Gamuyao, R., Niimi, Y., Hobo, T., Fukuda, M., Kojima, M., Takebayashi, Y., Fukushima, A., Himuro, Y., Kobayashi, M., Ackley, W., Hisano, H., Sato, K., Yoshida, A., Wu, J., Sakakibara, H., . . . Ashikari, M. (2020). Antagonistic regulation of the gibberellic acid response during stem growth in rice. *Nature*, *584*(7819), 109-114. <https://doi.org/10.1038/s41586-020-2501-8>



- Nardi, A. E., Machado, S., Almada, L. F., Paes, F., Silva, A. C., Marques, R. J., Amrein, R., Freire, R. C., Martin-Santos, R., Cosci, F., Hallak, J. E., Crippa, J. A., & Arias-Carrión, O. (2013). Clonazepam for the treatment of panic disorder. *Current Drug Targets*, 14(3), 353-364. <https://doi.org/10.2174/1389450111314030007>
- Neher, E., & Sakmann, B. (1976). Single-channel currents recorded from membrane of denervated frog muscle fibres. *Nature*, 260(5554), 799-802. <https://doi.org/10.1038/260799a0>
- Neher, E., Sakmann, B., & Steinbach, J. H. (1978). The extracellular patch clamp: A method for resolving currents through individual open channels in biological membranes. *Pflugers Arch*, 375(2), 219-228. <https://www.ncbi.nlm.nih.gov/pubmed/567789>
- Nguyen, D. T., Gopfert, J. C., Ikezawa, N., Macnevin, G., Kathiresan, M., Conrad, J., Spring, O., & Ro, D. K. (2010). Biochemical conservation and evolution of germacrene a oxidase in asteraceae. *Journal of Biological Chemistry*, 285(22), 16588-16598. <https://doi.org/10.1074/jbc.M110.111757>
- Nguyen, T. D., Faraldos, J. A., Vardakou, M., Salmon, M., O'Maille, P. E., & Ro, D. K. (2016). Discovery of germacrene a synthases in barnadesia spinosa: The first committed step in sesquiterpene lactone biosynthesis in the basal member of the asteraceae. *Biochemical and Biophysical Research Communications*, 479(4), 622-627. <https://doi.org/10.1016/j.bbrc.2016.09.165>
- Nguyen, T. D., Kwon, M., Kim, S. U., Fischer, C., & Ro, D. K. (2019). Catalytic plasticity of germacrene a oxidase underlies sesquiterpene lactone diversification. *Plant Physiology*, 181(3), 945-960. <https://doi.org/10.1104/pp.19.00629>
- Niehaus, T. D., Okada, S., Devarenne, T. P., Watt, D. S., Sviripa, V., & Chappell, J. (2011). Identification of unique mechanisms for triterpene biosynthesis in botryococcus braunii. *Proceedings of the National Academy of Sciences of the United States of America*, 108(30), 12260-12265. <https://doi.org/10.1073/pnas.1106222108>
- Nik, A. M., Pressly, B., Singh, V., Antrobus, S., Hulsizer, S., Rogawski, M. A., Wulff, H., & Pessah, I. N. (2017). Rapid throughput analysis of gaba(a) receptor subtype modulators and blockers using disbac(1)(3) membrane potential red dye. *Molecular pharmacology*, 92(1), 88-99. <https://doi.org/10.1124/mol.117.108563>
- Nybo, S. E., Saunders, J., & McCormick, S. P. (2017). Metabolic engineering of escherichia coli for production of valerenadiene. *Journal of Biotechnology & Bioengineering*, 262, 60-66. <https://doi.org/10.1016/j.jbiotec.2017.10.004>
- O'Maille, P. E., Malone, A., Dellas, N., Andes Hess, B., Smentek, L., Sheehan, I., Greenhagen, B. T., Chappell, J., Manning, G., & Noel, J. P. (2008). Quantitative exploration of the catalytic landscape separating divergent plant sesquiterpene synthases. *Nature Chemical Biology*, 4(10), 617-623. <https://doi.org/10.1038/nchembio.113>

- Obergrussberger, A., Friis, S., Brüggemann, A., & Fertig, N. (2021). Automated patch clamp in drug discovery: Major breakthroughs and innovation in the last decade. *Expert Opinion on Drug Discovery*, 16(1), 1-5. <https://doi.org/10.1080/17460441.2020.1791079>
- Olfson, M., King, M., & Schoenbaum, M. (2015). Benzodiazepine use in the united states. *JAMA Psychiatry*, 72(2), 136-142. <https://doi.org/10.1001/jamapsychiatry.2014.1763>
- Olsen, R. W., & Sieghart, W. (2009). Gaba a receptors: Subtypes provide diversity of function and pharmacology. *Neuropharmacology*, 56(1), 141-148. <https://doi.org/10.1016/j.neuropharm.2008.07.045>
- Özaydın, B., Burd, H., Lee, T. S., & Keasling, J. D. (2013). Carotenoid-based phenotypic screen of the yeast deletion collection reveals new genes with roles in isoprenoid production. *Metabolic Engineering*, 15, 174-183. <https://doi.org/10.1016/j.ymben.2012.07.010>
- Paddon, C. J., Westfall, P. J., Pitera, D. J., Benjamin, K., Fisher, K., McPhee, D., Leavell, M. D., Tai, A., Main, A., Eng, D., Polichuk, D. R., Teoh, K. H., Reed, D. W., Treynor, T., Lenihan, J., Fleck, M., Bajad, S., Dang, G., Dengrove, D., . . . Newman, J. D. (2013). High-level semi-synthetic production of the potent antimalarial artemisinin. *Nature*, 496(7446), 528-532. <https://doi.org/10.1038/nature12051>
- Paknikar, S. K., Kadam, S. H., Ehrlich, A. L., & Bates, R. B. (2013). Alternate biosynthesis of valerenadiene and related sesquiterpenes. *Natural Product Communications*, 8(9), 1195-1196. <https://www.ncbi.nlm.nih.gov/pubmed/24273843>
- Pan, A. C., Borhani, D. W., Dror, R. O., & Shaw, D. E. (2013). Molecular determinants of drug-receptor binding kinetics. *Drug Discovery Today*, 18(13-14), 667-673. <https://doi.org/10.1016/j.drudis.2013.02.007>
- Pateraki, I., Heskes, A. M., & Hamberger, B. (2015). Cytochromes p450 for terpene functionalisation and metabolic engineering. *Advances in Biochemical Engineering/Biotechnology*, 148, 107-139. [https://doi.org/10.1007/10\\_2014\\_301](https://doi.org/10.1007/10_2014_301)
- Peralta-Yahya, P. P., Ouellet, M., Chan, R., Mukhopadhyay, A., Keasling, J. D., & Lee, T. S. (2011). Identification and microbial production of a terpene-based advanced biofuel. *Nature Communications*, 2, 483. <https://doi.org/10.1038/ncomms1494>
- Picaud, S., Olsson, M. E., Brodelius, M., & Brodelius, P. E. (2006). Cloning, expression, purification and characterization of recombinant (+)-germacrene d synthase from zingiber officinale. *Archives of Biochemistry and Biophysics*, 452(1), 17-28. <https://doi.org/10.1016/j.abb.2006.06.007>
- Picciotto, M. R., Brunzell, D. H., & Caldarone, B. J. (2002). Effect of nicotine and nicotinic receptors on anxiety and depression. *Neuroreport*, 13(9), 1097-1106. <https://doi.org/10.1097/00001756-200207020-00006>

- Poulter, C. D., & Rilling, H. C. (1978). The prenyl transfer reaction. Enzymic and mechanistic studies of the 1'-4 coupling reaction in the terpene biosynthetic pathway. *Accounts of Chemical Research*, 11(8), 307-313. <https://doi.org/10.1021/ar50128a004>
- Pritchett, D. B., Sontheimer, H., Gorman, C. M., Kettenmann, H., Seeburg, P. H., & Schofield, P. R. (1988). Transient expression shows ligand gating and allosteric potentiation of gabaa receptor subunits. *Science*, 242(4883), 1306-1308. <https://www.ncbi.nlm.nih.gov/pubmed/2848320>
- Pyle, B. W., Tran, H. T., Pickel, B., Haslam, T. M., Gao, Z., MacNevin, G., Vederas, J. C., Kim, S. U., & Ro, D. K. (2012). Enzymatic synthesis of valerena-4,7(11)-diene by a unique sesquiterpene synthase from the valerian plant (*valeriana officinalis*). *FEBS Journal*, 279(17), 3136-3146. <https://doi.org/10.1111/j.1742-4658.2012.08692.x>
- Ramharter, J., & Mulzer, J. (2009). Total synthesis of valerenic acid, a potent gabaa receptor modulator. *Organic Letters*, 11(5), 1151-1153. <https://doi.org/10.1021/ol9000137>
- Rapid measurement of protein concentration by western analysis using colorimetric detection by bcip-nbt. (2006). *Cold Spring Harbor Protocols*, 2006(1), pdb.prot4254. <https://doi.org/10.1101/pdb.prot4254>
- Reider Apel, A., d'Espaux, L., Wehrs, M., Sachs, D., Li, R. A., Tong, G. J., Garber, M., Nnadi, O., Zhuang, W., Hillson, N. J., Keasling, J. D., & Mukhopadhyay, A. (2017). A cas9-based toolkit to program gene expression in *saccharomyces cerevisiae*. *Nucleic Acids Research*, 45(1), 496-508. <https://doi.org/10.1093/nar/gkw1023>
- Ricigliano, V., Kumar, S., Kinison, S., Brooks, C., Nybo, S. E., Chappell, J., & Howarth, D. G. (2016). Regulation of sesquiterpenoid metabolism in recombinant and elicited *valeriana officinalis* hairy roots. *Phytochemistry*, 125, 43-53. <https://doi.org/10.1016/j.phytochem.2016.02.011>
- Rising, K. A., Starks, C. M., Noel, J. P., & Chappell, J. (2000). Demonstration of germacrene a as an intermediate in 5-epi-aristolochene synthase catalysis. *Journal of the American Chemical Society*, 122(9), 1861-1866. <https://doi.org/10.1021/ja993584h>
- Ro, D. K., Paradise, E. M., Ouellet, M., Fisher, K. J., Newman, K. L., Ndungu, J. M., Ho, K. A., Eachus, R. A., Ham, T. S., Kirby, J., Chang, M. C., Withers, S. T., Shiba, Y., Sarpong, R., & Keasling, J. D. (2006). Production of the antimalarial drug precursor artemisinic acid in engineered yeast. *Nature*, 440(7086), 940-943. <https://doi.org/10.1038/nature04640>
- Robinson, O. J., Pike, A. C., Cornwell, B., & Grillon, C. (2019). The translational neural circuitry of anxiety. *Journal of Neurology, Neurosurgery, Psychiatry*, 90(12), 1353-1360. <https://doi.org/10.1136/jnnp-2019-321400>

- Rudolph, U., & Knoflach, F. (2011). Beyond classical benzodiazepines: Novel therapeutic potential of gabaa receptor subtypes. *Nature Reviews Drug Discovery*, 10(9), 685-697. <https://doi.org/10.1038/nrd3502>
- Russell, J. A. (1980). A circumplex model of affect. *Journal of Personality and Social Psychology*, 39(6), 1161-1178. <https://doi.org/10.1037/h0077714>
- Ruzicka, L. (1953). The isoprene rule and the biogenesis of terpenic compounds. *Experientia*, 9(10), 357-367. <https://www.ncbi.nlm.nih.gov/pubmed/13116962>
- Ryan, O. W., & Cate, J. H. (2014). Multiplex engineering of industrial yeast genomes using crispr. *Methods of Enzymology*, 546, 473-489. <https://doi.org/10.1016/B978-0-12-801185-0.00023-4>
- Ryan, O. W., Skerker, J. M., Maurer, M. J., Li, X., Tsai, J. C., Poddar, S., Lee, M. E., DeLoache, W., Dueber, J. E., Arkin, A. P., & Cate, J. H. (2014). Selection of chromosomal DNA libraries using a multiplex crispr system. *Elife*, 3. <https://doi.org/10.7554/eLife.03703>
- Rynkiewicz, M. J., Cane, D. E., & Christianson, D. W. (2002). X-ray crystal structures of d100e trichodiene synthase and its pyrophosphate complex reveal the basis for terpene product diversity. *Biochemistry*, 41(6), 1732-1741. <https://www.ncbi.nlm.nih.gov/pubmed/11827517>
- Sali, A., & Blundell, T. L. (1993). Comparative protein modelling by satisfaction of spatial restraints. *Journal of Molecular Biology*, 234(3), 779-815. <https://doi.org/10.1006/jmbi.1993.1626>
- Salmon, M., Laurendon, C., Vardakou, M., Cheema, J., Defernez, M., Green, S., Faraldos, J. A., & O'Maille, P. E. (2015). Emergence of terpene cyclization in artemisia annua. *Nature Communications*, 6, 6143. <https://doi.org/10.1038/ncomms7143>
- Sartori, S. B., & Singewald, N. (2019). Novel pharmacological targets in drug development for the treatment of anxiety and anxiety-related disorders. *Pharmacology & Therapeutics*, 204, 107402. <https://doi.org/10.1016/j.pharmthera.2019.107402>
- Sauer, R. T., & Baker, T. A. (2011). Aaa+ proteases: Atp-fueled machines of protein destruction. *Annual Review of Biochemistry*, 80, 587-612. <https://doi.org/10.1146/annurev-biochem-060408-172623>
- Schmidt, C. O., Bouwmeester, H. J., Bulow, N., & Konig, W. A. (1999). Isolation, characterization, and mechanistic studies of (-)-alpha-gurjunene synthase from solidago canadensis. *Archives of Biochemistry & Biophysics*, 364(2), 167-177. <https://doi.org/10.1006/abbi.1999.1122>
- Schneider, C. A., Rasband, W. S., & Eliceiri, K. W. (2012). Nih image to imagej: 25 years of image analysis. *Nature Methods*, 9(7), 671-675. <https://www.ncbi.nlm.nih.gov/pubmed/22930834>

- Schofield, P. R., Darlison, M. G., Fujita, N., Burt, D. R., Stephenson, F. A., Rodriguez, H., Rhee, L. M., Ramachandran, J., Reale, V., Glencorse, T. A., & et al. (1987). Sequence and functional expression of the gaba a receptor shows a ligand-gated receptor super-family. *Nature*, 328(6127), 221-227. <https://doi.org/10.1038/328221a0>
- Schrepfer, P., Buettner, A., Goerner, C., Hertel, M., van Rijn, J., Wallrapp, F., Eisenreich, W., Sieber, V., Kourist, R., & Bruck, T. (2016). Identification of amino acid networks governing catalysis in the closed complex of class i terpene synthases. *Proceedings of the National Academy of Sciences of the United States of America*, 113(8), E958-967. <https://doi.org/10.1073/pnas.1519680113>
- Schrodinger, LLC. (2015). *The pymol molecular graphics system, version 1.8*.
- Shackman, A. J., & Fox, A. S. (2016). Contributions of the central extended amygdala to fear and anxiety. *Journal of Neuroscience*, 36(31), 8050-8063. <https://doi.org/10.1523/JNEUROSCI.0982-16.2016>
- Shen, M. Y., & Sali, A. (2006). Statistical potential for assessment and prediction of protein structures. *Protein Science*, 15(11), 2507-2524. <https://doi.org/10.1110/ps.062416606>
- Shirneshan, E. (2013). *Cost of illness study of anxiety disorders for the ambulatory adult population of the united states* [University of Tennessee].
- Singh, B., & Sharma, R. A. (2015). Plant terpenes: Defense responses, phylogenetic analysis, regulation and clinical applications. *3 Biotech*, 5(2), 129-151. <https://doi.org/10.1007/s13205-014-0220-2>
- Starks, C. M., Back, K., Chappell, J., & Noel, J. P. (1997). Structural basis for cyclic terpene biosynthesis by tobacco 5-epi-aristolochene synthase. *Science*, 277(5333), 1815-1820. <https://www.ncbi.nlm.nih.gov/pubmed/9295271>
- Sterpenich, V., Vidal, S., Hofmeister, J., Michalopoulos, G., Bancila, V., Warrot, D., Dayer, A., Desseilles, M., Aubry, J.-M., Kosel, M., Schwartz, S., & Vutskits, L. (2019). Increased reactivity of the mesolimbic reward system after ketamine injection in patients with treatment-resistant major depressive disorder. *Anesthesiology*, 130(6), 923-935. <https://doi.org/10.1097/aln.0000000000002667>
- Stewart, J. J. P. (2016). *Mopac2016*. In Stewart Computational Chemistry. <HTTP://OpenMOPAC.net>
- Succol, F., Fiumelli, H., Benfenati, F., Cancedda, L., & Barberis, A. (2012). Intracellular chloride concentration influences the gabaa receptor subunit composition. *Nat Commun*, 3, 738. <https://doi.org/10.1038/ncomms1744>
- Takahashi, S., Yeo, Y., Greenhagen, B. T., McMullin, T., Song, L., Maurina-Brunker, J., Rosson, R., Noel, J. P., & Chappell, J. (2007). Metabolic engineering of sesquiterpene

- metabolism in yeast. *Biotechnology & Bioengineering*, 97(1), 170-181.  
<https://doi.org/10.1002/bit.21216>
- Takahashi, S., Yeo, Y. S., Zhao, Y., O'Maille, P. E., Greenhagen, B. T., Noel, J. P., Coates, R. M., & Chappell, J. (2007). Functional characterization of premnaspirodiene oxygenase, a cytochrome p450 catalyzing regio- and stereo-specific hydroxylations of diverse sesquiterpene substrates. *Journal of Biological Chemistry*, 282(43), 31744-31754.  
<https://doi.org/10.1074/jbc.M703378200>
- Tantillo, D. J. (2011). Biosynthesis via carbocations: Theoretical studies on terpene formation. *Natural Product Reports*, 28(6), 1035-1053.  
<https://doi.org/10.1039/c1np00006c>
- Tarshis, L. C., Yan, M., Poulter, C. D., & Sacchettini, J. C. (1994). Crystal structure of recombinant farnesyl diphosphate synthase at 2.6-Å resolution. *Biochemistry*, 33(36), 10871-10877. <https://www.ncbi.nlm.nih.gov/pubmed/8086404>
- Tateno, M., Stone, B. J., Srodulski, S. J., Reedy, S., Gawriluk, T. R., Chambers, T. M., Woodward, J., Chappell, J., & Kempinski, C. F. (2020). Synthetic biology-derived triterpenes as efficacious immunomodulating adjuvants. *Scientific Reports*, 10(1), 17090.  
<https://doi.org/10.1038/s41598-020-73868-6>
- Tauseef, M. (2012). Benzodiazepines revisited [Review]. *British Journal of Medical Practitioners*, 5(1).
- Tretter, V., Ehya, N., Fuchs, K., & Sieghart, W. (1997). Stoichiometry and assembly of a recombinant gabaa receptor subtype. *Journal of Neuroscience*, 17(8), 2728-2737.  
<https://www.ncbi.nlm.nih.gov/pubmed/9092594>
- Tretter, V., Jacob, T. C., Mukherjee, J., Fritschy, J. M., Pangalos, M. N., & Moss, S. J. (2008). The clustering of gaba(a) receptor subtypes at inhibitory synapses is facilitated via the direct binding of receptor alpha 2 subunits to gephyrin. *Journal of Neuroscience*, 28(6), 1356-1365. <https://doi.org/10.1523/JNEUROSCI.5050-07.2008>
- Trott, O., & Olson, A. J. (2010). Autodock vina: Improving the speed and accuracy of docking with a new scoring function, efficient optimization, and multithreading. *Journal of Computational Chemistry*, 31(2), 455-461. <https://doi.org/10.1002/jcc.21334>
- van Der Hoeven, R. S., Monforte, A. J., Breeden, D., Tanksley, S. D., & Steffens, J. C. (2000). Genetic control and evolution of sesquiterpene biosynthesis in *lycopersicon esculentum* and *l. Hirsutum*. *Plant Cell*, 12(11), 2283-2294.  
<https://www.ncbi.nlm.nih.gov/pubmed/11090225>
- Vattekkatte, A., Garms, S., & Boland, W. (2017). Alternate cyclization cascade initiated by substrate isomer in multiproduct terpene synthase from *medicago truncatula*. *Journal of Organic Chemistry*, 82(6), 2855-2861. <https://doi.org/10.1021/acs.joc.6b02696>



- Verwaal, R., Wang, J., Meijnen, J.-P., Visser, H., Sandmann, G., van den Berg, J. A., & van Ooyen, A. J. J. (2007). High-level production of beta-carotene in *saccharomyces cerevisiae* by successive transformation with carotenogenic genes from *xanthophyllomyces dendrorhous*. *Applied and Environmental Microbiology*, 73(13), 4342-4350. <https://doi.org/doi:10.1128/AEM.02759-06>
- Wang, X., Huo, X., Yang, R., Li, Z., Sun, Y., Qu, L., & Zeng, H. (2020). A novel fluorescence probe based on specific recognition of gabaa receptor for imaging cell membrane. *Talanta*, 219, 121317. <https://doi.org/10.1016/j.talanta.2020.121317>
- Williams, P. A., Cosme, J., Sridhar, V., Johnson, E. F., & McRee, D. E. (2000). Mammalian microsomal cytochrome p450 monooxygenase: Structural adaptations for membrane binding and functional diversity. *Molecular Cell*, 5(1), 121-131. [https://doi.org/10.1016/s1097-2765\(00\)80408-6](https://doi.org/10.1016/s1097-2765(00)80408-6)
- Wittchen, H. U., Jacobi, F., Rehm, J., Gustavsson, A., Svensson, M., Jönsson, B., Olesen, J., Allgulander, C., Alonso, J., Faravelli, C., Fratiglioni, L., Jennum, P., Lieb, R., Maercker, A., van Os, J., Preisig, M., Salvador-Carulla, L., Simon, R., & Steinhausen, H. C. (2011). The size and burden of mental disorders and other disorders of the brain in europe 2010. *European Neuropsychopharmacology*, 21(9), 655-679. <https://doi.org/10.1016/j.euroneuro.2011.07.018>
- Wong, J., d'Espaux, L., Dev, I., van der Horst, C., & Keasling, J. (2018). De novo synthesis of the sedative valerenic acid in *saccharomyces cerevisiae*. *Metabolic Engineering*, 47, 94-101. <https://doi.org/10.1016/j.ymben.2018.03.005>
- Yamaguchi, S., Saito, T., Abe, H., Yamane, H., Murofushi, N., & Kamiya, Y. (1996). Molecular cloning and characterization of a cDNA encoding the gibberellin biosynthetic enzyme ent-kaurene synthase b from pumpkin (*cucurbita maxima* l.). *Plant Journal*, 10(2), 203-213. <https://doi.org/10.1046/j.1365-313x.1996.10020203.x>
- Yamaguchi, S., Sun, T., Kawaide, H., & Kamiya, Y. (1998). The ga2 locus of *arabidopsis thaliana* encodes ent-kaurene synthase of gibberellin biosynthesis. *Plant Physiology*, 116(4), 1271-1278. <https://doi.org/10.1104/pp.116.4.1271>
- Yeo, Y. S., Nybo, S. E., Chittiboyina, A. G., Weerasooriya, A. D., Wang, Y. H., Gongora-Castillo, E., Vaillancourt, B., Buell, C. R., DellaPenna, D., Celiz, M. D., Jones, A. D., Wurtele, E. S., Ransom, N., Dudareva, N., Shaaban, K. A., Tibrewal, N., Chandra, S., Smillie, T., Khan, I. A., . . . Chappell, J. (2013). Functional identification of valerenal, 10-diene synthase, a terpene synthase catalyzing a unique chemical cascade in the biosynthesis of biologically active sesquiterpenes in *valeriana officinalis*. *Journal of Biological Chemistry*, 288(5), 3163-3173. <https://doi.org/10.1074/jbc.M112.415836>
- Yip, G. M., Chen, Z. W., Edge, C. J., Smith, E. H., Dickinson, R., Hohenester, E., Townsend, R. R., Fuchs, K., Sieghart, W., Evers, A. S., & Franks, N. P. (2013). A propofol binding site on mammalian gabaa receptors identified by photolabeling. *Nature Chemical Biology*, 9(11), 715-720. <https://doi.org/10.1038/nchembio.1340>

Yoshikuni, Y., Ferrin, T. E., & Keasling, J. D. (2006). Designed divergent evolution of enzyme function. *Nature*, *440*(7087), 1078-1082. <https://doi.org/10.1038/nature04607>

Yoshikuni, Y., Martin, V. J., Ferrin, T. E., & Keasling, J. D. (2006). Engineering cotton (+)-delta-cadinene synthase to an altered function: Germacrene d-4-ol synthase. *Chemical Biology*, *13*(1), 91-98. <https://doi.org/10.1016/j.chembiol.2005.10.016>

Zhang, T., Zhu, J., Xu, L., Tang, X., Cui, H., Wei, Y., Wang, Y., Hu, Q., Qian, Z., Liu, X., Tang, Y., Li, C., & Wang, J. (2019). Add-on rtms for the acute treatment of depressive symptoms is probably more effective in adolescents than in adults: Evidence from real-world clinical practice. *Brain Stimulation*, *12*(1), 103-109. <https://doi.org/10.1016/j.brs.2018.09.007>

Zhuang, X. (2013). *Engineering novel terpene production platforms in the yeast *saccharomyces cerevisiae** [Doctoral Dissertation, University of Kentucky]. [https://uknowledge.uky.edu/pss\\_etds/17](https://uknowledge.uky.edu/pss_etds/17)

Zhuang, X., & Chappell, J. (2015). Building terpene production platforms in yeast. *Biotechnology & Bioengineering*, *112*(9), 1854-1864. <https://doi.org/10.1002/bit.25588>



## VITA

1. Bachelor of Science in biochemistry from Lee University, Cleveland, TN (2014)
2. No professional positions held
3. **Zinck, G. E.**, & Chappell, J. (2021). Structurally Guided Reprogramming of Valerenadiene Synthase. *Biochemistry*, *60*(51), 3868-3878.

Kempinski, C. Jiang, Z. **Zinck, G.** Sato, SJ. Ge, Z. Clemente, TE. Chappell, J. Engineering linear, branched-chain triterpene metabolism in monocots. *Plant Biotechnol J.* 2019 Feb;17(2):373-385.

**Zinck, G.** and J. Chappell (2019). "Book Review of Herbal Medicines, Fourth Edition." *Journal of Natural Products* **82**(4): 1049-1049.

4. Garrett Edward Zinck